INHIBITION OF HYDROCARBON AUTOXIDATION BY NITROXIDE CATALYZED CROSS DISMUTATION OF ALKYLPEROXYL AND HYDROPEROXYL RADICALS

&

A NOVEL APPROACH TOWARD FLUORINATED POLYUNSATURATED LIPIDS

by

Kareem Harrison

A thesis submitted to the Department of Chemistry and Biomelcular Sciences

in conformity with the requirements for the degree of Master in Chemistry

University of Ottawa

Ottawa, Ontario, Canada

(December 2019)

Abstract

Nitroxides are intermediates in the accepted reaction mechanisms of the antioxidant activity of diarylamines and hindered alkyl amines. The parent amines are used as additives to preserve synthetic and natural hydrocarbon-based materials from oxidative degradation. New methodology which enables monitoring of hydrocarbon autoxidations at low rates of radical generation has revealed that diarylnitroxides and hindered nitroxides are far better inhibitors of unsaturated hydrocarbon autoxidation than their precursor amines, implying intervention of a previously overlooked mechanism. Experimental and computational investigations suggest that the nitroxides catalyze the cross-dismutation of alkylperoxyl and hydroperoxyl radicals to yield a hydroperoxide and O_2, thereby halting the autoxidation chain reaction. The hydroperoxyl radicals – key players in hydrocarbon combustion, but essentially unknown in autoxidation – are proposed to derive from a tunneling-enhanced intramolecular (1,4)-hydrogen-atom transfer/elimination sequence from oxygenated radical addition intermediates. These insights suggest that nitroxides are preferred additives for the protection of unsaturated hydrocarbon-based materials from autoxidation since they exhibit catalytic activity under conditions where their precursor amines are less effective and/or inefficiently converted to nitroxides *in situ*.

Polyunsaturated fatty acids (PUFAs) are highly autoxidizable lipids that are integral structural components of biological membranes as well as substrates for enzymes the produce inflammatory mediators implicated in a host of degenerative diseases. In particular, the interactions between these substrates and their respective native enzymes are hotly pursued since elucidation of the underlying mechanisms could lead to the discovery of better small molecule inhibitors for the ailments to which they contribute. In the past decade, an additional mode of cellular degeneration has been unveiled in the process of ferroptosis whose hallmark includes a sharp increase in the cellular pool of PUFA derived hydroperoxides. As a result, there is further incentive to uncover all mechanisms by which these inflammatory precursors are developed. Herein, progress toward the synthesis of fluorinated PUFAs is presented. These are proposed to be useful to probe the interactions of PUFAs with lipoxygenase enzymes, which metabolize polyunsaturated fatty acids to their hydroperoxide derivatives.

Statement of Originality

I hereby certify that all the work described in this thesis is the original work of the author, with exceptions for work performed by collaborators noted in the preface to each chapter. The work in this thesis finds its foundations rooted in a large bulk of previously published work. Any published (or unpublished) work by others is cited and fully acknowledged within the references herein.

Kareem Harrison

Acknowledgements

Over my time here, I have been extremely fortunate to work alongside a group of hard-working, dedicated, and incredibly knowledgeable people. I would like to thank my supervisor Derek Pratt for his tutelage, counsel, support and seemingly unending wealth of knowledge. I would also like to thank Keith Ingold for his insight into much of the chemistry I've worked with, and all of his helpful advice over the years.

A tremendous thank to all members of the Pratt Group (past and present). A big thanks to Evan Haidasz, Jean-Philippe Chauvin, Markus Griesser, Demar Pitter, Ron Shah, Zosia Zielinski, Omkar Zilka, Pierre Faudot-dit-Bel, Jia-Fei Poon, Luke Farmer, Emily Schaefer, Katie Shirley, Melodie Mallais, Spencer Short, Dmitry Saraev, and Anas Abou-Zaid. An extra special thanks to Ron for being my first mentor and providing me with the skills to mentor two very capable chemists in Neill Penner and Sarah Watt. I also want to give a huge thanks to my good friends Garrett Corkery, Alexander St. Jacques, Emily Lizurej, Enid Gibney and Derick Poirier and my wonderful mother Vedaline Clarke who have been my biggest supporters along this endeavour

Table of Contents

List of Schemes

List of Figures

List of Tables

List of Abbreviations

α-TOC	α-tocopherol
AAPH	2,2'-azobis-(2-amidinopropane) monohydrochloride
AC	acrolein
Ar_2NH	di-*tert*-butyl diphenylamine
Ar_2NO	di-*tert*-butyl diphenylnitroxide
BIAB	Iodosobenzene diacetate
BODIPY	4,4-difluoro-4-bora-3a,4a-diaza-s-indacene
BDE	bond dissociation enthalpy
BHA	butylated hydroxyanisole (2,6-di-*tert*-butyl-4-methoxyphenol)
BHT	butylated hydroxytoluene (2,6-di-*tert*-butyl-4-methylphenol)
COX	cyclooxygenase
CV	cyclic voltametry
CycOct	cyclooctene
DAST	diethylamino sulfur trifluoride
DCM	dichloromethane
DKIE	deuterium kinetic isotope effect
DPA	diphenylamine
DPPH	2,2-diphenyl-1-picrylhydrazyl
DPV	differential pulse voltametry
DMAP	4-dimethylaminopyridine
DMF	dimethylformamide
DMSO	dimethylsulfoxide
DTBNH	di-*tert*-butyl diphenylamine
DTBNO	di-*tert*-butyl diphenylnitroxide
e	efficiency of radical generation
EDG	electron donating group
EDFA	ethyl bromodifluoroacetate
EI	electron impact
EPR	electron paramagnetic resonance
EtOH	ethanol
Fer-1	ferrostatin-1
FLAP	5-lipoxygenase activating protein
GC	gas chromatography
GPX4	glutathione peroxidase 4
HALS	hindered amine light stabilizers
HOMO	highest occupied molecular orbital
HPLC	high-pressure liquid chromatography
HAT	hydrogen-atom transfer
HBA	hydrogen-bond acceptor
HBD	hydrogen-bond donor
HETE	hydroxyeicosatetraenoic acid
HNE	5-hydroxynonenal
HPETE	hydroperoxyeicosatetraenoic acid
In	initiator
IP	ionization potential
k_d	rate constant of initiator dissociation into radicals
k_i	rate constant of initiation

k_p	rate constant of propagation
KSE	kinetic solvent effect
k_t	rate constant of termination
Lip-1	liproxstatin-1
LOH	lipid derived alcohol
LOOH	lipid derived hydroperoxide
LT	leukotriene
LUMO	lowest unoccupied molecular orbital
LX	lipoxin
Lyso-PC	lysophophatidylcholine
MDA	malonyl dialdehyde
MnO_2	manganese dioxide
MUFA	monounsaturated fatty acid
n	stochiometric factor
NaH	sodium hydride
NHE	normal hydrogen electrode
Norb	norbornene
PCET	proton coupled electron transfer
PET	photoinduced electron transfer
PhCl	chlorobenzene
PMC	2,2,5,7,8-pentamethyl-6-chromanol
PUFA	polyunsaturated fatty acid
RCE	retro-carbonyl-ene
R_i	rate of initiation
RDS	rate-determining step
ROOH	substrate derived hydroperoxide
ROH	substrate derived alcohol
RTA	radical trapping antioxidant
sLOX	soybean lipoxygenase
SOMO	singly occupied molecular orbital
TCBC	trichlorobenzoyl chloride
TEMPO	(2,2,6,6-tetramethylpiperidin-1-yl) *N*-oxyl
TEMPH	2,2,6,6-tetramethylpiperidine
TFA	trifluoroacetic acid
THF	tetrahydrofuran
t_{inh}	length of time autoxidation remains inhibited
TIPS	triisopropylsilane
TMS	trimethylsilane
TS	transition state
UV-Vis	ultraviolet to visual light

Chapter 1

Background and Significance

1.1. Hydrocarbon Autoxidation

Petroleum derived products of every dimension are comprised of hydrocarbons. Industries that are built upon these products including fuels, plastics, cosmetics, polymers and fuel additives, are tirelessly in pursuit of methods and systems that protect their foundational materials. Autoxidation is the ubiquitous, radical-mediated oxygenation involved in the degradation of all hydrocarbons. Every hydrocarbon that exists in an aerobic environment is vulnerable to this process to some extent. This includes both saturated and unsaturated petroleum-based consumer goods such as fuels and polymers as well as biologically integral components such as lipids and terpenes.[1,2] The primary oxidation products from an autoxidation are substrate-derived hydroperoxide (ROOH) and/or peroxides (ROOR).[3] In addition, the relative lability of the weak O-O bond in these hydroperoxides and peroxides can breakdown and result in downstream oxidation products such as alcohols, aldehydes, ketones, esters, and carboxylic acids, all of which contribute to degradative structural and chemical changes from the parent substrate.[4,5]

Since the 1950's, a tremendous amount of work has been put into the mechanistic studies on how autoxidation proceeds on a variety of substrates. This includes implications of autoxidation on the onset of several degenerative diseases and its direct involvement in the shortening of petroleum-based consumer product longevity.[4] In general, autoxidation is comprised of the same three phases of any chain reaction: initiation, propagation and termination.[2] A fourth phase, inhibition, can be invoked with the addition of a radical-trapping antioxidant (RTA).[2] Initiation reactions generate new radicals within the reaction. Propagation reactions comprise the key chain-carrying steps that are largely responsible for hydroperoxide formation. Termination reactions are any reactions that remove chain-carrying radicals from an autoxidation, primarily in the form of the self-reaction of two substrate-derived radicals. Finally, intervening inhibition reactions arise from the cross reaction between substrate-derived radicals and radical-trapping antioxidants. A summary of the autoxidation process can be seen in Scheme 1.1. below.

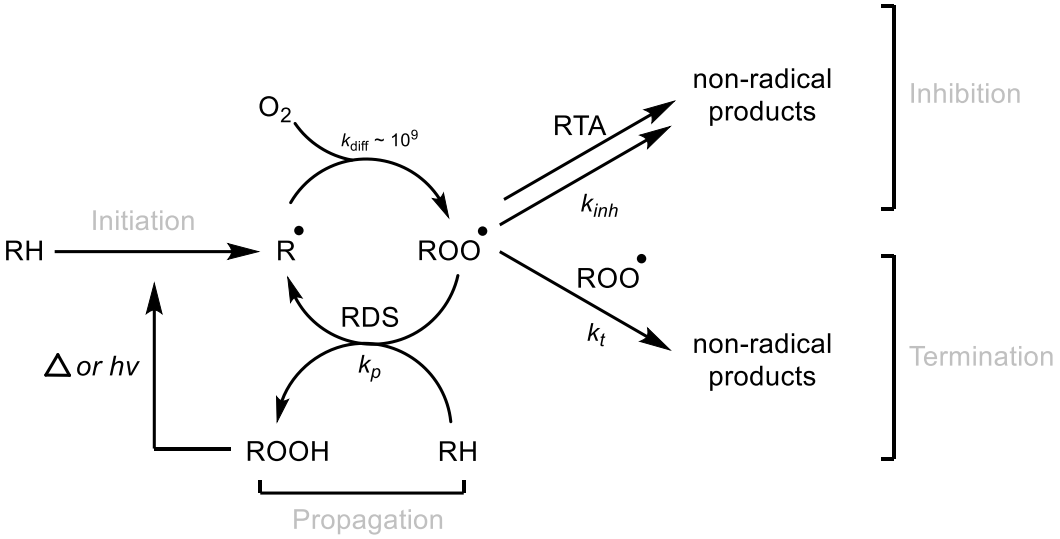

Scheme 1.1. General mechanism for hydrocarbon autoxidation and inhibition with radical trapping-antioxidants (RTA).

1.1.1. Initiation

An initiation reaction is brought about by thermal or photochemical induced bond cleavage of a susceptible bond in the reaction mixture (Eq 1.1).[6,7] This homolysis affords two initiator-derived radicals (In$^{\cdot}$) that react with the hydrocarbon substrate and generate the initial carbon centered radicals (Eq 1.2).[2]

$$In_2 \xrightarrow{R_i} 2\ In^{\bullet} \qquad (1.1)$$

$$In^{\bullet} + RH \longrightarrow InH + R^{\bullet} \qquad (1.2)$$

The resultant substrate-derived radical is trapped by triplet state molecular oxygen at rates approaching the diffusion limit ($k^{298\ K}$ = 3 x 10^9 M^{-1} s^{-1}) [2] , furnishing a substrate-derived peroxyl radical. This peroxyl radical can abstract a hydrogen atom from another molecule of substrate thus, propagating the chain. In addition, at elevated temperatures the resultant hydroperoxides can also decompose (O-O BDE ~ 45 kcal mol^{-1}) into substrate-derived alkoxyls and hydroxyl radicals which are also competent chain initiating radicals.[8] In effect, autoxidation is potentially autocatalytic and will lead to rapid decay of the native substrate as the number of initiating radicals generated spirals out of control.[9]

In effect, primary products from the autoxidation can further initiate the overall reaction. Thus, at elevated temperatures the rate of initiation (R_i) increases as more hydroperoxides are produced in the propagation steps. As a result, systems where the hydroperoxides are susceptible to decomposition are considered autocatalytic.[9] Moreover, hydroperoxide decomposition is not limited to just thermal or photochemical processes. Low-valent metal species such as (Fe (II) or mechanical components) can

reductively heterolyze the hydroperoxides through a Fenton-type reaction into radical-ion pairs ($RO^{\cdot}/HO^{-}$ or $RO^{-}/HO^{\cdot}$) where the radical component can serve as another competent chain-carrying radical.[10] The rate of initiation is critical to the success of establishing a competent autoxidation. Rates of initiation that are too high favour radical-radical reactions over radical-substrate reactions leading to short chain lengths (i.e. termination reactions or radical antioxidants reacting with substrate-derived radicals.[2] At lower rates of initiation, the inverse paradigm unfolds, radical-substrate reactions dominate whereas radical-radical reactions are minimized with the result being elongated chain lengths. The rate of initiation is characterized in equation 1.3.[2] The parameter 'e' is the efficiency of radical generation, which is influenced by solvent and temperature. The parameter k_d represents the rate constant for the decomposition of the initiator into radicals. The final parameter [In] is the concentration of the initiator multiplied by two since two radicals are typically furnished in the initiation step.

$$R_i = 2ek_d[\mathrm{In}] \qquad (1.3)$$

1.1.2. Propagation

Propagation reactions are the primary source of hydroperoxides in an autoxidation and the net sum of elementary propagation steps represents the net chemical transformation observed in autoxidation. Once the initiation step has furnished a substrate-derived alkyl radical, the first propagation step involves the rapid addition of molecular oxygen to yield the corresponding peroxyl radical ($k^{298\ K} = 3 \times 10^9\ M^{-1}\ s^{-1}$) (Eq 1.4).[11]

$$R^{\bullet} + O_2 \xrightarrow{k_{diff} \sim 10^9} ROO^{\bullet} \qquad (1.4)$$

The peroxyl radical then performs an H-atom abstraction on another molecule of the substrate to yield a new substrate-derived alkyl radical and a hydroperoxide (Eq 1.5).

$$ROO^{\bullet} + RH \xrightarrow{k_p} ROOH + R^{\bullet} \qquad (1.5)$$

Since this is the rate-limiting step of the propagation sequence, its rate second order rate constant (k_p) is proportional to the rate of the autoxidation (Eq 1.6), where [ROOH] is the concentration of the substrate-derived hydroperoxides, k_t is the rate constant of termination, [RH] is the concentration of substrate and R_i is the rate of initiation.

$$k_p = \frac{[ROOH]\sqrt{2k_t}}{[RH]\sqrt{R_i}} \qquad (1.6)$$

It is influenced by the C-H bond dissociation enthalpy (BDE) of the most susceptible substrate-derived C-H bond. In effect, fully saturated substrates autoxidize relatively slowly under ambient conditions while allylic, benzylic or alpha-alkoxy substituted positions react significantly faster due to conjugative effects (Figure 1.1).[12,13,14]

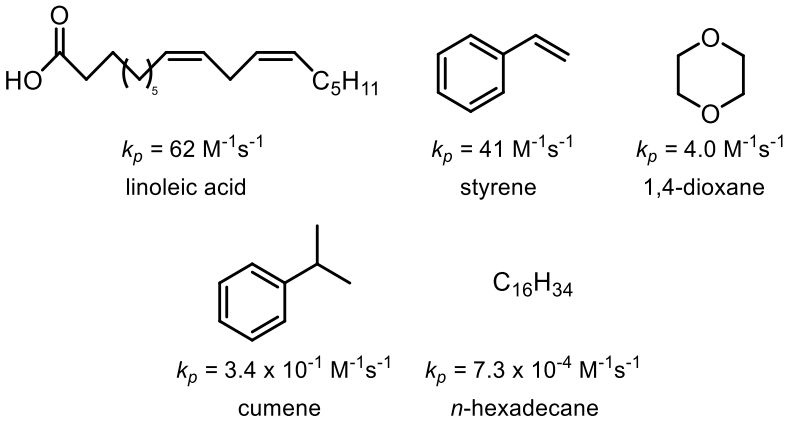

Figure 1.1. Structures and associated rate constants of propagation (k_p) of various studied hydrocarbon substrates with peroxyl radicals calculated at 303K.

Alkenyl substrates also undergo peroxyl addition to the double bond furnishing a peroxy alkyl radical that can be trapped by oxygen and propagate the chain.[13] Alternatively, they can undergo intramolecular homolytic substitution to yield epoxides and chain-initiating alkoxyl radicals. Alkenyl aromatic compounds such as styrene autoxidize primarily via this addition pathway to generate co-polymers of oxygen and substrate (Scheme 1.2).[15,16]

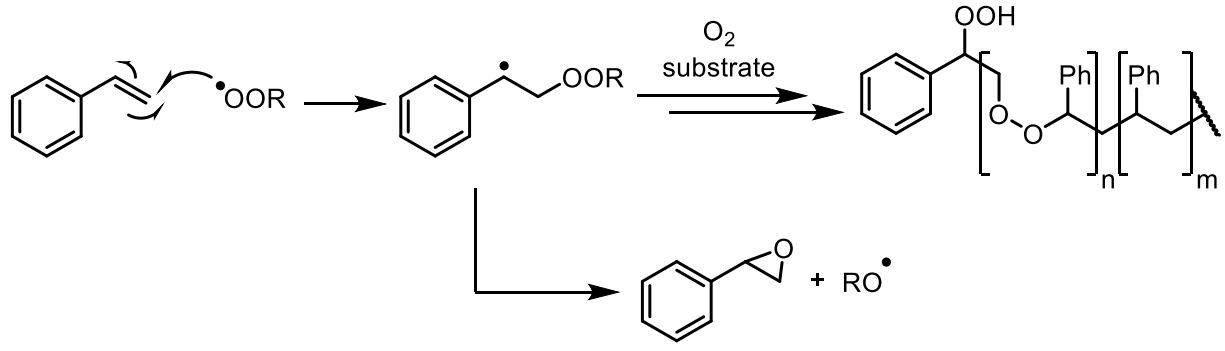

Scheme 1.2. Primary reaction of a peroxyl radical with styrene and formation of oxygen-substrate co-polymers in the autoxidation of styrene.

1.1.3. Termination

Termination reactions occur between two substrate-derived radicals and give rise to non-radical products thereby removing the radicals from the overall reaction (Eqs 1.7-1.9).[17] While termination can occur between any substrate derived radical shown below, the rapid reaction between alkyl radicals and oxygen effectively reduces the pool of alkyl radicals such that the recombination of two peroxyl radicals becomes the predominant termination pathway.

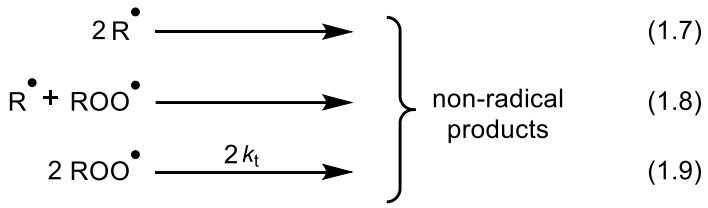

The combination of two peroxyl radicals leads to a largely unstable tetroxide intermediate that rapidly fragments through a mechanism first suggested by Russell.[18] Initially described for tertiary peroxyls, the transient tetroxide fragments asymmetrically to generate an alkoxyl radical and a trioxyl species that also fragments within the solvent cage to liberate triplet oxygen and a second alkoxyl. With no readily abstractable hydrogen atoms, the two nascent alkoxyls undergo in-cage recombination to furnish the dialkylperoxide.[17] The rate of termination is highly dependent on the structure of the peroxyl radical.[19] Recent computational studies by Coote provide evidence that a similar mechanism operates for primary and secondary peroxyls except that the nascent alkoxyls can disproportionate to afford a ketone, triplet oxygen and an alcohol.[20]

Tertiary peroxyls exhibit markedly lower rate constants of termination compared to their structurally analogous secondary and primary counterparts. This is most clearly shown in the reduction of methyl group substitution at the benzylic position in a peroxyl radical termination series comprised of cumene ($k_t = 2.3 \times 10^4$ $M^{-1}s^{-1}$), ethylbenzene ($k_t = 2.0 \times 10^7$ $M^{-1}s^{-1}$) and toluene ($k_t = 1.5 \times 10^8$ $M^{-1}s^{-1}$).[13,21] In the instance of tertiary peroxyls it is suggested that the lack of an abstractable alpha-hydrogen atom increases the likelihood that the peroxyls will escape the solvent cage further propagating the chain by reacting with substrate rather than terminating through recombination (Scheme 1.3). [20]

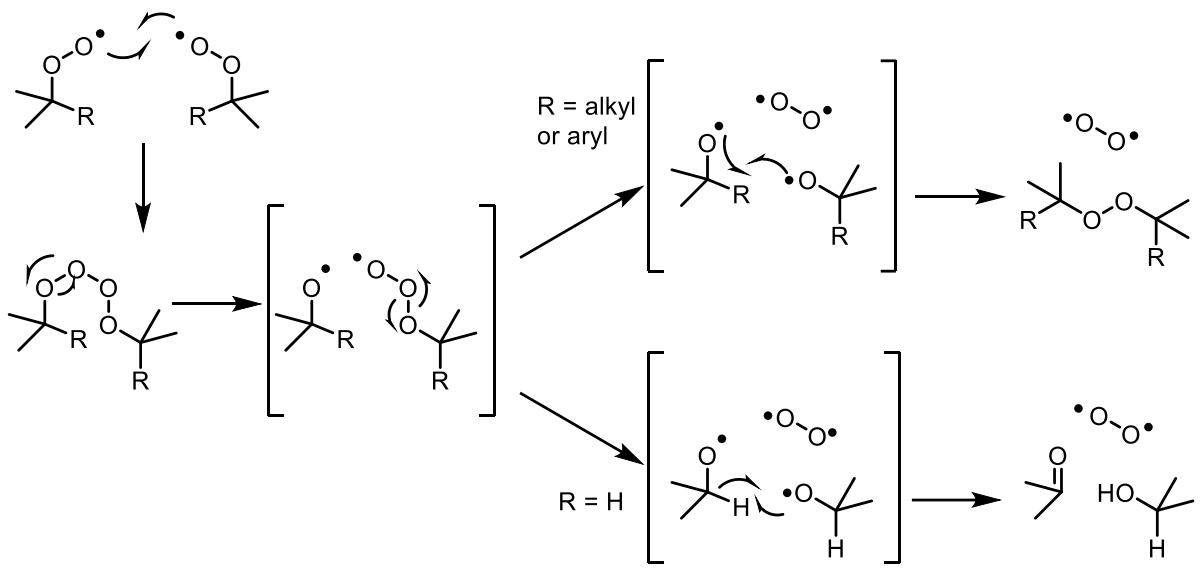

Scheme 1.3. Proposed mechanisms for Russell termination of two substrate-derived peroxyl radicals.

Overall, the kinetics of an uninhibited autoxidation with a constant R_i (assuming no autocatalysis), is described by the following equation. (Eq 1.10).[2]

$$\frac{\delta[\mathrm{ROOH}]}{\delta t} = \frac{-\delta[\mathrm{O_2}]}{\delta t} = \frac{k_p[\mathrm{RH}]\sqrt{R_i}}{\sqrt{2k_t}} \qquad (1.10)$$

1.2. Inhibition of Autoxidation

Antioxidants are compounds that remove radical species from an autoxidation via processes distinct from termination reactions. Preventative antioxidants serve to decrease the rate of radical chain initiation; they decompose the produced hydroperoxides or other initiating compounds in the autoxidation system.[1,2] These compounds take the form of nucleophilic two-electron reducing species capable of converting hydroperoxides to their corresponding alcohols. In contrast, radical-trapping antioxidants (RTAs) inhibit autoxidation by trapping the chain-propagating radicals. Primarily, this involves the trapping of substrate-derived peroxyl radicals.[1,2] Under certain conditions (low O_2 concentration), alkyl radicals may be trapped to inhibit propagation, however, the RTAs must be administered in exceedingly high concentrations to kinetically outcompete oxygen addition.[22,23,24,25] As such, the primary parameter used to determine RTA efficacy is the rate at which it can trap peroxyl radicals. [2]

1.2.1. Kinetic Parameters of Autoxidation Inhibition

Inhibited autoxidations initiated at a constant rate generally follow the kinetics described in equation 1.11, when the propagating peroxyl radicals are trapped to yield non-propagating species. [2] As such, the rate constant for the reaction of a peroxyl radical with an RTA, k_{inh}, can be determined from the initial rate of hydroperoxide formation during the inhibited portion of the autoxidation.

$$\frac{\delta[\mathrm{ROOH}]}{\delta t} = \frac{-\delta[\mathrm{O_2}]}{\delta t} = \frac{k_p[\mathrm{RH}]R_i}{nk_{inh}[\mathrm{RTA}]} \qquad (1.11)$$

The other notable parameter used to assess RTA efficacy is the stoichiometric factor, *n*, which accounts for the average number of radicals trapped per molecule of RTA. The stoichiometric number can be derived from equation 1.12, where t_{inh} is the length of time the autoxidation is identified to be inhibited by the RTA.

$$R_i = \frac{n[\mathrm{RTA}]}{t_{inh}} \qquad (1.12)$$

1.2.2. Phenol and Diarylamine Antioxidants

In response to the growing demand for petrochemical preservation, phenolic and diarylaminic compounds were developed and comprise two of the three most commonly used antioxidant motifs in industrial applications.[1,2] Both classes trap peroxyl radicals via a proton-coupled electron transfer (PCET) stemming from the activated O-H or N-H bonds, characterized by an inhibition rate constant of roughly $10^4\ M^{-1}\ s^{-1}$ for both BHT and diphenylamine shown below (Scheme 1.4.).[26,27] Each of these PCET processes align with an Evans-Polanyi relationship such that the bond dissociation enthalpies (BDE) of these reactive bonds and the rate constants of inhibition in their respective inhibition reactions correlate positively as the substituents on the aryl rings vary. This relationship indicates that the weaker bonds in the radical trapping antioxidants are instrumental in faster trapping of peroxyl radicals.

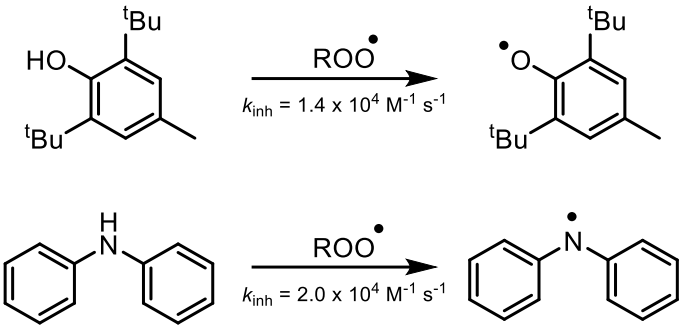

Scheme 1.4. Reactions of BHT and diphenylamine with peroxyl radicals, and their associated rate constants.

In addition, the BDE's also exhibit positive Hammett correlations with respect to σ_p^+ such that the BDE of the reactive bond decreases in the presence of stronger electron donating groups.[28,29] This is attributed to the stabilizing effect an electron donating group would have on the electron-deficient RTA-derived radical produced by the PCET reaction.[30,31,32,33]

Most phenols exhibit a RTA reaction stoichiometry of $n = 2$ under ambient conditions, where the first chain propagating peroxyl radical is trapped via a PCET mechanism and the second trapping occurs via combination of the resultant phenoxyl radical and another peroxyl radical.[34] Increasing the temperatures beyond ambient conditions decreases the phenolic stoichiometric number (e.g. $n = 1.2$ for BHT at 160 °C).[35] Crucially, the RTA-derived radical after the initial peroxyl radical trapping event must remain inert to H-atom abstraction from the substrate or ROOH, otherwise it would serve as a chain transfer agent and help maintain the autoxidation rather than inhibit it. 2,2,5,7,8-Pentamethyl-6-chromanol (PMC), an analogue of α-tocopherol (the most active form of Vitamin E), is known to trap peroxyls through a well-defined mechanism (Scheme 1.5).[36] This is presumably due to increased probability of non-productive side reactions with the phenoxyl radical and/or heightened rates of initiation as the initial dialkylperoxide products also homolyze at these temperatures.[37]

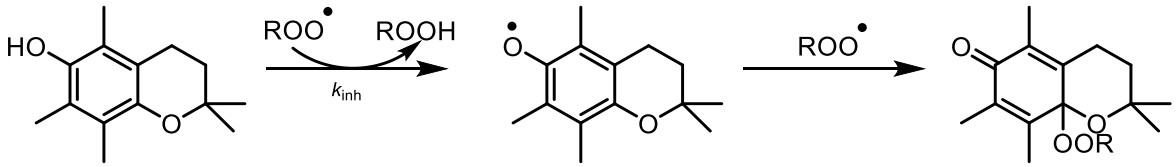

Scheme 1.5. Inhibition mechanism for peroxyl radical trapping by a phenolic RTA (PMC).

Conversely, diarylaminic RTAs feature a stoichiometric number of 2 at ambient temperatures but exhibit higher stoichiometric numbers at elevated temperatures (>120 °C).[36,38,39] This observation suggests that the inhibition reaction affords a product that is also a competent RTA. In the 1990's Korcek *et. al*

observed that an autoxidation of hexadecane inhibited by *bis*(4-octylphenyl)nitroxide at 160 °C yielded the corresponding amine in quantities up to 70%.[40] Moreover, another autoxidation proposed containing a mixture of *O*-alkyl *bis*(4-octylphenyl) alkoxyamines also afforded the parent amine in yields up to 64%. Given that these aminic derivatives appeared to revert to the parent amine, a catalytic cycle was proposed (Scheme 1.6) to depict the apparent regeneration of the initial diarylaminic RTA and its high stochiometric numbers exhibited at elevated temperatures.

Analysis of the proposed intermediates unveils the decomposition of the *N*, *N*-diarylalkoxyamine to regenerate the amine as the rate-determining step. This decomposition is envisioned to proceed either via N-O bond homolysis followed by in-cage disproportionation of the resultant diarylaminyl and alkoxyl radicals[41] At the same temperatures, Haidasz *et* al elucidated that the alkoxyamines formed from diphenylamines and unsaturated substrates or *N*-phenyl-*β*-naphthylamine and saturated substrates diarylamines needed to fragment via a concerted retro-carbonyl-ene reaction in order to observe this catalytic radical trapping activity.[42]

Through employment of recombination of substrate – derived alkyl radicals and nitroxide and the disproportionation, the RTA can be competently turned overusing the substrate itself as a reducing equivalent after the initial peroxyl radical trapping event (Scheme 1.6).

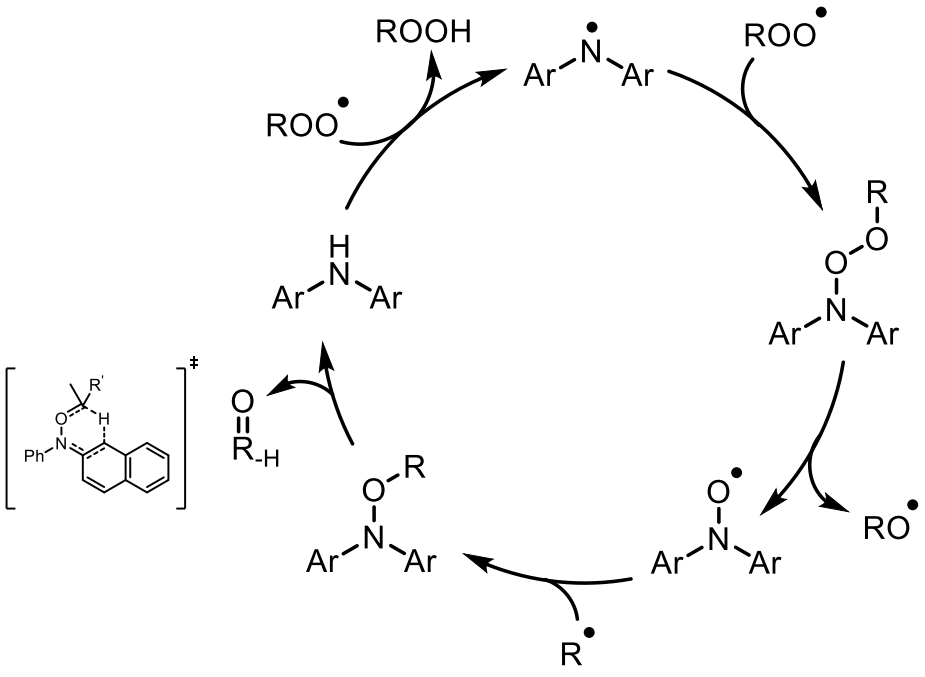

Scheme 1.6. Proposed mechanism for the catalytic activity of diarylamine RTAs (Korcek Cycle).

1.2.3. Hindered Alkyl Amines

A third class of RTA commonly used in industry is hindered alkyl amines, also known as hindered amine light stabilizers. These key additives to plastics and other petroleum-derived products are structurally based upon a 2° or 3° hindered alkyl amine. It is believed that dialkylnitroxides play a pivotal role in the RTA activity of HALS in an analogous, but distinct, manner to the role of diarylnitroxides in the RTA activity of diarylamines. Hindered nitroxides such as 2,2,6,6-tetramethylpiperidine-*N*-oxyl (TEMPO) have been reported to trap peroxyl radicals with very high stoichiometric numbers. TEMPO has been reported to trap peroxyls in paraffin oil at 130 °C with a stoichiometric number of 510. [40] The prevailing dogma on nitroxides is that they are unreactive to peroxyl radicals but very reactive toward alkyl radicals. In reacting with alkyl radicals, the nitroxide is converted to its alkoxyamine derivative which is suggested to decompose in some fashion to recover the nitroxide as the most active form of the RTA. This cycle is generally depicted as the 'Denisov Cycle' shown below (Scheme 1.7).

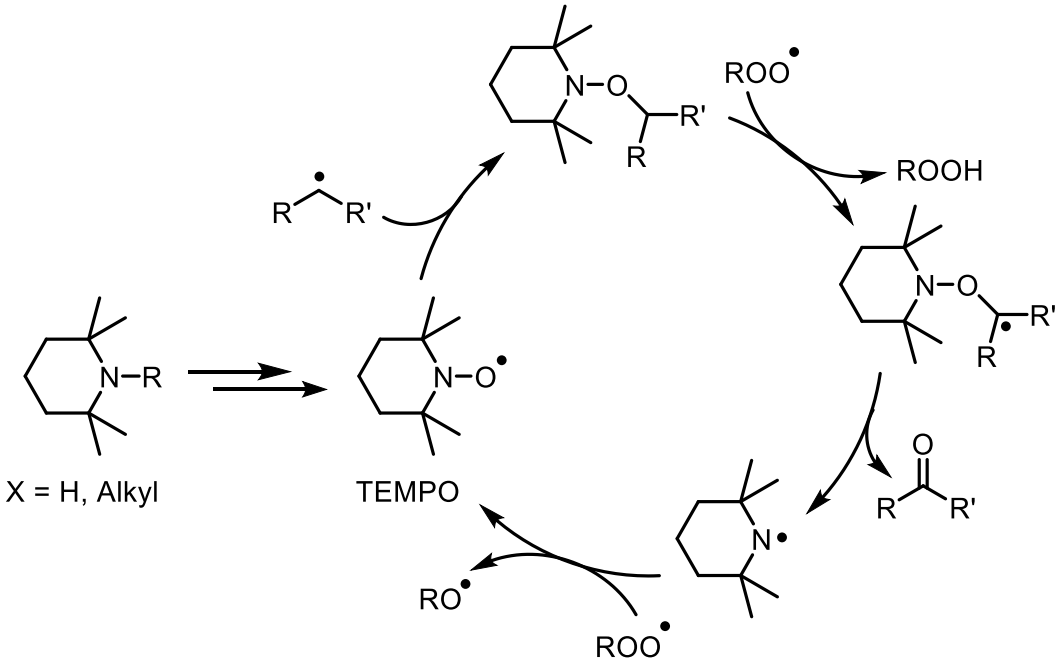

Scheme 1.7. General scheme for the catalytic activity of hindered alkyl amines.

It has been shown previously that nitroxides such as TEMPO do not react with peroxyl radicals but react exceptionally well with alkyl radicals at rates of $k_{inh} \sim 10^8$ M^{-1} s^{-1} at 30 °C. [23,24]As a result, nitroxides are proposed to first trap alkyl radicals to form alkoxyamines such (e.g. TEMPOR). The regeneration of the nitroxide in the cycle has been under extended investigation and was rationalized by the involvement of H-atom abstraction from the alkoxyamine followed by quick β-fragmentation of the

resultant carbon centered radical. Lastly, the newly generated hindered aminyl radical could then be oxidized back to the parent nitroxide (Scheme 1.7).[43]

More recently, our group has shown that acid may play a role in the turnover of nitroxides after their rapid trapping of oxygen centered radicals.[44] Weak acids, such as carboxylic acids, promote nitroxide mediated inhibition for extended time frames which support the high stoichiometric numbers measured previously at 130 °C by Bolsman, Blok and Frins.[40] It was also found that the nitroxides were not being consumed during the reaction despite the large number of apparent peroxyl radicals trapped. It is known that nitroxides can disproportionate to an oxoammonium ion and hydroxylamine in (k_{inh} = 2.4 x 10^6 M^{-1} s^{-1}) under acidic conditions. However, the rate constant of inhibition found for the nitroxide in this system was found to be much larger (k_{inh} 7.0 x 10^8 M^{-1} s^{-1} with 4.3 mM TFA). It was found that the nitroxide in solution was protonated and has been found to be a formal hydrogen atom donor in a PCET reaction. The resultant oxoammonium ion is then reduced back to the nitroxide and exemplifies the elevated capacity for the nitroxide catalytic turnover (Scheme 1.8).

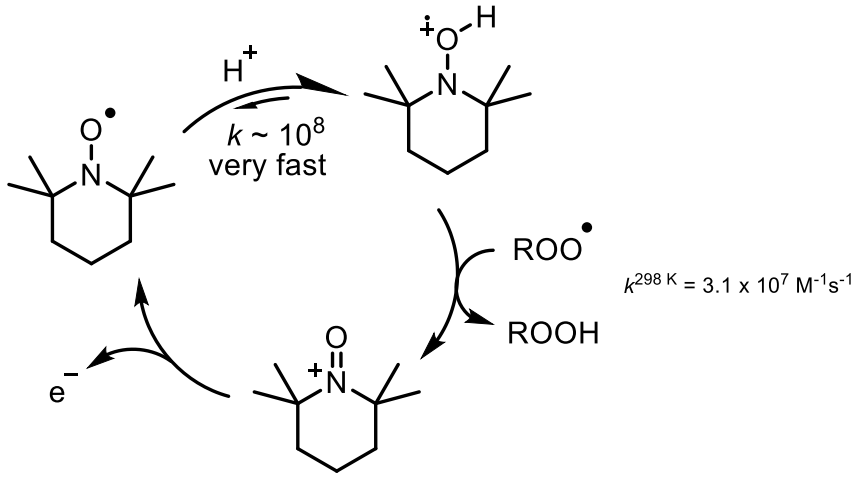

Scheme 1.8. Proposed mechanism for the acid-catalyzed RTA activity of nitroxides.

Similar to diarylamines, hindered alkyl amines and their derivative nitroxides can be regenerated in several distinct pathways based on the autoxidation conditions to exhibit potent radical-trapping efficacy.

1.3. Measuring the Activity of Radical Trapping Antioxidants

The efficacy of radical trapping antioxidants is assessed by their ability to trap chain carrying peroxyl radicals, and in certain instances, alkyl radicals. The mechanisms behind these radical trapping

events have been studied for decades and several techniques have been developed to monitor RTA efficacy. [44,45]

1.3.1. Continuous Visible Light Spectrophotometric Inhibited Co-autoxidations

Recently, a technique was developed to capture all the valuable kinetic data obtained from an inhibited autoxidation with the accessibility and high-throughput nature of a spectrophotometric qualitative antioxidant assays. A spectrophotometric approach that employs BODIPY based signal carriers in an inhibited co-autoxidation was developed by Haidasz et al.[46] The BODIPY probes were conjugated to a 1-phenylbutadiene or styrene unit that when oxidized, the break in conjugation would blue-shift the lambda max of the dye outside the set wavelength of the spectrophotometer. This competing process could then be used as a continuous, indirect reporter of the rate of autoxidation (Scheme 1.9).

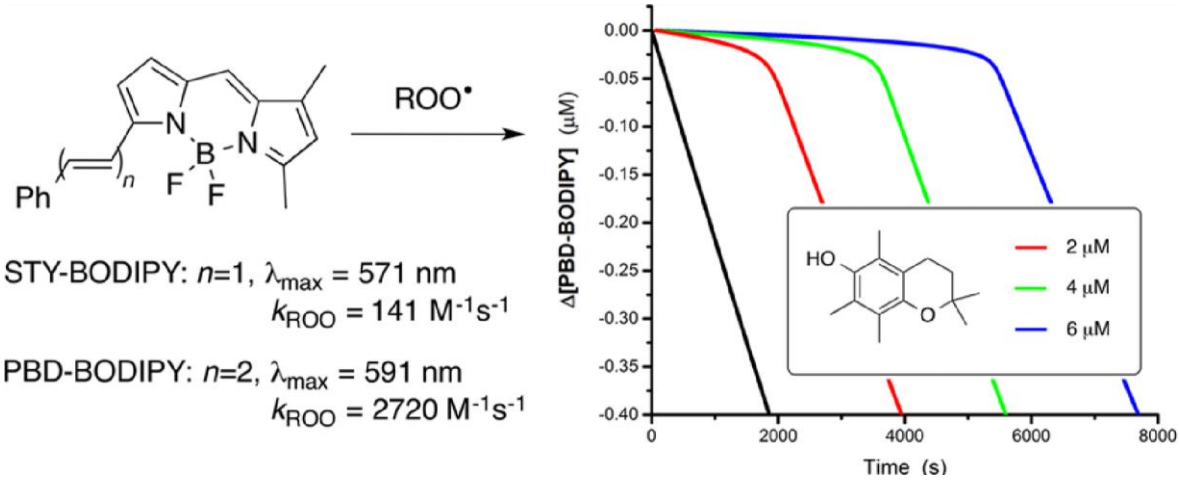

Scheme 1.9. STY-BODIPY and PBD-BODIPY as signal carriers in the autoxidation of organic substrates. Co-autoxidations of styrene (4.3 M) and PBD-BODIPY (10 μM) in PhCl initiated with AIBN (1 mM) at 37 °C (black) inhibited by 2 μM (red) 4 μM (green) and 6 μM (blue) of PMC (blue). Reaction progress was monitored at 591 nm (ε = 139,000 M^{-1} cm^{-1}). Reprinted (adapted) with permission from E. A. Haidasz, A. T. M. Van Kessel and D. A. Pratt, *J. Org. Chem*., 2016, **81**, 737–744. Copyright (2019) American Chemical Society.

The rate constant for propagation of the autoxidation of the BODIPY dye could be obtained by measuring its rate consumption in co-autoxidations with variable concentrations of dye, assuming a steady-state of peroxyl radicals. The rate of BODIPY dye consumption plotted against the dye concentration affords a linear correlation where the slope comprises k_{BODIPY}, R_i and k_t as shown in eq. 1.13. The rate of initiation can be approximated from literature values, if available for the given substrate under the same conditions. Alternatively, and preferably, it can be determined from the inhibition period (t_{inh}) of an autoxidation containing an antioxidant of known stoichiometry and concentration run carried out under the exact autoxidation conditions as the test antioxidant. Typically, 2,2,5,7,8-pentam-

ethylchroman-7-ol (PMC) is used for this purpose because of its well-defined reaction mechanism in the trapping of peroxyl radicals giving rise to stoichiometry of $n = 2$.[46]

$$\frac{-\delta[\text{PBD-BODIPY}]}{\delta t} = \frac{k_{\text{PBD-BODIPY}}[\text{PBD-BODIPY}]R_i}{nk_{inh}[\text{RTA}]} \qquad (1.13)$$

With k_{BODIPY} and R_i known, the inhibition rate constant of the unknown antioxidant can be calculated using equations 1.11 and 1.12 with the term for k_p substituted with k_{BODIPY} as seen in equation 1.13. The kinetic data obtained from this technique generates data which is indistinguishable from those obtained from oxygen consumption methods with the operational benefit of employing a standard UV-Vis spectrophotometer over more specialized differential pressure apparatuses. Moreover, once the key kinetic parameters k_{BODIPY} and R_i for the given co-autoxidation have been established, this technique enables rapid mechanistic studies, such as measurements of kinetic solvent effects and kinetic isotope effects. [46]

1.4. Lipid Peroxidation

1.4.1. Lipid Peroxidation

Unsaturated lipids are oxidatively labile hydrocarbons and serve as perfectly viable substrates for autoxidative systems. Following an initiation event, the lipid derived alkyl radical has oxygen rapidly added to it to form the lipid derived peroxyl which can go on to perform another hydrogen atom transfer and propagate the chain reaction (Scheme 1.10).[47]

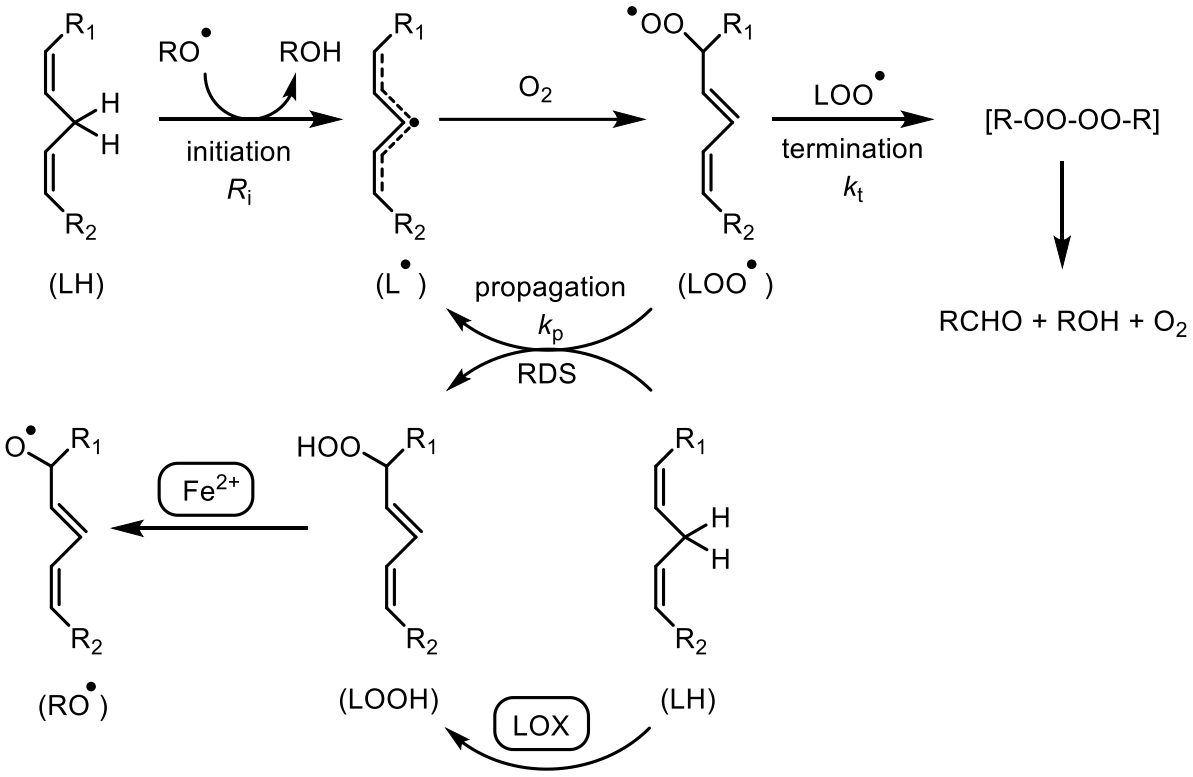

Scheme 1.10. Free radical autoxidation mechanism of lipid substrates both in the presence and absence of an enzyme (LOX).

The rate determining step in this process is the formal hydrogen atom transfer (HAT) from a labile C-H bond on a molecule of substrate to a peroxyl radical. In effect, the strength of the C-H that is broken dictates the rate of oxidation. This is best illustrated in the scheme below where substrate units that can best stabilize the resultant alkyl radical exhibit a higher rate constant of propagation (k_p) over other structurally similar motifs (Scheme 1.11).[48]

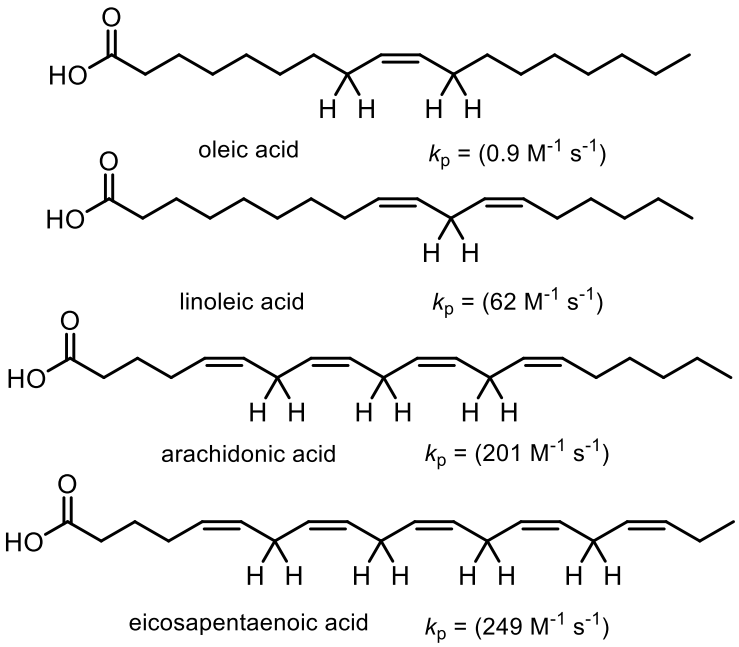

Scheme 1.11. Selected polyunsaturated lipids and their associated rate constants of propagation with peroxyl radicals at 298 K.

As the degree of lipid unsaturation increases from oleic acid to eicosapentaenoic acid, the rate constant of propagation (k_p) also increases in correspondence to higher lability of the allylic hydrogen atom most susceptible to HAT in each lipid molecule. The transition from the k_p of oleic acid at 0.9 M^{-1} s^{-1} to the k_p of linoleic acid at 62 M^{-1} s^{-1} highlights the weakening of the C-H bonds in the allylic position of oleic acid versus the *bis*-allylic C-H bonds in linoleic acid. As more bisallylic units are made available in the higher order polyunsaturated lipids the respective k_p's also increase in magnitude as a result of increasing the number of labile C-H bonds.[48]

In the 1980s, Porter and co-workers elucidated many important features of the mechanism of unsaturated lipid autoxidation.[49,50] They showed that the primary products of radical autoxidation of diene fatty acids were the diene hydroperoxides. Notably, methyl linoleate, the methyl ester of linoleic acid can be oxidized at the *bis*-allylic position at C11, and the nascent pentadienyl radical oxygenated at either of the three separate carbon positions (C9, C11 and C13). Addition of molecular oxygen is reversible with the rates of β-fragmentation of the various isomers determining the distribution of the hydroperoxide products formed in a methyl linoleate autoxidation.[50] The various isomers are depicted below in (Scheme 1.12).

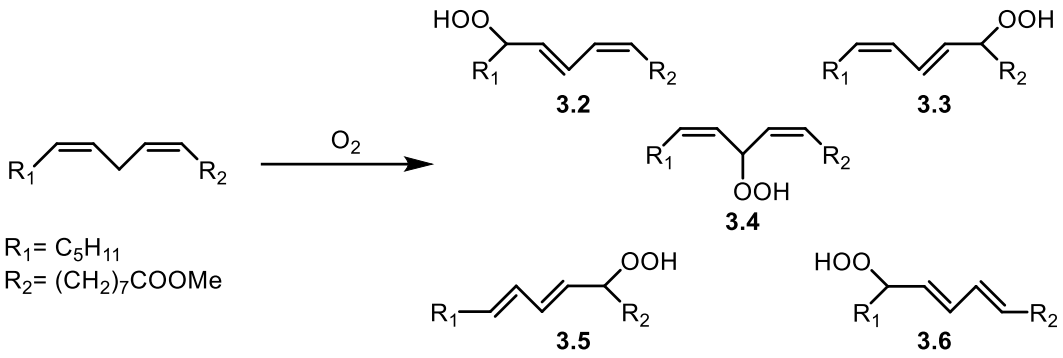

Scheme 1.12. Products of methyl linoleate autoxidation.

In the presence of a hydrogen atom donor, the two *trans, cis* products (**3.2, 3.3**) and the single skipped diene product (**3.4**) dominate the product profile as the kinetic products. In the absence of a good hydrogen atom donor, β-fragmentation predominates, and the product profile skews toward the more stable *trans* products (**3.5, 3.6**). The rate constant of propagation (k_p), the rates of β-fragmentation (k_β) and the rate constant of inhibition (k_{inh}) of a given antioxidant are all contributors to an autoxidation. The relative rates of these processes ultimately determine the final product distribution (Scheme 1.15).

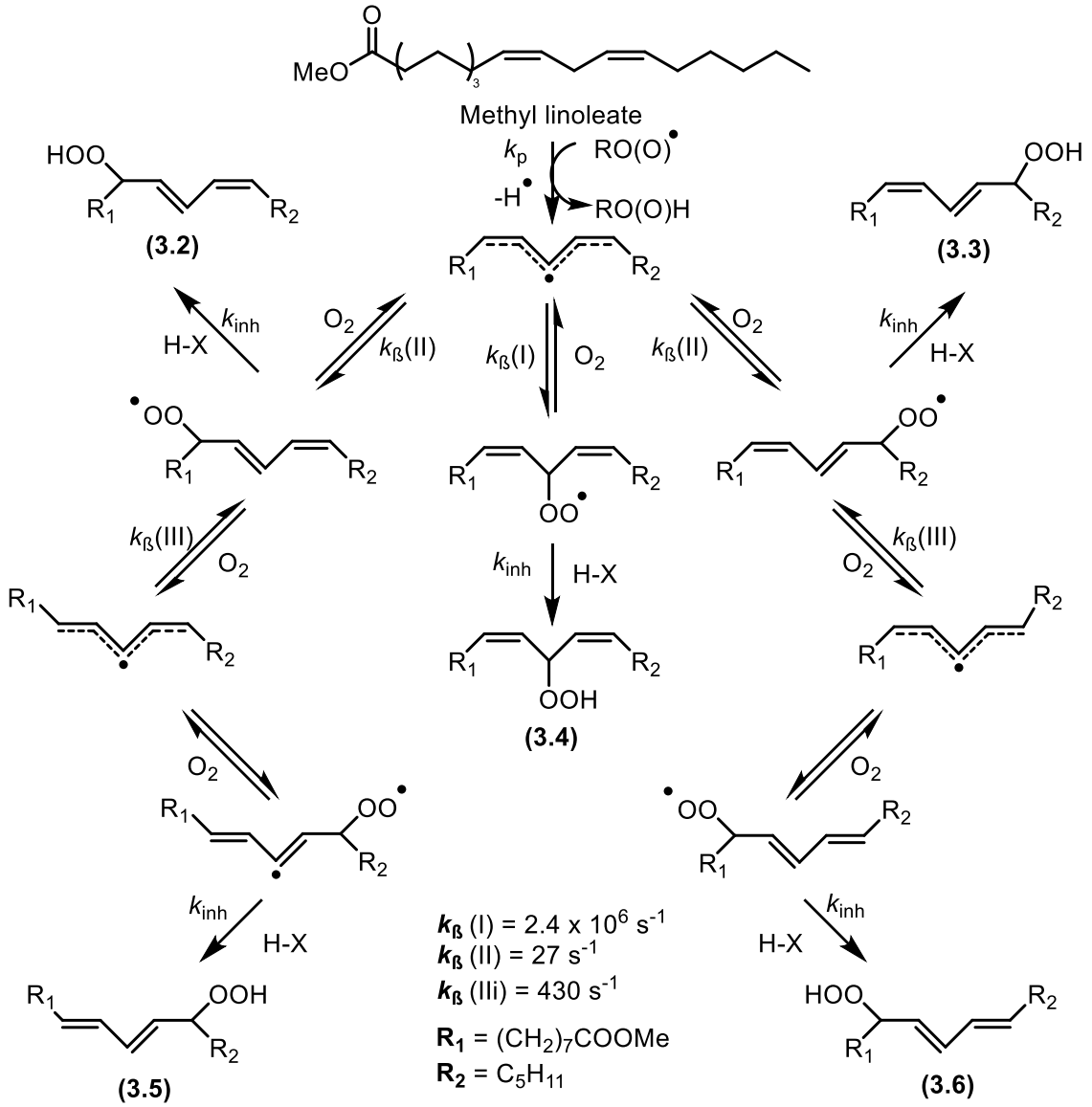

Scheme 1.13. Mechanism and distribution of methyl linoleate autoxidation.

Methyl linoleate is the simplest polyunsaturated fatty acid (PUFA) susceptible to autoxidation giving rise to five major products. In contrast, arachidonic acid with its four successive skipped diene units gives rise to a much more complex product distribution of hydroperoxyeicosatetraenoic acids (HPETEs) and other products resulting from intermolecular reactions of the initially produced peroxyl radicals. [51,52]

These HPETE products have been implicated in a number of pathophysiologies when generated *in vivo* due to their disruption of cell membranes and their propensity to breakdown into electrophilic

species such as acrolein (AC), 4-hydroxy-2-noneal (HNE) and malondialdehyde (MDA), all known for their cytotoxicity (Scheme 1.14). These activated aldehydic compounds pose a great risk to cells due to their propensity to form adducts with DNA and nucleophilic proteins, leading to improper DNA replication, DNA mutations and protein misfolding, all of which can trigger the onset of degenerative diseases. The products of these lipid oxidation events are implicated in a wide array of pathophysiological states. These implications have spurred on the pursuit to determine the mechanisms by which lipid peroxidation occurs and what preventative measures can be taken to slow its progression.[53,54,55]

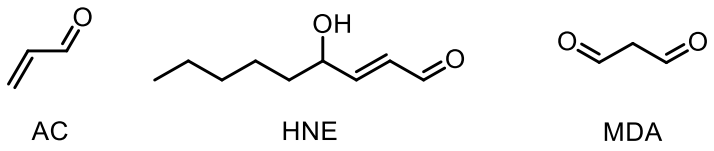

Scheme 1.14. Metabolic end-products of lipid hydroperoxides.

1.4.2. Enzyme-catalyzed Lipid Peroxidation

Lipid peroxidation can also be achieved by enzymatic processes fully independent of autoxidation. Two enzyme classes will be discussed: lipoxygenases (LOXs) and cyclooxygenases (COXs). COXs, also known as prostaglandin endoperoxide synthases, and LOXs, use PUFAs such as arachidonic acid and linoleic acid as substrates and catalyze the production of myriad lipid-derived signaling molecules. COX enzymes catalyze the formation of prostanoids (prostaglandins, prostacyclins and thromboxanes) while LOX enzymes catalyze the formation of HPETEs and leukotrienes.[56] These lipid-derived products are mediators for a bevy of physiological responses including inflammation, immunity, pain, fever, homeostatic regulation and renal functionality.[56,57] Leukotrienes and HPETEs are principally involved in the pathophysiology of asthma and allergic responses. Since lipoxygenases facilitate the production of these inflammatory mediators, methods that inhibit these enzymes are important respiratory disease treatment.[57]

1.4.3. Lipoxygenases

Lipoxygenases are a class of non-heme iron containing enzymes that catalyze the peroxidation of PUFAs to generate their fatty acid hydroperoxide derivatives.[57,58,59,60] The native enzyme is activated by low levels of endogenous lipid peroxides which first oxidize the inactive ferrous Fe^{2+} form to the active ferric Fe^{3+} form via proton-coupled electron transfer (PCET) mechanism. The active ferric form mediates a tightly controlled stereoselective hydrogen atom abstraction at the central C-3 position of a 1,4-cis, cis pentadiene (*bis*-allyl) unit to afford a delocalized pentadienyl radical intermediate. The enzyme channels molecular oxygen to the pentadienyl radical and regioselectively dioxygenates the substrate antarafacial

to the abstracted hydrogen atom to afford a peroxyl radical. The peroxyl radical is formally reduced by the ferrous Fe(II)-H_2O centre to yield the fatty acid hydroperoxide and restore the Fe(III)-OH active form. The reduction step is purportedly achieved via a tunneling-enhanced PCET mechanism as well, whereby the electron tunnels to the ferric iron while the proton transfers simultaneously to the hydroxide ligand (Scheme 1.15). [57,58,59,60]

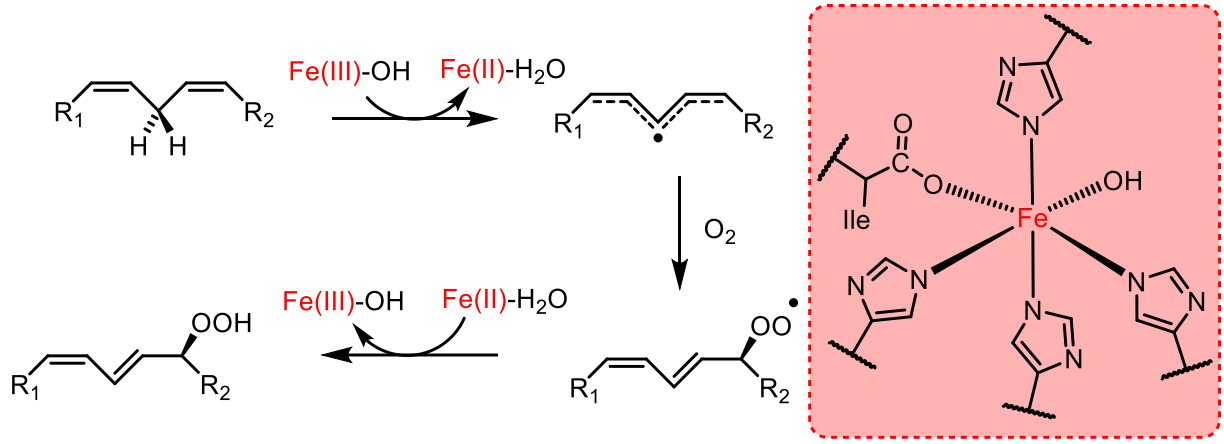

Scheme 1.15. Proposed mechanism for the initial reaction catalyzed by lipoxygenases with coordination sphere of the active site iron centre. Depiction of 5-LOX active site chiral environment shown in red.

Three-dimensional structures of native lipoxygenases have proven incredibly difficult to obtain due to the enzyme's instability at a wide range of conditions. Lipoxygenases are found ubiquitously in biological organisms including plants and mammals – and more recently in coral, mosses, fungi and various bacteria strains.[59] Plants have three isoforms of lipoxygenase named LOX-1, LOX-2 and LOX-3.[61] The native substrate for plant lipoxygenases is linoleic acid which notably contains only one 1,4-*cis*, *cis* pentadiene unit that is susceptible to oxidation. Presently, six isoforms of mammalian lipoxygenases have been identified: 5-LOX, 15-LOX-1, 15-LOX-2, 12*S*-LOX, Platelet Type 12-LOX and eLOX-3. The 5-LOX, 12*S*-LOX and 15-LOX-1 isoforms have been linked to various human pathophysiological conditions. [57] The native substrate for mammalian lipoxygenases is the considerably more complex arachidonic acid, which contains three 1,4-*cis*, *cis* pentadiene units.

LOXs are monomeric proteins that range from 95-100 kDa in size with two domains: an N-terminal barrel domain proximally involved to the membrane binding site and an α-helical domain. [57,58,59,60] There is a single iron atom octahedrally coordinated within the active site by a water-hydroxide ligand and 5 basic amino acid side chain units. Plants LOXs employ three histidines, one asparagine and the free carboxylate of the C-terminal isoleucine in the iron coordination site. In contrast, mammalian LOXs employ four histidines and a similar recruitment of the carboxylate of the C-terminal isoleucine.[59]

The diverse product output of LOX enzymes is made possible by changes in substrate binding. The binding pocket's width and depth tightly control the substrate's entry and positioning of the central carbon of the *bis*-allylic unit in accordance to the coordinated iron centre. Steric shielding and the oxygen channeling event are also dictated by the enzyme's conformation.[59]

1.4.3.1. 5-Lipoxygenase

Human 5-lipoxygenase (5-LOX) catalyzes the peroxidation of arachidonic acid at the 5-position to afford 5-HPETE, a precursor to leukotrienes. Leukotriene derivatives participate in allergenic immune responses and contribute significantly to inflammation in lung bronchioles resulting in airway constriction, asthma and bronchitis.[51,52] 5-LOX containing cell types are abundant, being found in dendritic cells, B-lymphocytes, monocytes, mast cells and granulocytes (Scheme 1.16).[57]

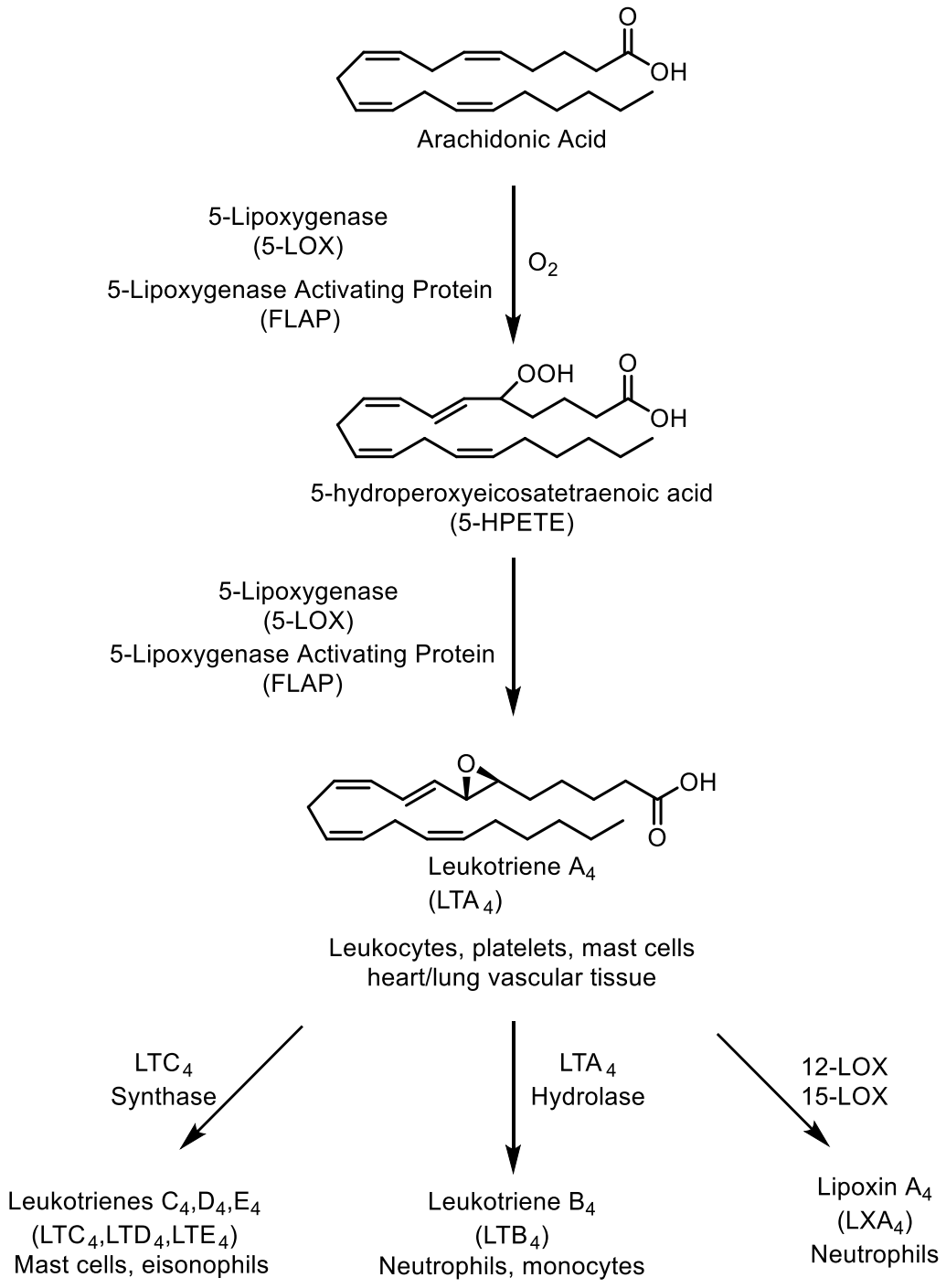

Scheme 1.16. Enzymatic arachidonic acid peroxidation via the lipoxygenase pathway to afford various inflammation mediating metabolites in their respective cell types.

Due to its pathophysiological proclivity, complete tertiary structure elucidation of native 5-LOX would be valuable for effective structure-activity relationships within the active site and pharmaceutical

compounds aimed at treating asthma and bronchitis. The complete tertiary structure of active 5-LOX has proven elusive due to the membrane bound enzymes marked instability.[62] The catalytic iron centre inactivates in the presence of oxygen and renders analysis extremely difficult.

The three dimensional structure of 5-LOX has been pursued for decades and Newcomer *et al* were the first to report on a stably engineered human 5-LOX based on the known structures of rabbit 15-LOX and coral 8-LOX.[62] Two key areas were identified to human 5-LOX's enhanced instability compared to the other LOX variants including rabbit 8-LOX, coral 8-LOX and indeed human 8-LOX and human 15-LOX.[63,64] In addition to the iron centre's oxidizability, leucine 655 in most LOX homologies is replaced by a lysine in 5-LOX and this amino acid variant causes the iron centre to orient itself differently within the active site. Also, common salt bridges that are used to affix the peptide chain to the membrane are absent in 5-LOX that are present in other LOX structures including 8-LOX and 15-LOX.[62] The replaced lysine unit was inspired by sequences in coral 8-LOX, integrated with the exchange of two cysteine residues for alanines allowed for increased stability of the engineered enzyme. The activity of the enzyme construct was monitored through detection of the initial 5S-HPETE product and downstream leukotriene A_4 product via high performance liquid chromatography (HPLC).[62,63]

Analysis of the substrate-enzyme co-crystal structure brought forth additional evidence that the iron centre is coordinated to three histidine residues analogous to other lipoxygenases. However, the engineered human 5-LOX showcased a peculiar substrate cavity where two aromatic amino acid residues (Phe177 and Tyr181) appeared to have sealed off substrate entry via a cork-shaped arrangement.[62] A significant question remains on how the native substrate arachidonic acid docks into the substrate cavity given the blockage caused by the aromatic residues, either the cork structure needs to unwind when the enzyme is active, or the other end of the cavity needs to undergo a conformational change.

1.4.3.2. 15*S*-Lipoxygenase

In contrast to the implications of 5-LOX in respiratory pathophysiology, 15-LOX products have been linked to cardiovascular disease particularly in their promotion of vascular permeability and coronary artery restriction.[64,65] Of the six types of human lipoxygenases, two are 15-LOXs that dioxygenate arachidonic acid at the C_{15} position. Reticulocyte 15*S*-LOX-1 is typically found in reticulocytes and eosinophils while epithelial 15*S*-LOX-2 is found in epithelial cells.[64,66] 15*S*-LOX-1 facilitates the production of lymph node metastasis promoters and signals the recruitment of breast cancer cells.[67] While there is a 40% amino acid sequence match between the two 15*S*-LOX isoforms, the structural changes that may dictate the difference in product distribution and dioxygenation selectivity at the C -15 position remain unclear.[64,66]

1.4.3.3. 12-Lipoxygenase

Like 15-LOX, there are two isoforms of 12-LOX, but they differ in the stereochemistry of the HPETEs products that are produced: 12*S*-LOX makes 12*S*-HPETE and 12*R*-LOX makes 12*R*-HPETE. These 12-LOXs have been linked to atherogenesis derived from oxidized LDL.[68,69,70] Depending on the cell type, epidermal, platelet or leukocyte, either or both isoforms can be found.12-LOX initially dioxygenates arachidonic acid at the C-12 position to generate the 12-hydroperoxy product (12-HPETE).[68] Prostate cancer appears to be linked to platelet-type 12*S*-lipoxygenase activity and skin barrier junctions appear to be influenced by 12*R*-lipoxygenases activity.[71] Predictions on the active site of 12-LOX has led to speculation that the active site is roughly 6% larger than that found in 15-LOX and could contribute to the difference in specificity.[68,69]

1.4.3.4. Epidermal lipoxygenase-3

Epidermal lipoxygenase-3 (eLOX3) is the sixth human isoform of lipoxygenases. This isoform is involved in epithelial barrier formations but does not feature the typical lipoxygenase behaviour of fatty acid deoxygenation in any capacity.[72] eLOX3 takes its place in the lipoxygenase family due to its peptide sequence sharing 58% similarity to 12*R*-LOX. Its enzymatic activity is centered around the isomerization of a fatty acid derived hydroperoxide to epoxy-alcohols and ketones.[72,73] The link between mode of action and physiological response is still not fully understood (Scheme 1.17).

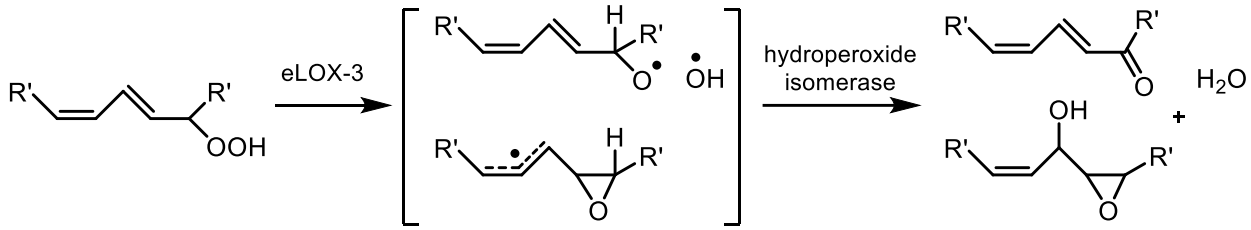

Scheme 1.17. eLOX-3 mediated conversion of lipid hydroperoxides to epoxy-alcohols and ketones.

1.4.4. Lipoxygenase Inhibition

5-LOX has been a target for drug development for several decades. Its enzymatic function lies at the front of a critical inflammation cascade in the leukotriene pathway and contributes heavily in chronic respiratory pathophysiology. The goal to address these ailments is of global concern as mitigating leukotriene production is essential to alleviating the production of inflammatory mediators. Research in leukotriene product inhibition has led to the development of montelukast, zafirlukast and pranlukast, all three target downstream leukotriene receptors with varying degrees of efficacy (Scheme 1.18).[74]

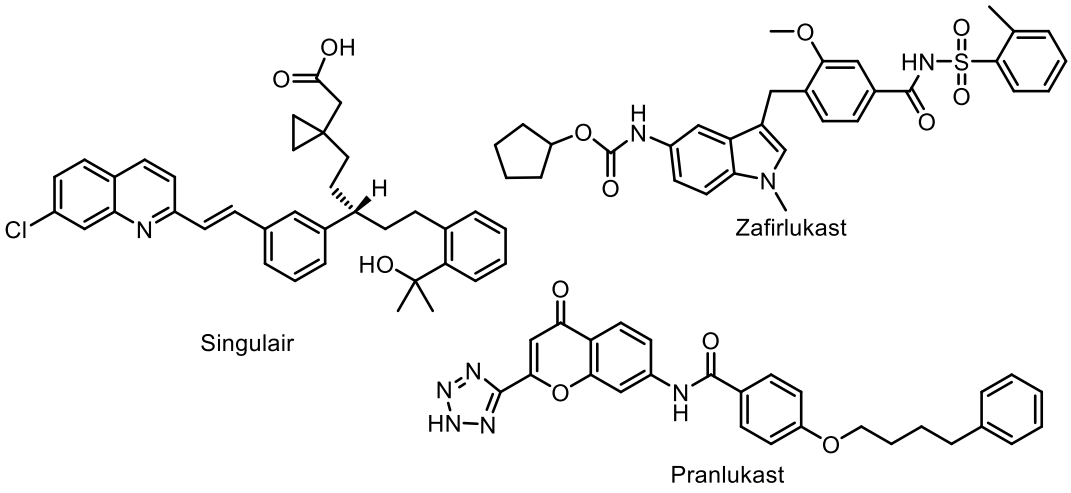

Scheme 1.18. Cysteinyl-leukotriene type 1 receptors.

A more elegant solution would be to target 5-LOX directly and shutdown the entire cascade. The few drugs on the market aimed at this goal suffer from toxicity issues. To date Zileuton is the only 5-LOX specific inhibitor believed to function by binding the catalytic iron core of the active site with its hydroxamic acid warhead. However, the key hydroxamic acid also carries several side effects due to oxidative lability - namely poor bioavailability and a short half-life.[74,75]

CAY10649 is a newer thiazolinone compound discovered through virtual screening that has also demonstrated direct inhibition of 5-LOX (Scheme 1.19).[76]

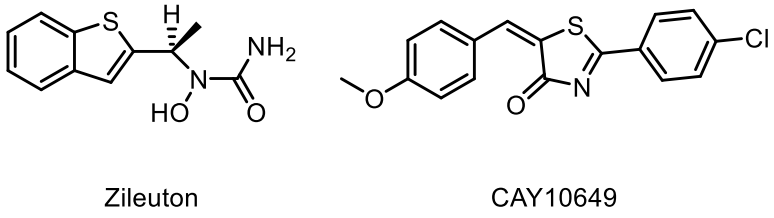

Scheme 1.19. Isoform-specific 5-LOX inhibitors.

1.5. Ferroptosis

Lipid peroxidation has been implicated in numerous forms of human pathophysiology over decades. However, in 2012, a unique mode of cell death dubbed 'ferroptosis' was linked directly to lipid peroxidation.[77] Ferroptosis is a non-apoptotic form of cell death associated with an unregulated build-up of lipid hydroperoxides. Ferroptosis was initially characterized by glutathione depletion by system x_c^- inhibitor erastin resulting in caspase-independent cell death.[78] Glutathione is the reducing co-substrate for glutathione peroxidase 4 (GPX4), which is the sole enzyme capably of detoxifying phospholipid hydroperoxides (LOOH) by reduction to their corresponding phospholipid alcohols (LOH). Ferroptosis can also be induced by GPX4 inhibition by RSL3, or induced deletion of the GPX4 encoding gene.[79,80] In effect, mechanisms that involve glutathione depletion or GPX4 inhibition result in a buildup of lipid hydroperoxides that can sensitize the cell to ferroptosis.[77,81]

Lipid hydroperoxide concentrations can increase via autoxidation of polyunsaturated lipids or enzyme-mediated peroxidation of lipids.[82] This led to the implication that lipoxygenase inhibition could contribute to ferroptosis resistance in cells and was supported by the evidence that known LOX inhibitors were shown to be cytoprotective in ferroptotic assays.[83,84,85] It has been shown that cells can exhibit resistance to ferroptosis when LOX activity is inactivated by small interfering RNAs.[84] However, only pharmacological inhibitors of LOX were shown to rescue *gpx4*$^{-/-}$ knockout mice.[80] As such, it was unclear how lipoxygenases were critical to ferroptosis other than their inhibition appeared to confer ferroptoptic resistance.[86]

Using high-throughput screening, ferrostatin-1 (Fer-1) and liproxstatin-1 (Lip-1) were identified as potent ferroptosis inhibitors.[85,87] Fer-1 and Lip-1 compared remarkably well to the LOX inhibitors such as the 5-LOX inhibitor zileuton and the general LOX inhibitor NDGA. Notably, Fer-1 and Lip-1 are not potent inhibitors of LOX but are potent radical-trapping antioxidants. Given the select potencies of Fer-1 and Lip-1 as potent RTAs, but poor LOX inhibitors, it appears that ferroptotic resistance is derived from global lipid hydroperoxide reduction rather than directly inhibiting lipoxygenases.[86] Thus, lipoxygenase inhibition merely contributes to a reduction in the overall pool of lipid hydroperoxides available. Moreover, other isoform-specific LOX inhibitors were shown to be poorly correlated to ferroptosis inhibition based on lipoxygenase inhibitory performance but rather these inhibitors were shown to be competent RTAs.[86] Correlations of RTA efficacy and ferroptosis inhibition of these purported lipoxygenase inhibitors much more clearly distinguishes which compounds are effective as ferroptosis inhibitors. A compiled scheme of the various known inducers and inhibitors of ferroptosis are shown in Scheme 1.20.

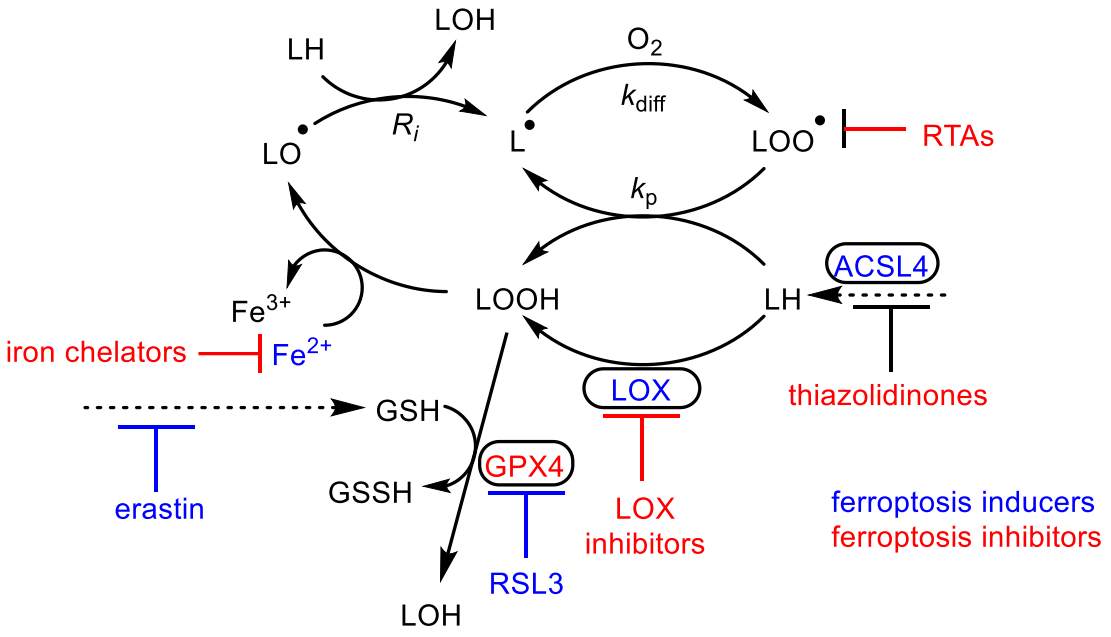

Scheme 1.20. Demonstrative schema of small molecule and enzymatic ferroptosis inducers and inhibitors of (phospho)lipid hydroperoxides (LH). Reprinted and adapted with permission from (R. Shah, M. S. Shchepinov and D. A. Pratt, *ACS Cent. Sci*., 2018, **4**, 387–396.]. Copyright [2018] American Chemical Society

Thereby, a mechanism that can contribute to the overall pool of lipid hydroperoxides can also sensitize a cell towards ferroptosis if it overwhelms the capacity for GPX4 to reduce the present pool of lipid hydroperoxides.

Recent results by Pratt and Stockwell also support the efficacy in modulating the *bis*-allylic methylene unit in arachidonic acid and linoleic acid.[88,89] Previous syntheses have been developed where all three *bis*-allylic units of arachidonic acid were systematically functionalized with deuterium atoms.[90] These deuterated analogues were developed to see if they had an observable kinetic isotope effect in enzymatic and non-enzymatic lipid hydroperoxide production. This was a tenable hypothesis given that the enzymes are known to react via a hydrogen atom abstraction event that would most likely be involved in the rate limiting step. HEK293 cell lines were transfected to overexpress each of the human lipoxygenase isoforms implicated in disease: 5-LOX, 12-LOX and 15-LOX-1 rendering them sensitized to ferroptosis. When these transfected cell lines were supplemented with 7,7,10,10,13,13-d6-arachidonic acid and ferroptosis was induced using GPX4 inhibitor RSL3, it was observed that a significant population of cells were protected from ferroptotic cell death. This only held true when all three *bis*-allylic sites (6 hydrogen atoms total) were fully exchanged from hydrogen to deuterium. Cells

supplemented with deuterated arachidonic acid analogues where only one or two of the three methylene sites were functionalized showed minimal ferroptosis resistance in this regard. Curiously, additional experiments showed that only 20% of the total lipid pool in the cells had to be supplemented with 7,7,10,10,13,13-d6-arachidonic acid in order to remain ferroptotically resistant.

Dixon and co-workers revealed that monounsaturated fatty acids (MUFAs) such as oleic acid also appear to show an inhibitory effect on ferroptosis in cells where GPX4 has been suppressed.[89] The authors noted that based on the observations that oleic acid did not reactivate the expression of GPX4 or decrease the expression of ACSL4, a ferroptosis inducer, that it must inhibit ferroptosis ether downstream or in parallel to GPX4 activity. MUFAs were also shown to block plasma membrane lipid hydroperoxide accumulation by the supplanting of more reactive PUFAs from being incorporated into phospholipids.

1.6. Research Objectives

Korcek and co-workers put forth the notion that diarylamines could be regenerated in high temperature inhibited autoxidations in a cyclic process that featured diarylamines as a key intermediate. In a similar context, Denisov and co-workers also invoked the regeneration of hindered alkyl nitroxides in elevated temperature autoxidations after the parent hindered alkyl amine had been oxidized. Recently, it was observed that hindered alkyl nitroxides and diarylnitroxides displayed stoichiometric numbers and rate constants of inhibition that significantly exceeded those of their parent hindered alkyl amines and diarylamines in styrene/PBD-BODIPY and hexadecane/PBD-BODIPY co-autoxidations while the opposite observation was made in cumene/STY-BODIPY autoxidations. This observation was very surprising considering the prevailing dogma that nitroxides did not react directly with peroxyl radicals. It was unclear how a purportedly inert RTA could seemingly outperform its parent compound through what must be a distinct and overlooked mechanistic pathway. A few hypotheses were developed based on the peculiar observations as follows:

Given that nitroxides alone do not react with peroxyl radicals in hydrocarbon-based systems, they must be converted into a compound that is a highly competent RTA. The foregoing preliminary investigations suggest that this reactivity is particularly important in *olefinic* substrates, suggesting that the olefinic substrate is somehow involved. Lastly, the reactive RTA must be sufficiently regenerated *in-situ* given the stoichiometric numbers measured reaching quantities well above those of the parent amines. Thus, the objectives of this project are:

- Uncover the material in the autoxidation of an autoxidizable unsaturated substrate that leads to the regeneration of nitroxides *in situ* using continuous visible light spectrophotometric inhibited co-autoxidations
- Probe the effect that rates of initiation have on this phenomenon given that most previous studies were conducted at relatively high rates of initiation
- Untangle the contributing components that both the Korcek and Denisov cycles apparently seem to exhibit in this underlying mechanism

Lipid peroxidation has been linked and associated with myriad pathophysiological conditions including asthma, atherosclerosis, dementias and most recently, ferroptosis. Lipoxygenase enzymes are known to metabolize polyunsaturated fatty acids with their initial products being the lipid hydroperoxide derivatives. These lipid hydroperoxide intermediates are the precursor to a host of secondary metabolites

that signal the onset of various degenerative diseases. Moreover, the hallmark of ferroptosis is the unregulated build-up of hydroperoxide species. It would be useful to probe to what extent lipoxygenase-mediated lipid hydroperoxide production has as a contributor toward ferroptosis.

Current purported lipoxygenase inhibitors often target downstream enzymatic processes with mediocre efficiency and/or high toxicity. In order to improve the efficacy of future lipoxygenase inhibitor generations, further developments must be made in lipoxygenase mechanism elucidation and ultimately, active site substrate-enzyme co-crystallization and modelling. Cyclooxygenase mechanism elucidation was greatly aided through co-crystallization of the native enzyme with their native arachidonic acid substrate. Similar attempts with lipoxygenases and their native linoleic acid substrates have been unsuccessful to date. A strategy involving synthetic substrate analogues toward active site substrate-enzyme co-crystallization is to be evaluated for lipoxygenases herein.

The objectives of this project are:

- Synthesize an unnatural substrate analogue of lipoxygenases to facilitate protein crystallization and elucidate native active site-substrate binding interactions
- Explore methods to exchange labile hydrogen atoms with fluorine atoms that would render the active moiety on the substrate analogue inert to lipoxygenase metabolism
- Examine to what extent selective inhibition of lipoxygenases using redox inactive inhibitors has on the onset of ferroptosis by limiting the pool of lipoxygenase-mediated hydroperoxides

1.7. References

1 K. U. Ingold, *Chem. Rev.*, 1961, **61**, 563–589.
2 K. U. Ingold and D. A. Pratt, *Chem. Rev.*, 2014, **114**, 9022–9046.
3 R. K. Jensen, S. Korcek, L. R. Mahoney and M. Zinbo, *J. Am. Chem. Soc.*, 1979, **101**, 7574–7584.
4 W. A. Pryor and N. A. Porter, *Free Radic. Biol. Med.*, 1990, **8**, 541–543.
5 C. Schneider, K. A. Tallman, N. A. Porter and A. R. Brash, *J. Biol. Chem.*, 2001, **276**, 20831–20838.
6 H. R. Cooper and H. W. Melville, *J. Chem. Soc.*, 1951, 1984–1993.
7 H. R. Cooper and H. W. Melville, *J. Chem. Soc.*, 1951, 1994–2002.
8 D. V Avila, C. E. Brown, K. U. Ingold and J. Lusztyk, *J. Am. Chem. Soc.*, 1993, **115**, 466–470.
9 R. K. Jensen, S. Korcek, M. Zinbo and M. D. Johnson, *Int. J. Chem. Kinet.*, 1990, **22**, 1095–1107.
10 H. J. H. Fenton, *J. Chem. Soc. Trans.*, 1894, **65**, 899–910.
11 B. Maillard, K. U. Ingold and J. C. Scaiano, *J. Am. Chem. Soc.*, 1983, **105**, 5095–5099.
12 R. K. Jensen, S. Korcek and M. Zinbo, *Int. J. Chem. Kinet.*, 1994, **26**, 673–680.
13 J. A. Howard and K. U. Ingold, *Can. J. Chem.*, 1967, **45**, 793–802.
14 J. A. Howard and K. U. Ingold, *Can. J. Chem.*, 1969, **47**, 3809–3815.
15 F. R. Mayo, A. A. Miller and G. A. Russell, *J. Am. Chem. Soc.*, 1958, **80**, 2500–2507.
16 J. A. Howard and K. U. Ingold, *Can. J. Chem.*, 1962, **40**, 1851–1864.
17 R. Lee, G. Gryn'ova, K. U. Ingold and M. L. Coote, *Phys. Chem. Chem. Phys.*, 2016, **18**, 23673–23679.
18 J. A. Howard, K. Adamic and K. U. Ingold, *Can. J. Chem.*, 1969, **47**, 3793–3795.
19 G. A. Russell, *J. Am. Chem. Soc.*, 1957, **79**, 3871–3877.
20 J. A. Howard, *Reactions of organic peroxyls in organic solvents 'Peroxyl Radicals'*, Wiley, New York, Z.B. Alfas., 1997.
21 R. F. Enes, A. C. Tomé, J. A. S. Cavaleiro, R. Amorati, M. G. Fumo, G. F. Pedulli and L. Valgimigli, *Chem. – A Eur. J.*, 2006, **12**, 4646–4653.
22 I. T. Brownlie and K. U. Ingold, *Can. J. Chem.*, 1967, **45**, 2427–2432.
23 V. W. Bowry and K. U. Ingold, *J. Am. Chem. Soc.*, 1992, **114**, 4992–4996.
24 J. Sobek, R. Martschke and H. Fischer, *J. Am. Chem. Soc.*, 2001, **123**, 2849–2857.
25 E. A. Haidasz, D. Meng, R. Amorati, A. Baschieri, K. U. Ingold, L. Valgimigli and D. A. Pratt, *J. Am. Chem. Soc.*, 2016, **138**, 5290–5298.
26 J. M. Mayer, D. A. Hrovat, J. L. Thomas and W. T. Borden, *J. Am. Chem. Soc.*, 2002, **124**, 11142–11147.
27 G. A. DiLabio and E. R. Johnson, *J. Am. Chem. Soc.*, 2007, **129**, 6199–6203.
28 J. J. Hanthorn, R. Amorati, L. Valgimigli and D. A. Pratt, *J. Org. Chem.*, 2012, **77**, 6895–6907.
29 R. Amorati and L. Valgimigli, *Org. Biomol. Chem.*, 2012, **10**, 4147–4158.
30 D. A. Pratt, G. A. DiLabio, L. Valgimigli, G. F. Pedulli and K. U. Ingold, *J. Am. Chem. Soc.*, 2002, **124**, 11085–11092.
31 D. A. Pratt, G. A. DiLabio, P. Mulder and K. U. Ingold, *Acc. Chem. Res.*, 2004, **37**, 334–340.
32 J. A. Howard and K. U. Ingold, *Can. J. Chem.*, 1963, **41**, 1744–1751.
33 M. Lucarini, P. Pedrielli, G. F. Pedulli, L. Valgimigli, D. Gigmes and P. Tordo, *J. Am. Chem. Soc.*, 1999, **121**, 11546–11553.
34 G. W. Burton and K. U. Ingold, *J. Am. Chem. Soc.*, 1981, **103**, 6472–6477.
35 J. Igarashi, R. K. Jensen, J. Lusztyk, S. Korcek and K. U. Ingold, *J. Am. Chem. Soc.*, 1992, **114**, 7727–7736.
36 L. R. Mahoney, *Angew. Chemie Int. Ed. English*, 1969, **8**, 547–555.
37 J. Lerchová, J.; Nikiforov, C. A.; Pospíšil, *J. Polym. Sci. Polym. Symp*, 2007, 249–253.
38 I. T. Brownlie and K. U. Ingold, *Can. J. Chem.*, 1966, **44**, 861–868.

39 J. R. Thomas and C. A. Tolman, *J. Am. Chem. Soc.*, 1962, **84**, 2930–2935.
40 T. A. B. M. Bolsman, A. P. Blok and J. H. G. Frijns, *Recl. des Trav. Chim. des Pays-Bas*, 1978, **97**, 310–312.
41 R. Amorati and L. Valgimigli, *Free Radic. Res.*, 2015, **49**, 633–649.
42 E. A. Haidasz, R. Shah and D. A. Pratt, *J. Am. Chem. Soc.*, 2014, **136**, 16643–16650.
43 B. Li and D. A. Pratt, *Free Radic. Biol. Med.*, 2015, **82**, 187–202.
44 R. Amorati, P. T. Lynett, L. Valgimigli and D. A. Pratt, *Chem. – A Eur. J.*, 2012, **18**, 6370–6379.
45 C. Lee, L. Xu, M. Singhal, P. Mendes, S. Hoops, J. Pahle, N. Simus, R. Gauges, S. Sahle and U. Kummer, *Bioinformatics*, 2006, **22**, 3067–3074.
46 E. A. Haidasz, A. T. M. Van Kessel and D. A. Pratt, *J. Org. Chem.*, 2016, **81**, 737–744.
47 J. L. Bolland, *Q. Rev. Chem. Soc.*, 1949, **3**, 1–21.
48 Z. A. M. Zielinski and D. A. Pratt, *J. Org. Chem.*, 2017, **82**, 2817–2825.
49 N. A. Porter, *Acc. Chem. Res.*, 1986, **19**, 262–268.
50 N. A. Porter, B. A. Weber, H. Weenen and J. A. Khan, *J. Am. Chem. Soc.*, 1980, **102**, 5597–5601.
51 M. Peters-Golden and T. G. Brock, *Prostaglandins, Leukot. Essent. Fat. Acids*, 2003, **69**, 99–109.
52 R. A. Lewis, K. F. Austen and R. J. Soberman, *N. Engl. J. Med.*, 1990, **323**, 645–655.
53 T. M. Yau, *Mech. Ageing Dev.*, 1979, **11**, 137–144.
54 A. Tanel and D. A. Averill-Bates, *Free Radic. Biol. Med.*, 2007, **42**, 798–810.
55 A. Nishikawa, R. Sodum and F.-L. Chung, *Lipids*, 1992, **27**, 54–58.
56 C. D. Funk, *Science*, 2001, **294**, 1871-1875.
57 J. Z. Haeggström and C. D. Funk, *Chem. Rev.*, 2011, **111**, 5866–5898.
58 C. Schneider, D. A. Pratt, N. A. Porter and A. R. Brash, *Chem. Biol.*, 2007, **14**, 473–488.
59 A. Andreou and I. Feussner, *Phytochemistry*, 2009, **70**, 1504–1510.
60 M. H. Glickman and J. P. Klinman, *Biochemistry*, 1996, **35**, 12882–12892.
61 M. J. Nelson, *Biochemistry*, 1988, **27**, 4273-4278.
62 N. C. Gilbert, S. G. Bartlett, M. T. Waight, D. B. Neau, W. E. Boeglin, A. R. Brash and M. E. Newcomer, *Science.*, 2011, **331**, 217–219.
63 M. L. Oldham, A. R. Brash and M. E. Newcomer, *J. Biol. Chem.* , 2005, **280**, 39545–39552.
64 S. A. Gillmor, A. Villaseñor, R. Fletterick, E. Sigal and M. F. Browner, *Nat. Struct. Biol.*, 1997, **4**, 1003–1009.
65 D. Steinberg, S. Parthasarathy, T. E. Carew, J. C. Khoo and J. L. Witztum, *N. Engl. J. Med.*, 1989, **320**, 915–924.
66 A. R. Brash, W. E. Boeglin and M. S. Chang, *Proc. Natl. Acad. Sci.*, 1997, **94**, 6148 LP – 6152.
67 D. Kerjaschki, Z. Bago-Horvath, M. Rudas, V. Sexl, C. Schneckenleithner, S. Wolbank, G. Bartel, S. Krieger, R. Kalt, B. Hantusch, T. Keller, K. Nagy-Bojarszky, N. Huttary, I. Raab, K. Lackner, K. Krautgasser, H. Schachner, K. Kaserer, S. Rezar, S. Madlener, C. Vonach, A. Davidovits, H. Nosaka, M. Hämmerle, K. Viola, H. Dolznig, M. Schreiber, A. Nader, W. Mikulits, M. Gnant, S. Hirakawa, M. Detmar, K. Alitalo, S. Nijman, F. Offner, T. J. Maier, D. Steinhilber and G. Krupitza, *J. Clin. Invest.*, 2011, **121**, 2000–2012.
68 T. Yoshimoto and Y. Takahashi, *Prostaglandins Other Lipid Mediat.*, 2002, **68**–**69**, 245–262.
69 S. Xu, T. C. Mueser, L. J. Marnett and M. O. Funk, *Structure*, 2012, **20**, 1490–1497.
70 C. D. Funk and T. Cyrus, *Trends Cardiovasc. Med.*, 2001, **11**, 116–124.
71 D. Nie, G. G. Hillman, T. Geddes, K. Tang, C. Pierson, D. J. Grignon and K. V Honn, *Cancer Res.*, 1998, **58**, 4047-4051.
72 Z. Yu, C. Schneider, W. E. Boeglin and A. R. Brash, *Arch. Biochem. Biophys.*, 2006, **455**, 188–196.
73 Y. Zheng and A. R. Brash, *J. Biol. Chem.* , 2010, **285**, 39876–39887.
74 C. H. Fanta, *Drug Therapy for Asthma REPLY*, 2009, vol. 360.
75 P. Lu, M. L. Schrag, D. E. Slaughter, C. E. Raab, M. Shou and A. D. Rodrigues, *Drug Metab.*

Dispos., 2003, **31**, 1352 LP – 1360.
76 B. Hofmann, S. Barzen, C. B. Rödl, A. Kiehl, J. Borig, A. Živković, H. Stark, G. Schneider and D. Steinhilber, *J. Med. Chem.*, 2011, **54**, 1943–1947.
77 S. J. Dixon, K. M. Lemberg, M. R. Lamprecht, R. Skouta, E. M. Zaitsev, C. E. Gleason, D. N. Patel, A. J. Bauer, A. M. Cantley, W. S. Yang, B. Morrison and B. R. Stockwell, *Cell*, 2012, **149**, 1060–1072.
78 N. Yagoda, M. von Rechenberg, E. Zaganjor, A. J. Bauer, W. S. Yang, D. J. Fridman, A. J. Wolpaw, I. Smukste, J. M. Peltier, J. J. Boniface, R. Smith, S. L. Lessnick, S. Sahasrabudhe and B. R. Stockwell, *Nature*, 2007, **447**, 865.
79 W. S. Yang and B. R. Stockwell, *Chem. Biol.*, 2008, **15**, 234–245.
80 A. Seiler, M. Schneider, H. Förster, S. Roth, E. K. Wirth, C. Culmsee, N. Plesnila, E. Kremmer, O. Rådmark, W. Wurst, G. W. Bornkamm, U. Schweizer and M. Conrad, *Cell Metab.*, 2008, **8**, 237–248.
81 S. Doll, B. Proneth, Y. Y. Tyurina, E. Panzilius, S. Kobayashi, I. Ingold, M. Irmler, J. Beckers, M. Aichler, A. Walch, H. Prokisch, D. Trümbach, G. Mao, F. Qu, H. Bayir, J. Füllekrug, C. H. Scheel, W. Wurst, J. A. Schick, V. E. Kagan, J. P. F. Angeli and M. Conrad, *Nat. Chem. Biol.*, 2016, **13**, 91.
82 H. Yin, L. Xu and N. A. Porter, *Chem. Rev.*, 2011, **111**, 5944–5972.
83 V. E. Kagan, G. Mao, F. Qu, J. P. F. Angeli, S. Doll, C. S. Croix, H. H. Dar, B. Liu, V. A. Tyurin, V. B. Ritov, A. A. Kapralov, A. A. Amoscato, J. Jiang, T. Anthonymuthu, D. Mohammadyani, Q. Yang, B. Proneth, J. Klein-Seetharaman, S. Watkins, I. Bahar, J. Greenberger, R. K. Mallampalli, B. R. Stockwell, Y. Y. Tyurina, M. Conrad and H. Bayır, *Nat. Chem. Biol.*, 2016, **13**, 81.
84 W. S. Yang, K. J. Kim, M. M. Gaschler, M. Patel, M. S. Shchepinov and B. R. Stockwell, *Proc. Natl. Acad. Sci.*, 2016, **113**, 4966-4975.
85 J. P. Friedmann Angeli, M. Schneider, B. Proneth, Y. Y. Tyurina, V. A. Tyurin, V. J. Hammond, N. Herbach, M. Aichler, A. Walch, E. Eggenhofer, D. Basavarajappa, O. Rådmark, S. Kobayashi, T. Seibt, H. Beck, F. Neff, I. Esposito, R. Wanke, H. Förster, O. Yefremova, M. Heinrichmeyer, G. W. Bornkamm, E. K. Geissler, S. B. Thomas, B. R. Stockwell, V. B. O'Donnell, V. E. Kagan, J. A. Schick and M. Conrad, *Nat. Cell Biol.*, 2014, **16**, 1180.
86 O. Zilka, R. Shah, B. Li, J. P. Friedmann Angeli, M. Griesser, M. Conrad and D. A. Pratt, *ACS Cent. Sci.*, 2017, **3**, 232–243.
87 R. Skouta, S. J. Dixon, J. Wang, D. E. Dunn, M. Orman, K. Shimada, P. A. Rosenberg, D. C. Lo, J. M. Weinberg, A. Linkermann and B. R. Stockwell, *J. Am. Chem. Soc.*, 2014, **136**, 4551–4556.
88 R. Shah, M. S. Shchepinov and D. A. Pratt, *ACS Cent. Sci.*, 2018, **4**, 387–396.
89 L. Magtanong, P.-J. Ko, M. To, J. Y. Cao, G. C. Forcina, A. Tarangelo, C. C. Ward, K. Cho, G. J. Patti, D. K. Nomura, J. A. Olzmann and S. J. Dixon, *Cell Chem. Biol.*, 2019, **26**, 420-432.
90 M. A. Fomich, A. V Bekish, D. Vidovic, C. R. Lamberson, I. L. Lysenko, P. Lawrence, J. T. Brenna, O. L. Sharko, V. V Shmanai and M. S. Shchepinov, *ChemistrySelect*, 2016, **1**, 4758–4764.

Chapter 2

Inhibition of Hydrocarbon Autoxidation by Nitroxide Catalyzed Cross-Dismutation of Alkylperoxyl and Hydroperoxyl Radicals

Preface

Nitroxides are putative intermediates in the accepted reaction mechanisms of the diarylamine and hindered amine antioxidants that are universally added to preserve synthetic and natural hydrocarbon-based materials. New methodology which enables monitoring of hydrocarbon autoxidations at low rates of radical generation has revealed that diarylnitroxides and hindered nitroxides are far better inhibitors of unsaturated hydrocarbon autoxidation than their precursor amines, implying intervention of a different mechanism. Experimental and computational investigations suggest that the nitroxides catalyze the cross-dismutation of hydroperoxyl and alkylperoxyl radicals to yield O_2 and a hydroperoxide, thereby halting the autoxidation chain reaction. The hydroperoxyl radicals – key players in hydrocarbon combustion, but essentially unknown in autoxidation – are proposed to derive from a tunneling-enhanced intramolecular (1,4-) hydrogen-atom transfer/elimination sequence from oxygenated radical addition intermediates. These insights suggest that nitroxides are preferred additives for the protection of hydrocarbon-based materials from autoxidation since they exhibit catalytic activity under conditions where their precursor amines are less effective and/or inefficiently converted to nitroxides in situ. The following chapter was reproduced and readapted from (K. A. Harrison, E. A. Haidasz, M. Griesser and D. A. Pratt, *Chem. Sci.*, 2018, **9**, 6068–6079.) with permission from the Royal Society of Chemistry. Copyright (2018). The work was performed in conjunction with former graduate student Dr. Evan A. Haidasz who conducted some of the initial styrene and cumene inhibited autoxidations as well as former post-doctoral fellow Dr. Markus Griesser who performed the computational work and EPR analysis.

2.1. Introduction

Autoxidation, the archetype free radical chain reaction, limits the lifetime of all hydrocarbon-based materials – natural products such as lipids and terpenes as well as synthetic products such as plastics and lubricants. Unsaturated moieties within these materials render them particularly sensitive to autoxidation; they are activated toward H-atom abstraction by chain-carrying peroxyl radicals and can also undergo addition reactions to propagate the chain process (Figure 2.1A.). Diarylamines and hindered aliphatic amines comprise two of the three key types of radical-trapping antioxidants (RTAs)

commonly added to preserve hydrocarbon-based materials.[1,2] Extensive investigations since the mid-1950s have established that diarylamines trap 2 peroxyl radicals at ambient temperatures,[3,4] but at elevated temperatures trap far more[5] by a catalytic mechanism (the "Korcek Cycle", Figure 2.1B)[6,7] involving the formation of diarylnitroxide intermediates.[8,9] In contrast, hindered amines are not RTAs at ambient temperatures, but at elevated temperatures or prolonged irradiation[5] they lead to nitroxides which trap radicals in a distinct, but still catalytic manner (the "Denisov Cycle", Figure 2.1C).[10,11]

Although nitroxides are key intermediates in both the Korcek and Denisov cycles, they do not react with peroxyl radicals directly in these mechanisms – and thereby adhere to the longstanding dogma that nitroxides do not react with oxygen-centred radicals. This belief is based largely on the seminal work of Thomas[8] and Ingold[12], who showed that diphenylnitroxide and 4-oxo-2,2,6,6-tetramethylpiperidin-1-oxyl were not particularly effective at inhibiting the autoxidation of cumene and styrene, respectively. Instead, it was proposed that they only retard the autoxidation by competing with O_2 for the chain-carrying alkyl radicals – a difficult competition since the reaction of nitroxides with alkyl radicals is at least an order of magnitude slower[13,14] than that of O_2.[15–17] Paradoxically, this reaction is invoked in both the Korcek and Denisov cycles, implying that catalytic RTA activity arises only when the intermediate nitroxide concentration exceeds that of O_2.

We recently made the stunning observation that diarylnitroxides and hindered nitroxides are far better inhibitors of unsaturated hydrocarbon autoxidation than are their precursor amines at ambient to moderate temperatures (*vide infra*). These results were obtained at lower rates of radical generation than those typically employed in laboratory experiments, implying that the mechanism responsible operates at lower steady state concentrations of radicals – a situation representative of most 'real world' applications. Moreover, these results suggest a different mechanism of antioxidant activity for the nitroxides than those expected based upon the Korcek and Denisov mechanisms – insight which could be leveraged for the design and development of badly needed new antioxidant technology. Our observations are presented below, alongside our efforts to elucidate the mechanism and a discussion of the practical implications of these insights: most importantly, that nitroxides should be considered as additives to increase the longevity of both natural and synthetic hydrocarbon-based materials in lieu of currently used amines.

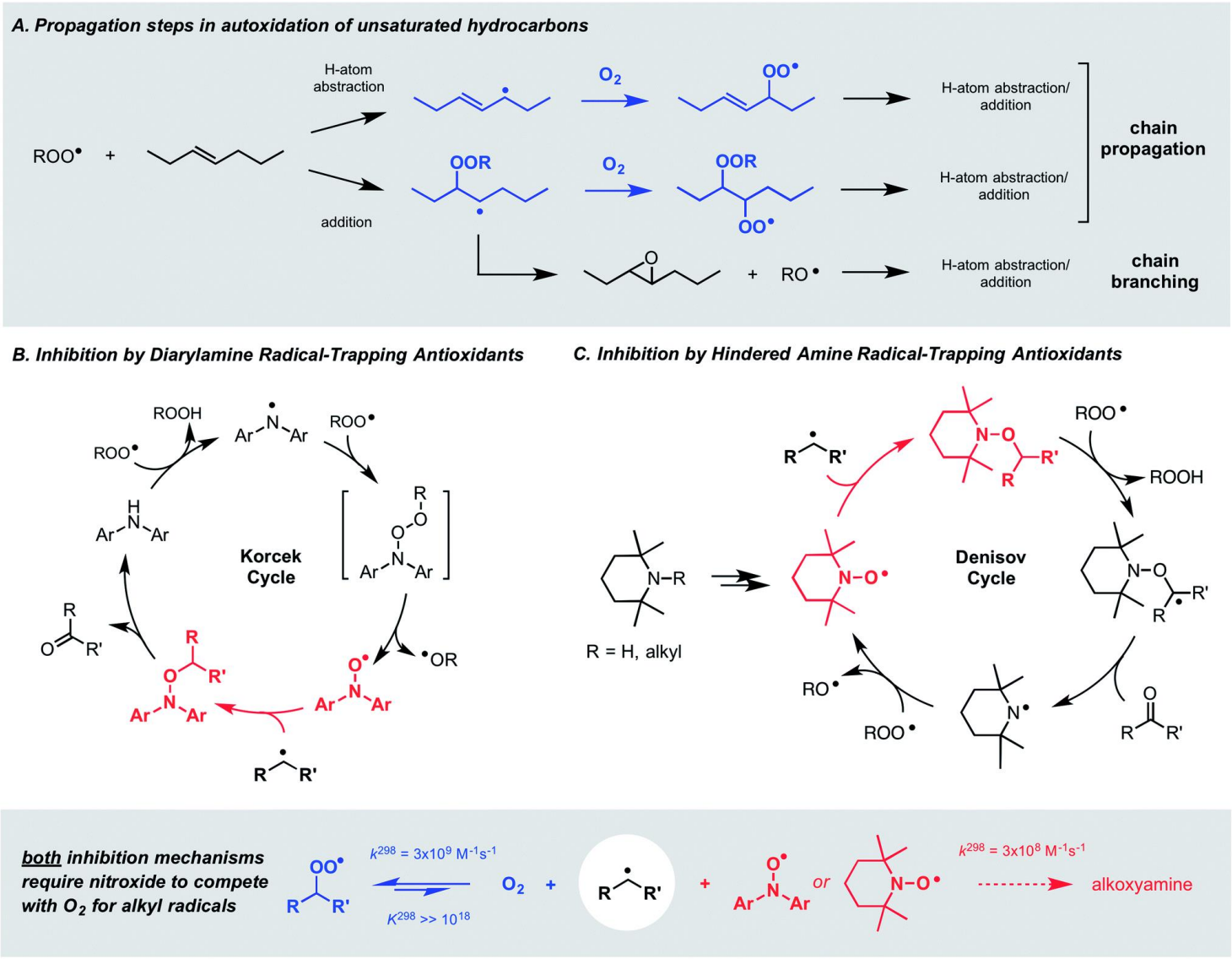

Figure 2.1. (A) The key propagation steps in the autoxidation of unsaturated hydrocarbons. (B and C) The Korcek and Denisov mechanisms believed responsible for the catalytic inhibition of hydrocarbon autoxidation by diarylamine and hindered amine antioxidants.

2.2. Results

2.2.1. Styrene and cumene autoxidations at low rates of radical generation inhibited by nitroxides

We recently reported a method to monitor inhibited autoxidations of hydrocarbons which makes use of highly absorbing and highly autoxidizable probes as signal carriers (e.g. STY-BODIPY, Figure 2.1A).[18] The consumption of the probe is monitored by conventional spectrophotometry, and since its reactivity toward peroxyl radicals can be independently determined (e.g. $k_{\text{STY-BODIPY}} = 4012\ M^{-1}s^{-1}$ in styrene/chlorobenzene at 70 °C, see Figure 2.1A-B and Supporting Information), the inhibition rate constant (k_{inh}) of an added RTA and the stoichiometry of the inhibition (n, i.e. how many chain-carrying radicals are trapped by each molecule of RTA) can be easily derived from the data as in Figure 2.1B. During our efforts to validate this approach – by comparison to measurements using the venerable O_2 uptake method[19–21]- we obtained unexpected results in autoxidations of styrene inhibited by 4,4'-di-*tert*-butyldiphenylamine and its corresponding nitroxide (hereafter Ar_2NH and Ar_2NO, respectively). To our great surprise, the nitroxide was a significantly better RTA than the amine (Fig. 2.1C) – not just in terms of its kinetics ($k_{inh} = 7.9\times10^6\ M^{-1}s^{-1}$ for Ar_2NO compared to $k_{inh} = 7.9\times10^5\ M^{-1}s^{-1}$ for Ar_2NH), but in that the nitroxide trapped significantly more radicals than the amine ($n = 10.6\pm0.2$ for Ar_2NO compared to $n = 2.1\pm0.2$ for Ar_2NH).[22] These results stand in stark contrast to the seminal results obtained by Thomas[8] and Ingold.[12] Since Thomas had used cumene as the autoxidizable substrate, we carried out autoxidations of cumene instead, again using STY-BODIPY as the signal carrier,[18] but under otherwise identical conditions to Thomas (0.29 M cumene in chlorobenzene, initiated by 1.0 mM AIBN at 68.5 °C and inhibited by 50 μM of diphenylamine). Our results were fully consistent with Thomas' observations, in terms of both reactivity and stoichiometry, i.e. $n = 2.3\pm0.1$ for Ar_2NH and $n = 1.1\pm0.1$ for Ar_2NO (Fig S1). Recognizing that Ingold's styrene autoxidations had been carried out under significantly different conditions from our own, we attempted experiments using Ingold's conditions (7.24 M styrene in *o*-dichlorobenzene, initiated by 4.3 mM AIBN at 65 °C and inhibited by 4.3 mM antioxidant).

Unfortunately, it was impossible to monitor reaction progress by STY-BODIPY consumption due to the absorbance of the massive amounts of antioxidant and/or its oxidation products. However, when the antioxidant and initiator concentrations were reduced to those of Thomas (50 μM and 1 mM, respectively), we observed a relative reactivity that was consistent with what had been reported by Ingold, *i.e.*, Ar_2NH was more reactive than Ar_2NO (Fig. S2‡). Interestingly, the nitroxide still possessed a longer inhibition time than the amine. Ingold couldn't report on the stoichiometry of the inhibition due to the length of the inhibited time at the antioxidant concentrations he employed.

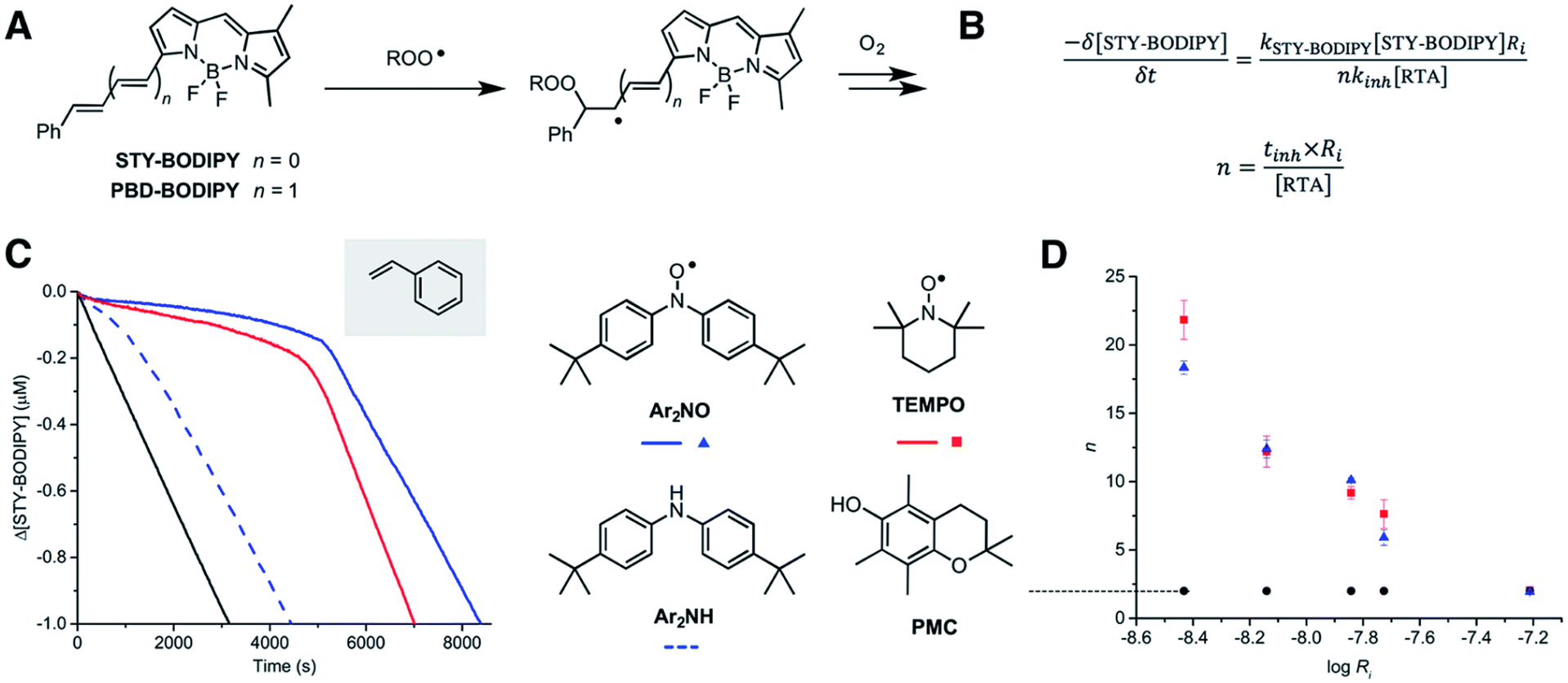

Figure. 2.2. Preliminary studies. (A) STY-BODIPY and PBD-BODIPY can be used as signal carriers in the autoxidation of organic substrates. (B) The rate constants (k_{inh}) and stoichiometries (n) for the reactions of inhibitors (RTAs) with chain-carrying peroxyl radicals can be derived from the initial rate of probe consumption and the duration of the inhibited periods (t_{inh}), respectively. (C) Co-autoxidations of styrene (3.5 M) and STY-BODIPY (10 μM) in PhCl initiated with di-*tert*-butylperoxide (218 mM) at 70 °C (black) and inhibited by Ar_2NO, Ar_2NH and TEMPO (2 μM). (D) Stoichiometry of peroxyl radical-trapping by Ar_2NO, TEMPO and PMC as a function of rate of initiation of styrene autoxidations at 70 °C (obtained using 62.5, 125, 250, 375 and 1000 μM AIBN). Reaction progress was monitored at 571 nm (ε = 97 235 M^{-1} cm^{-1}).

Given these interesting results, corresponding data were obtained with 2,2,6,6-tetramethylpiperidine-*N*-oxyl (hereafter TEMPO), the quintessential nitroxide. The results are shown alongside those for Ar_2NO in Fig. 2.2C. (The corresponding tetramethylpiperidine was not investigated as it is known to be unreactive to peroxyl radicals; its N-H BDE is ca. 10 kcal/mol higher than that of diphenylamine).[23]

Consistent with previous work,[23–26] TEMPO was unable to inhibit the autoxidation of cumene (data not shown), but consistent with the foregoing results, it inhibited the autoxidation of styrene with kinetics and stoichiometry similar to those observed for Ar_2NO, i.e. $k_{inh} = 2.1\times10^6$ $M^{-1}s^{-1}$ and $n = 9.3\pm0.9$. Thus, the RTA activity is largely independent of the nitroxide structure, but strongly dependent on both the structure of the substrate and the rate of initiation of the autoxidation. This last point can be seen clearly from the results in Figure 2.2D., where the stoichiometry determined from a series of nitroxide-inhibited autoxidations of styrene are plotted as a function of the rate of initiation (through an [AIBN] range of 62.5 μM to 1 mM). The variation in n is remarkable, spanning $n = 18.3\pm0.5$ and 21.9 ± 1.4 at $R_i = 3.7\times10^{-9}$ M/s to $n = 1.9\pm0.2$ and 2.1 ± 1.4 at $R_i = 6.1\times10^{-8}$ M/s for Ar_2NO and TEMPO, respectively. Laboratory autoxidations are generally carried out at high rates of initiation for practical reasons (ease of measurement by established methods, convenient timescale). In the 'real world', autoxidations proceed relatively slowly. It is important to note that the foregoing experiments were carried out at 70 °C to facilitate comparison with Thomas and Ingold's seminal data. Corresponding experiments carried out at 37 °C yielded similar trends, albeit with lower values of n for similar R_i (e.g. $n = 10.9 \pm 0.1$ and 10.1 ± 0.1 at $R_i = 2.8 \times 10^{-9}$ M s^{-1} for Ar_2NO and TEMPO, respectively – see Supporting Information for additional data).

2.2.2. Nitroxides are effective inhibitors of unsaturated, but not saturated, hydrocarbons

To better understand the substrate dependence of this reactivity, investigations were expanded to include autoxidations of other activated hydrocarbons. Since styrene and cumene differ in the presence/absence of a reactive alkene, autoxidizable substrates were selected that either possess an alkene (cyclooctene and norbornene) or do not (ethylbenzene and dioxane). Representative results for these substrates are shown in Figure 2.3 below.

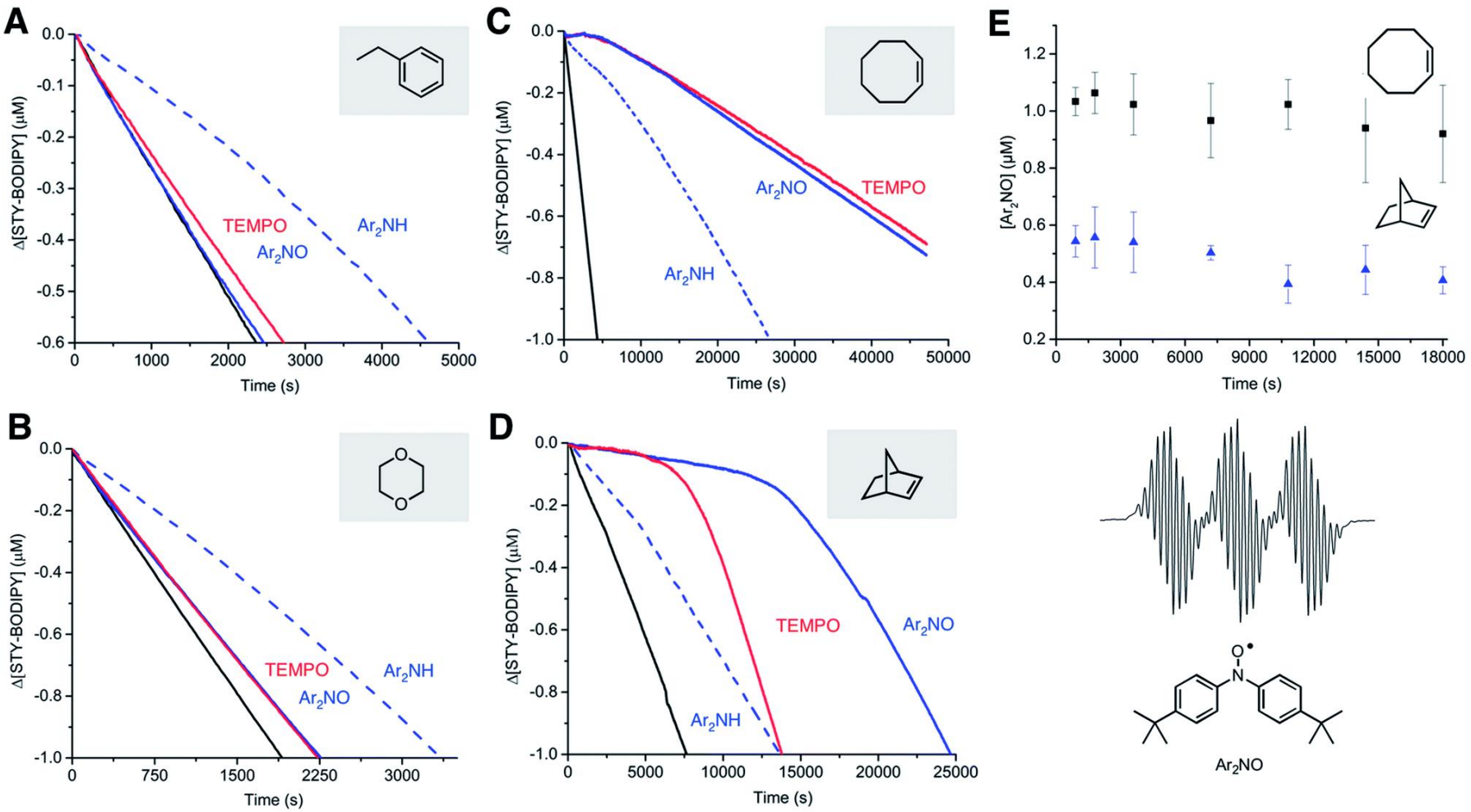

Figure 2.3. Substrate Dependence. Co-autoxidations of STY-BODIPY (10 μM) and ethylbenzene (3.3 M, A), cyclooctene (3.1 M, B) norbornene (1.0 M, C) and dioxane (2.9 M, D) in chlorobenzene initiated with di-tert-butylperoxide (87 mM for ethylbenzene, 218 mM for cyclooctene, norbornene and dioxane) at 70 °C (black) and inhibited by TEMPO, Ar_2NO and Ar_2NH (2 μM). Reaction progress was monitored at 569 nm in A (ε = 123,481 $M^{-1}cm^{-1}$), 568 nm in B (ε = 113,982 M^{-1} cm^{-1}), 568 nm in C (ε = 118,405 M^{-1} cm^{-1}) and 569 nm in D (ε = 122,873 $M^{-1}cm^{-1}$). (E) Concentration of Ar_2NO determined by EPR (spectrum shown) during Ar_2NH-inhibited co-autoxidations.

In a strikingly consistent fashion, autoxidations of the substrates that possess an unsaturation were very effectively inhibited by the nitroxides whereas those lacking one, were not. Moreover, while the diarylamine expectedly inhibited the autoxidation of all the substrates, it was noticeably more effective in the unsaturated ones, retarding the autoxidations well past the initial inhibited periods corresponding to $n = 2$. Since diarylamines are known to be converted to diarylnitroxides under autoxidative conditions (*i.e.* Fig 2.1) this suggests that the retardation of autoxidations of cyclooctene and norbornene beyond the nominal inhibition period result from the *in situ* formation of nitroxide. Indeed, when the autoxidations were followed by EPR spectroscopy, significant concentrations of nitroxide were observed, reaching a steady-state concentration (*ca.* 50% and 20% of the initial amine concentration for cyclooctene and norbornene, respectively) around the same time as the autoxidation rate became constant. Taken together, these results suggest that, in unsaturated hydrocarbons, nitroxides must be converted to very efficient RTAs.

2.2.3. The *in situ* formation of hydroxylamines accounts for the observed inhibition of autoxidation in unsaturated substrates

Since nitroxide-derived alkoxyamines have long been implicated as key intermediates in the RTA activity of diarylamines (Figure 2.1B) and hindered amines (Figure 2.1C), we sought to determine if they contribute to the observed reactivity in styrene. Thus, *O*-phenethyl *N*, *N*-(4-*tert*-butylphenyl) hydroxylamine and the corresponding *O*-phenethylated 2,2,6,6-tetramethylpiperidine-*N*-ol were synthesized (see Supporting Information) and their reactivity in the styrene autoxidations were assessed. The phenethyl substituent was chosen due to its similarity to the propagating benzylic radicals that would combine with the nitroxides in inhibited autoxidations of styrene. The data, which show that the alkoxyamines are unreactive, are given in Figure 2.4A and 2.4B.

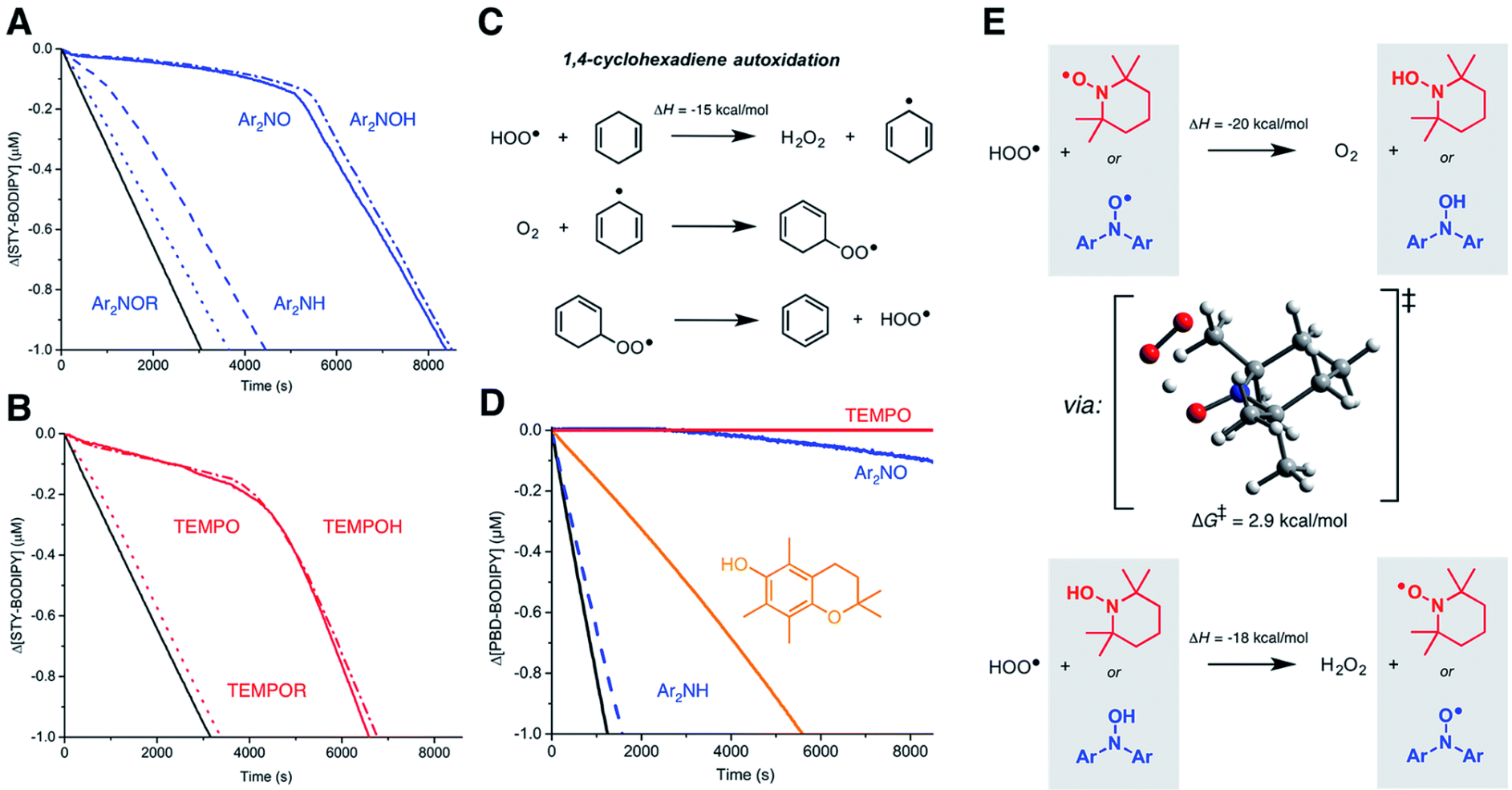

Figure 2.4. Mechanistic studies. (A) Co-autoxidations of styrene (3.5 M) and STY-BODIPY (10 μM) in PhCl initiated with di-*tert*-butylperoxide (218 mM) at 70 °C (black) and inhibited by 2 μM of Ar$_2$NOR (dotted line), Ar$_2$NH (dashed line), Ar$_2$NO (solid line) and Ar$_2$NOH (dotted/dashed line). (B) Co-autoxidations carried out under the same conditions and inhibited by TEMPOR (dotted line), TEMPO (solid line) and TEMPOH (dotted/dashed line). Reaction progress was monitored at 571 nm (ε = 97 235 M^{-1} cm^{-1}). (C) Mechanism of 1,4-cyclohexadiene autoxidation. (D) Co-autoxidations of 1,4-CHD (0.26 M) and PBD-BODIPY (10 μM) in chlorobenzene at 30 °C initiated by di-*tert*-butylperoxide (218 mM, black) and inhibited by 2 μM of TEMPO (red line), Ar$_2$NO (blue line), PMC (orange line) and Ar$_2$NH (dashed line). Reaction progress was monitored at 591 nm (ε = 130 797 M^{-1} cm^{-1}). (E) Nitroxide-catalyzed dismutation of hydroperoxyl radicals showing the CBS-QB3-calculated TS structure for the reaction of TEMPO with HOO$^{\cdot}$.

For comparison, we also investigated the corresponding hydroxylamines, which are clearly excellent inhibitors. The initial rates yield k_{inh} = (8.5±1.3)×10^6 and (3.0±0.7)×10^6 M^{-1} s^{-1} for Ar_2NOH and TEMPOH, respectively, the latter in excellent agreement with literature precedent (k_{inh} = 3.0×10^6 M^{-1} s^{-1} at 30 °C).[26] To the best of our knowledge, this is the first time a rate constant has been determined for a diarylhydroxylamine in a non-aqueous solvent; it is slightly greater than for TEMPOH, likely due to lower steric hindrance. The reaction stoichiometry is essentially +1 radical relative to the nitroxide (viz. 11.6±0.1 and 10.0±0.2, respectively), consistent with an initial H-atom transfer from the hydroxylamine to produce the nitroxide, which then reacts as when it is added directly.

The similar initial rates of the autoxidations inhibited by the hydroxylamines and nitroxides prompted us to consider if nitroxides could be reduced to hydroxylamines in situ. Recent work by Litwinienko and Amorati[27] has shown that 1,4-cyclohexadiene (hereafter 1,4-CHD) autoxidations are very efficiently inhibited by phenols because the hydroperoxyl radicals (HOO•) that are known to carry the autoxidation of 1,4-CHD (Figure 2.4C)[28] can regenerate the phenol following its initial chain-breaking reaction. Amazingly, 1,4-CHD/PBD-BODIPY co-autoxidations were perpetually inhibited by either TEMPO or Ar2NO (Figure 2.5C). Both nitroxides were demonstrably better than PMC, a truncated analog of Vitamin E and one of the most reactive phenolic antioxidants known. (Phenols are the other key type of RTA commonly added to preserve hydrocarbon-based materials.) This is presumably due to the more efficient conversion of nitroxides to chain-breaking hydroxylamines upon reduction by HOO• compared to the PMC-derived radical, which can also react via addition to the aryl ring giving inactive peroxyl-phenoxyl adducts.[27] TEMPO was observed to be a slightly better inhibitor than Ar_2NO, perhaps since the latter can (like the PMC-derived phenoxyl) undergo competitive addition of HOO• to the aryl ring. It is interesting that this reactivity trend is opposite of what is observed in styrene and norbornene, where Ar_2NO is more effective than TEMPO, perhaps because alkylperoxyl addition is more reversible than HOO• addition.

Although the O–H bonds of hydroxylamines are considerably weaker than the O–H bonds of even the most reactive phenols (compare BDEs of 70 and 78 kcal mol^{-1} in TEMPOH[29] and PMC,[30] respectively), the reaction is still highly exothermic. The barrier for the H-atom transfer from HOO$^{\cdot}$ to TEMPO is predicted by CBS-QB3[31] to be $\Delta G^{\ddagger}$ = 2.9 kcal mol^{-1}, corresponding to a rate constant of 2 × 10^{10} M^{-1} s^{-1} upon application of transition state theory. Thus, the reaction is predicted to be diffusion-controlled.[32] It is interesting to note the *syn*-orientation of the substituents on the oxygen atoms between which the H-atom is being transferred (Figure 2.4E). Although this is unexpected based on steric considerations, it is typical of reactions of peroxyl radicals with H-atom donors that possess an α-heteroatom (*e.g.* ROO$^{\cdot}$ + H–OSR,[33] H–OSeR,[34] H–SSR[35]) or unsaturation (*e.g.* H–OAr[36], H–NHAr[37]) due to secondary orbital interactions between the substituents.

2.2.4. A tunneling-enhanced 1,4-HAT/elimination sequence leads to hydroperoxyl formation in unsaturated hydrocarbon autoxidation

To the best of our knowledge, there has been no investigation of the intervention of HOO˙ in the propagation of autoxidation of simple monounsaturated hydrocarbons such as styrene, cyclooctene and norbornene. To assess whether HOO˙ could be formed from chain-propagating intermediates in the autoxidation of these substrates, we turned to computation. It has been suggested that hydroperoxyl radicals contribute to the propagation of autoxidation of activated unsaturated substrates, such as acrylates and substituted 1,3-butadienes. Multiple mechanistic possibilities were advanced.[38] However, prior to investigating these reactions, we sought to clarify the pathway operating in the autoxidation of 1,4-CHD.

The precise mechanism of HOO• formation in 1,4-CHD autoxidation has been a matter of some debate. Howard and Ingold had originally proposed a unimolecular elimination from the cyclohexadienylperoxyl radical (as shown in Figure 2.4C).[28] Hendry and Schuetzle subsequently argued that the reaction must involve direct H-atom transfer from the cyclohexadienyl radical to O_2.[39] Subsequent reports seem split between the two mechanisms.[40–44]

Our CBS-QB3 calculations suggest that the cyclohexadienylperoxyl is a bound structure that leads to HOO• and benzene via a concerted 1,4-HAT/elimination transition structure that intrinsic reaction coordinate (IRC) calculations confirm connect the two stationary points. No transition state structure was identified for the direct H-atom transfer mechanism.[45] The predicted barrier for this process ($\Delta G^{\ddagger}$ = 15.4 kcal/mol) is strikingly similar to that of the bimolecular propagation reaction of hydroperoxyl and 1,4-cyclohexadiene ($\Delta G^{\ddagger}$ = 15.2 kcal/mol). Confidence in the calculations comes from the excellent agreement between the predicted rate constant for the latter reaction and the known k_p for 1,4-CHD autoxidation (1610 $M^{-1}s^{-1}$ *vs.* 1400 $M^{-1}s^{-1}$,[28] respectively), as well as the thermodynamics of that step (ΔG = −14.2 kcal/mol), which is fully consistent with the difference in bond dissociation enthalpies (BDEs) between 1,4-CHD (74.5 kcal/mol)[46] and H_2O_2 (87.5 kcal/mol).[47]

In contrast to 1,4-CHD, styrene is well known to propagate by addition. Thus, the analogous 1,4-HAT/elimination process to produce HOO• may be expected to come from the propagating peroxyl radical show on the top left in Figure 2.5A. A transition state structure for the 1,4-HAT in this intermediate was readily identified, but in lieu of being concerted with HOO• elimination as for 1,4-CHD, IRC calculations indicate that no stationary point connects it and the transition state for β-fragmentation of the neighbouring O-O bond. Although a transition state structure could be identified for the elimination of HOO•, it is 15.3 kcal/mol higher in energy.

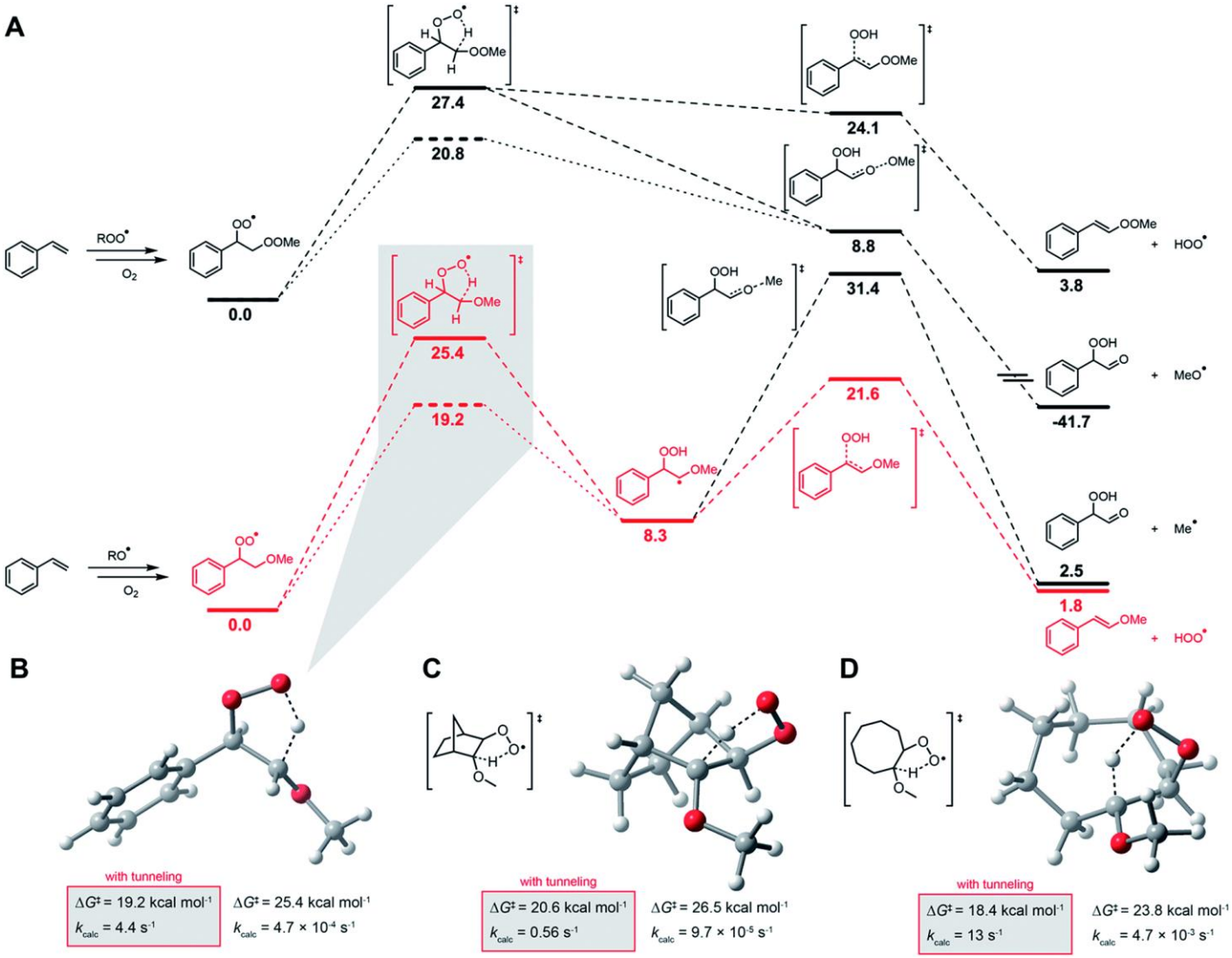

Figure 2.5. Computational Investigations. (A) CBS-QB3-Computed free energy profile for HOO• formation from peroxyl radical intermediates arising in styrene autoxidation. Energy of the tunneling-enhanced 1,4-HAT TS is given by the dashed line. Methylperoxyl and methoxyl are used as models of chain-propagating alkylperoxyl and alkoxyl radicals, respectively. Transition state structures for the 1,4-HAT in the *β*-alkoxyalkylperoxyl radicals derived from styrene (B), norborene (C) and cyclooctene (D).

The propagation of styrene autoxidation by peroxyl radical addition competes with the intramolecular S_H^i reaction that yields styrene epoxide and an alkoxyl radical which subsequently adds to styrene to continue the chain. Styrene oxide has been reported to account for as much as 39% of the products in a styrene autoxidation,[48] and is expectedly influenced by the partial pressure of O_2.[49] The alkoxyl radicals formed as a result – as well as alkoxyl radicals formed simply from homolysis of the styrene/oxygen copolymer products – add to styrene to yield a benzylic radical that is subsequently oxygenated to yield the chain-propagating peroxyl radical shown on the bottom left of Figure 2.5A. A transition state structure for the 1,4-HAT from this intermediate was also readily identified, but this time IRC calculations connect it to the product α-alkoxyalkyl radical. From this intermediate, HOO• elimination proceeds in favour of the β-fragmentation of the alkoxy C-O bond ($\Delta G^{\ddagger}$ = 13.3 kcal/mol for the former compared to 23.1 for the latter). The preceding 1,4-HAT has a much higher barrier but is predicted to be greatly enhanced by quantum tunneling with k = 4.4 s^{-1} (70 °C).

Corresponding calculations for cyclooctene and norbornene provide similar insight: elimination from the oxygenated intermediate arising from alkoxyl addition to the double bond is predicted to be a viable route to HOO• formation, with similar (tunneling-corrected) rate constants of 13 and 0.56 s^{-1} (70 °C), respectively. It should be noted that the autoxidation of norbornene[50,51] and cyclooctene[52,53] is known to produce even more epoxide than styrene. Complete potential energy surfaces for the relevant chain-propagating steps of cyclooctene and norbornene autoxidation are given in the Supporting Information.

2.2.5. Kinetic isotope effects support the proposed mechanism

If hydroperoxyl radicals are the stoichiometric reductants in nitroxide-inhibited autoxidations of unsaturated hydrocarbons, a kinetic isotope effect should be observed upon the addition of an acidic deuterium source to the medium due to the HOO•/DOO• equilibrium (the pK_a of HOO• is 4.9).[54] Thus, TEMPO-inhibited and Ar_2NO-inhibited styrene/STY-BODIPY co-autoxidations were repeated in the presence of either 1% MeOH or MeOD. The results are shown in Figure 2.6A. In both cases, the addition of MeOD had a pronounced effect on both the initial rate of the autoxidation and the duration of the inhibited period. From the initial rates, DKIEs of k_H/k_D = 4.2 and 3.3 can be calculated for TEMPO and Ar_2NO, respectively. The magnitude of these DKIEs are very similar to those reported by Brownlie and Ingold for inhibition of styrene autoxidations by structurally-related hydroxylamines.[12] These results are consistent with equilibration of HOO• with TEMPO/Ar_2NO to produce TEMPOH/Ar_2NOH as the chain-breaking antioxidant *in situ* (Figure 2.6B).[55–58]

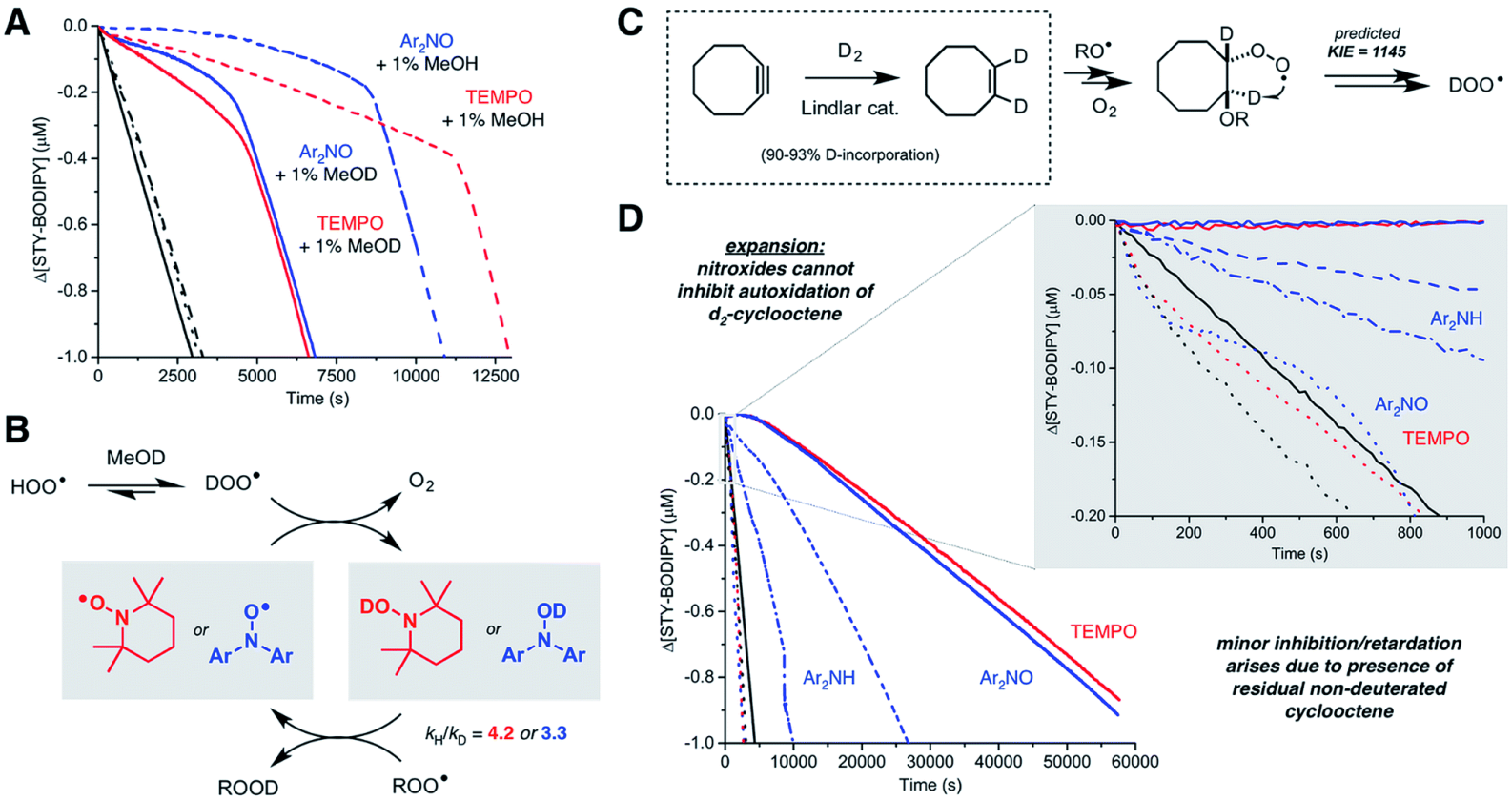

Figure. 2.6. Kinetic isotope effect studies. (A) Co-autoxidation of styrene (3.5 M) and STY-BODIPY (10 μM) in PhCl initiated with di-*tert*-butylperoxide (218 mM) at 70 °C (black) and inhibited by either Ar_2NO (2 μM, blue) or TEMPO (2 μM, red) in the presence of 1% v/v MeOH (dashed lines) or MeOD (solid lines). Reaction progress was monitored at 571 nm (ε = 97 235 M^{-1} cm^{-1}). (B) Dynamic exchange of the acidic proton in $HOO^{\cdot}$ with the acidic deuteron in MeOD is expected to precede the nitroxide-catalyzed cross-dismutation of hydroperoxyl and alkylperoxyl radicals, leading to the observed kinetic isotope effects. (C) Synthesis of 1,2-d_2-cyclooctene and the predicted kinetic isotope effect on $HOO^{\cdot}$ production. (D) Co-autoxidation of cyclooctene or 1,2-d_2-cyclooctene (3.1 M) and STY-BODIPY (10 μM) in PhCl initiated with di-*tert*-butylperoxide (218 mM) at 70 °C (black line) and inhibited by 2 μM of either Ar_2NO (blue line), TEMPO (red) or Ar_2NH (dashed blue line). Corresponding traces with deuterated substrate are represented by dotted lines. Inset: expansion of the initial portion of the autoxidation. Reaction progress was monitored at 568 nm (ε = 118 405 $M^{-1}cm^{-1}$).

Given the computational prediction that HOO• can be formed from unsaturated hydrocarbons by a quantum tunneling-enhanced intramolecular 1,4-HAT from a β-alkoxyalkylperoxyl intermediate, we sought to replace the vinylic H-atoms of one of the substrates above with deuterium to suppress the ability of nitroxides to inhibit the autoxidation. We selected cyclooctene for these experiments since 1,2-d_2-cyclooctene could be easily accessed simply by catalytic deuteration of cyclooctyne over Lindlar's catalyst (Figure 2.6C). The results of STY-BODIPY/1,2-d_2-cyclooctene co-autoxidations inhibited by TEMPO and Ar_2NO are plotted alongside the corresponding data for cyclooctene in Figure 2.6D.

The difference in the cyclooctene and 1,2-d_2-cyclooctene data could not be more dramatic. Substitution of the nominally unreactive alkene H-atoms of the substrate with deuterium atoms all but precludes inhibition of the reaction by the nitroxides. The very small effect of the nitroxides on the reaction progress in the autoxidation (which is visible only upon expanding the initial portion of the reaction progress data as in the inset to Figure 2.6D) is presumably due to the formation of a small amount of HOO• from the residual proteated cyclooctene also undergoing autoxidation. Although catalytic deuteration of cyclooctene is essentially quantitative to prepare 1,2-d_2-cyclooctene, the starting cyclooctyne is prepared from cyclooctene, which is difficult to remove (see Supporting Information for more details). In stark contrast, the initial rates of the Ar_2NH-inhibited autoxidations of cyclooctene and 1,2-d_2-cyclooctene are very similar (see inset to Figure 2.6D) and the reaction progress only diverges once the nitroxide formed *in situ* is responsible for inhibition of the autoxidation (evident over the longer reaction time shown in Figure 2.6D).

Overall, this result is fully consistent with the intramolecular 1,4-HAT of the β-alkoxyalkylperoxyl intermediate being key to the activity of the nitroxides, and that the contribution of this reaction to the propagation of autoxidation of these substrates is greatly enabled by quantum mechanical tunneling.

2.3. Discussion

Hindered aliphatic nitroxides such as TEMPO derivatives have long been considered unreactive to alkylperoxyl radicals, and as such, are not generally considered inhibitors of hydrocarbon autoxidation under most conditions (except at low partial pressures of O_2, where alkyl radicals can be trapped). In contrast, diarylnitroxides had been shown to react with peroxyl radicals, albeit it more slowly than their parent amines. Given the difference in reactivity of hindered nitroxides and diarylnitroxides, it was proposed that peroxyl radical addition to one of the aryl rings of the diarylnitroxide is possible (Scheme 2.1).[12]

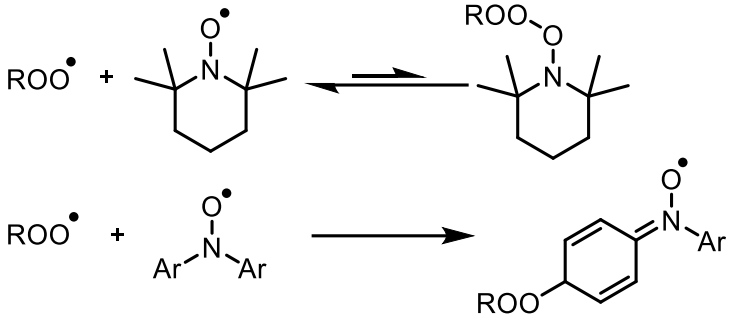

Scheme 2.1. Hindered aliphatic nitroxides do not react with alkylperoxyl radicals; (di)arylnitroxides react by addition to the aryl ring(s).

In recent years, some exceptions to this dogma have begun to appear (i.e. nitroxides undergo electron transfer to peroxyl radicals in aqueous solution,[17,59] and nitroxides undergo acid-promoted reactions with peroxyl radicals in organic solution),[18,26] but they are under specific conditions. As such, we were initially very surprised to obtain the results in Figure 2.1, where both hindered aliphatic nitroxides and diarylnitroxides are similarly good inhibitors of styrene autoxidation – better even than the corresponding diphenylamine. The results of subsequent experiments have clarified that nitroxides are excellent inhibitors of unsaturated hydrocarbon autoxidation at low rates of radical generation. Mechanistic studies have enabled the proposition of a mechanism that does not require the reaction of a nitroxide with an alkylperoxyl radical, but rather, a hydroperoxyl radical. Reaction of the resultant hydroxylamine with an alkylperoxyl radical traps a second chain-carrying radical and regenerates the nitroxide. The similarity in the apparent k_{inh} observed for the nitroxides and the k_{inh} observed for the authentic hydroxylamines implies that the reaction of nitroxide with HOO˙ is faster than hydroxylamine + ROO˙, such that hydroxylamine accumulates to serve as the key chain-breaking species.[60] Overall, this mechanism can be characterized as a nitroxide-catalyzed cross-dismutation of hydroperoxyl and alkylperoxyl radicals. A similar reaction sequence was once proposed to explain the superoxide dismutase activity of hindered nitroxides in aqueous solution, but was subsequently dismissed on kinetic grounds in favour of the half reactions involving conversion of TEMPO to its corresponding oxoammonium ion and back.[61]

More than a century of research in combustion chemistry has shown that the major initial products formed in the high temperature (>300 °C) gas phase oxidation of simple alkanes are alkenes containing the same number of carbons. This observation has been ascribed to the elimination of HOO˙ from alkylperoxyl intermediates.[62] The 1,4-HAT/elimination sequence connecting the alkylperoxyl radicals and alkenes have been the subject of extensive investigations, particularly for ethylperoxyl radicals due to their computational tractability.[63] There would appear to be a consensus that, in the case of simple alkylperoxyl radicals, the 1,4-HAT and elimination take place in a concerted fashion. However, as the putative β-hydroperoxyalkyl radical is more stable both pathways are possible,[64] or the step-wise process dominates.[65] The step-wise path is anticipated to be greatly

enhanced by quantum mechanical tunneling since the transition state involves little atomic movement other than the H-atom being transferred. Indeed, kinetic isotope effects derived for the 1,4-HAT in the step-wise formation of hydroperoxyl from *n*-propylperoxyl are predicted to decrease with temperature from 9.5 at 648 K to 6.2 at 703 K[66] – implying that at ambient temperatures they would be massive. Indeed, our calculations suggest that elimination of HOO˙ from chain-propagating alkylperoxyl radicals in unsaturated hydrocarbon autoxidation is stepwise and greatly enhanced by tunneling. Furthermore, the lack of inhibition of nitroxides in autoxidations of d_2-cyclooctene clearly corroborate the prediction that the reaction is greatly enhanced by tunneling.

In the condensed phase, the elimination of HOO˙ from alkylperoxyl intermediates formation is known only for very specific hydrocarbons, *e.g.* 1,4-CHD and 1,4-dihydronaphthalene.[28] Ingold first demonstrated that the autoxidation of these substrates is propagated primarily by HOO˙; initially due to their extremely rapid termination rate constants ($k_t = 6.3 \times 10^8$ M^{-1} s^{-1} in chlorobenzene at 30 °C; >200-fold greater than that measured for cyclohexene), and subsequently confirmed his assertion simply by washing the solutions with water and determining H_2O_2 by iodometric titration (which corresponded to *ca.* 95% of all the peroxide formed). The identification of substrates that propagate to only a small extent by hydroperoxyl radicals would have been extremely challenging due to their small contribution to k_t and low yields of H_2O_2. Instead, the foregoing suggest that these substrates can be revealed indirectly by the ability of nitroxides to inhibit their autoxidation.

At first glance, the relative contribution of the 1,4-HAT/elimination pathway that is proposed to yield HOO˙ from chain-propagating alkylperoxyl radicals may be reflected in the relative efficacy of the nitroxides as inhibitors of autoxidation. Indeed, we find that while 1,4-CHD autoxidation is perpetually inhibited by the addition of TEMPO, the nitroxide is relatively less effective in styrene, norbornene and cyclooctene. However, rationalizing the trends observed for styrene, norbornene and cyclooctene is complicated by the fact that styrene and norbornene propagate exclusively by addition (necessary to produce the intermediate peroxyl radical from which the 1,4-HAT/elimination is proposed to take place), whereas cyclooctene propagates largely, but not exclusively, by addition.[52,53] Moreover, because the 1,4-HAT and subsequent elimination is competitive only at low rates of initiation where radical–radical reactions are minimized, the differences in termination rate constants are also expected to contribute. Nevertheless, it appears that of the three substrates, the nitroxides are most effective in cyclooctene, perhaps because (as predicted by theory), the rate constant for the key 1,4-HAT is largest. Overall, it seems reasonable to propose that any substrate from which epoxides have been observed in autoxidations – even as minor products – should yield at least some HOO˙ and therefore, be protected by nitroxides.

Since linear unsaturated hydrocarbons such as those which are abundant in petroleum-derived products and biological lipids autoxidize largely by H-atom abstraction, it is unclear from the

foregoing if the proposed mechanism contributes to their autoxidation and, thus, that they can be inhibited efficiently by nitroxides. Therefore, we carried out co-autoxidations of 1-hexadecene and PBD-BODIPY to find that not only are they inhibited by the addition of each nitroxide (Figure 2.7), but that the inhibited periods correspond to massive stoichiometric factors: $n = 117 \pm 7$ for Ar_2NO and even greater for TEMPO.

For comparison, Ar_2NH is characterized by $n = 23 \pm 3$, which presumably arises since (some of) the amine is converted to the nitroxide *in situ* (detected by EPR, see Supporting Information). This is a striking result; the catalytic radical-trapping antioxidant activity of diarylamines is almost universally ascribed to the Korcek cycle (Figure 2.1B), but at these temperatures, Ar_2NOR is not readily converted to Ar_2NH, and even if it were, Ar_2NH is still significantly less effective than Ar_2NO.[67] It must be emphasized that this is not the only evidence that diarylamines and/or diarylnitroxides catalytically trap radicals via an alternative to the Korcek cycle. For example, an oft-overlooked result of the seminal work of Bolsman et al.[5] is that 4'4-dinitrodiphenylnitroxide is a catalytic inhibitor of paraffin autoxidation at 130 °C, while the corresponding amine is completely ineffective. This could not be explained by the Korcek mechanism and lead the authors to argue that the amines themselves are not involved in the catalytic cycle of diarylamine antioxidants but need to be 'activated' to the catalytic radical-trapping antioxidant: the nitroxide. It is tempting to suggest that the paraffin oil used by Bolsman et al. (Shell ONDINA 33) contained sufficient unsaturation to produce $HOO^{\bullet}$ and enable protection by the nitroxide.

Likewise, this mechanism can account for the 'non-classical' stoichiometries (i.e. $n > 2$) observed for diarylamines in autoxidations carried out at ambient temperatures. For example, some time ago, Lucarini and co-workers reported that phenoxazine was not only among the fastest RTAs ever reported ($k_{inh} = 2.9\times10^7$ $M^{-1}s^{-1}$), but that it trapped an amazing 5 radicals in styrene autoxidations (at 50 °C). Very recently, we revisited this chemistry[68] and found that phenoxazine trapped 10 radicals in styrene at 37 °C – a result which can now be readily explained by the fact that our rate of initiation was lower than Lucarini's, enabling 1,4-HAT/elimination to contribute more to the autoxidation. Interestingly, in our recent studies we were also able to see two distinct phases within the inhibited period of the autoxidation, which can now be understood as an initial phase in which the parent amine traps peroxyl radicals, and a secondary phase wherein the amine-derived nitroxide reacts with $HOO^{\bullet}$ and traps peroxyl radicals as the corresponding hydroxylamine.

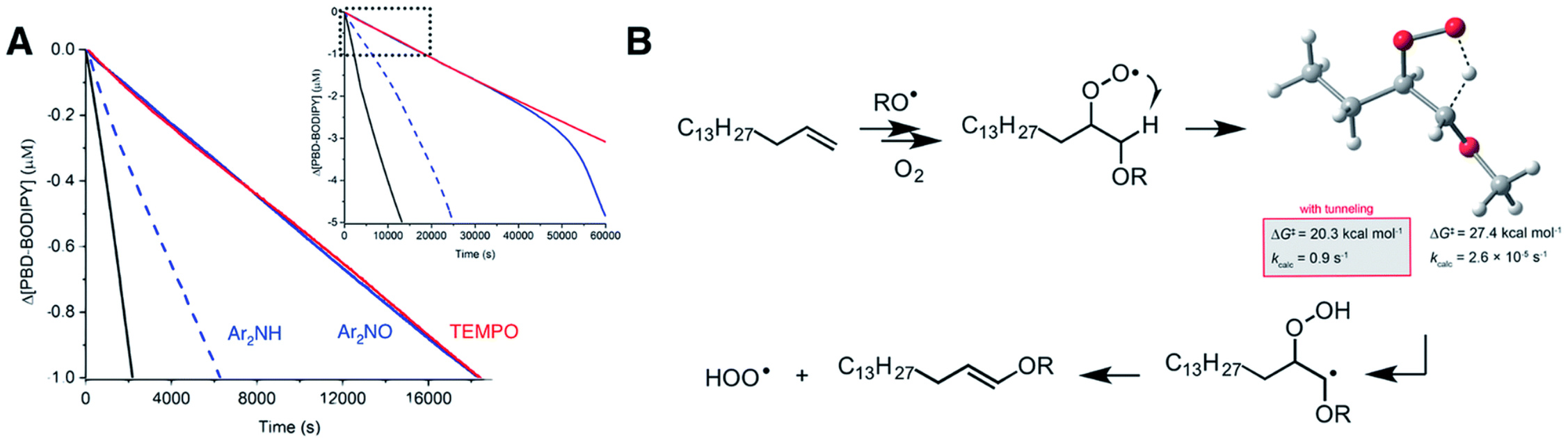

Figure 2.7. (A) Co-autoxidation of 1-hexadecene (2.68 M) and PBD-BODIPY (10 μM) in PhCl initiated with dicumyl peroxide (1 mM) at 100 °C (black line) and inhibited by 2 μM of Ar_2NO (blue line), TEMPO (red line) or Ar_2NH (blue dashed line). Inset: Expanded timescale showing the end of the inhibited periods for Ar_2NO and Ar_2NH. Reaction progress was monitored at 586 nm (ε = 119,166 $M^{-1}cm^{-1}$). (B) Relevant steps for HOO formation in a 1-hexadecene autoxidation along with the calculated transition state structure and activation parameters for the key 1,4-HAT reaction for comparison with corresponding processes in for styrene, cyclooctene and norbornene (Figure 2.5B-D).

2.4. Conclusions

Autoxidations of unsaturated hydrocarbons are very efficiently inhibited by nitroxides and/or compounds which react readily to produce nitroxides under autoxidative conditions. The utilization of HOO• formed in situ as a stoichiometric reductant accounts for the catalytic behaviour of the nitroxides and/or their precursors without invoking a mechanism that requires the formation – and decomposition – of alkoxyamines. Alkoxyamine intermediates are invoked in the Korcek and Denisov mechanisms that have been widely accepted to account for the catalytic active of diarylamines and hindered aliphatic amines, respectively. However, these mechanisms can be expected to apply only when the nitroxide is present at much higher concentrations than O_2, since alkoxyamine formation requires that the nitroxide react with an alkyl radical even though this reaction is characterized by a rate constant that is 10-fold lower than that of the reaction of alkyl radicals with O_2.

Moreover, elevated temperatures are required to convert the alkoxyamine back to the amine at a relevant rate, making it impossible to explain the catalytic reactivity of nitroxides and/or their precursors at ambient to moderate temperatures. The nitroxide-catalyzed cross-dismutation of HOO• and ROO• can account for observations that cannot be explained by the Korcek and Denisov cycles. This mechanism may be most relevant for hindered aliphatic amines/nitroxides since they are used in more applications at ambient temperatures where the rate of initiation is low, and radical-radical reactions are minimized.

2.5. Experimental Procedures

Inhibited Autoxidations

The co-autoxidations were carried out according to our previously published methodology.[18] Briefly, the substrate (1-2 mL) was loaded into a 3 mL cuvette along with the appropriate volume of PhCl such that the final volume of the sample was 2.5 mL. The cuvette was placed into the thermostatted sample holder of a UV−vis spectrophotometer and allowed to equilibrate to the appropriate temperature. STY-BODIPY or PBD-BODIPY (12.5 μL of a 2.0 mM solution in 1,2,4-trichlorobenzene) was then added followed by 50-100 μL of a solution of initiator in PhCl. The solution was thoroughly mixed. The consumption of the probe was monitored for 10-20 min to ensure that the reaction was proceeding with a constant rate, after which the test compound (10 μL of a 500 μM solution) was added, the solution thoroughly mixed once again, and the absorbance readings resumed. Inhibition rate constants (k_{inh}) and stoichiometries (n) were derived from the reaction progress traces analyzed using the equations in Figure 2.1B (see Supporting Information for representative examples).

An analogous procedure was followed when determining nitroxide concentration by EPR in diarylamine-inhibited autoxidations. Reactions were performed under identical conditions in a heat-

block at 70 °C and individual vials removed after the indicated time intervals and transferred to EPR tubes. Spectra were recorded on a Bruker EMXplus (X-band) spectrometer equipped with an ER 4119HS cavity and the radical concentration was determined using the quantitative EPR package of the Bruker Xenon software.

Calculations

Calculations were carried out using the CBS-QB3 complete basis set method[31] as implemented in the Gaussian 16 suite of programs.[69] Rate constants were calculated via transition state theory at 70 °C. The intramolecular hydrogen abstraction step was also calculated using small curvature tunnelling corrections.[70] The evaluation of different calculation methodologies using the oxidation of 1,4-cyclohexadiene as a model are described in the supporting information.

Synthesis of 1,2-d_2-cyclooctene.

A flame-dried 50 mL round-bottomed flask with magnetic stirrer was flushed with N_2, fitted with a rubber septum and charged with cyclooctyne (4.8 g, 44.6 mmol, 1.0 equiv.) in acetone (45 mL). The solution was sparged with N_2 for 5 minutes. Lindlar's catalyst ($Pd/CaCO_3$, poisoned with Pb) (0.48 g, 10 mol%) was added in one portion and the mixture was sparged for an additional 5 minutes. The atmosphere was evacuated and replaced with D_2 via a syringe adapted lecture bottle (1.5 L, 187.3 mmol, 4.2 equiv, 1 bar. 99.99% purity) (The reaction was gently warmed to 30 ^oC and stirred for 36 h. Once the starting material was consumed (as judged by ^1H NMR analysis), the reaction was filtered through a thin pad of Celite/silica gel and the filtrate vacuum distilled. The title product was collected (20 mbar / 63 ^oC) as a clear oil (3.0 g, 60%) following initial removal of acetone (30 mbar / 35 ^oC).[71] ^1H NMR (400 MHz; $CDCl_3$): δ (ppm): 5.62 (m, 0.2H), 2.13 (m, 4H), 1.50 (m, 8H). ^{13}C NMR (101 MHz; $CDCl_3$): 130.0, 29.5, 26.6, 25.3. HRMS (EI) m/z for $C_8H_{12}D_2$, calc: 112.1221, found 112.1256.

2.6. References

1 K. U. Ingold, *Chem. Rev.*, 1961, **61**, 563–589.
2 K. U. Ingold and D. A. Pratt, *Chem. Rev.*, 2014, **114**, 9022–9046.
3 C. E. Boozer, G. S. Hammond, C. E. Hamilton and J. N. Sen, *J. Am. Chem. Soc.*, 2002, **77**, 3233–3237.
4 M. Lucarini, P. Pedrielli, G. Franco Pedulli, L. Valgimigli, D. Gigmes and P. Tordo, *J. Am. Chem. Soc.*, 1999, **121**, 11546–11553.
5 T. A. B. M. Bolsman, A. P. Blok and J. H. G. Frijns, *Recl. des Trav. Chim. des Pays-Bas*, 1978, **97**, 313–319.
6 R. K. Jensen, S. Korcek, M. Zinbo and J. L. Gerlock, *J. Org. Chem.*, 2002, **60**, 5396–5400.
7 E. A. Haidasz, R. Shah and D. A. Pratt, *J. Am. Chem. Soc.*, 2014, **136**, 16643–16650.
8 J. R. Thomas and C. A. Tolman, *J. Am. Chem. Soc.*, 2002, **84**, 2930–2935.
9 K. Adamic, M. Dunn and K. U. Ingold, *Can. J. Chem.*, 1969, **47**, 287–294.
10 E. T. Denisov, *Polym. Degrad. Stab.*, 1989, **25**, 209–215.
11 G. Gryn'ova, K. U. Ingold and M. L. Coote, *J. Am. Chem. Soc.*, 2012, **134**, 12979–12988.
12 I. T. Brownlie and K. U. Ingold, *Can. J. Chem.*, 1967, **45**, 2427–2432.
13 A. L. J. Beckwith, V. W. Bowry and K. U. Ingold, *J. Am. Chem. Soc.*, 1992, **114**, 4983–4992.
14 V. W. Bowry and K. U. Ingold, *J. Am. Chem. Soc.*, 1992, **114**, 4992–4996.
15 B. Maillard, K. U. Ingold and J. C. Scaiano, *J. Am. Chem. Soc.*, 1983, **105**, 5095–5099.
16 E. A. Haidasz, D. Meng, R. Amorati, A. Baschieri, K. U. Ingold, L. Valgimigli and D. A. Pratt, *J. Am. Chem. Soc.*, 2016, **138**, 5290–5298.
17 M. Griesser, R. Shah, A. T. Van Kessel, O. Zilka, E. A. Haidasz and D. A. Pratt, *J. Am. Chem. Soc.*, 2018, **140**, 3798–3808.
18 E. A. Haidasz, A. T. M. Van Kessel and D. A. Pratt, *J. Org. Chem.*, 2016, **81**, 737–744.
19 L. Valgimigli and D. A. Pratt, *Encycl. Radicals Chem. Biol. Mater.*, 2012.
20 B. Li and D. A. Pratt, *Free Radic. Biol. Med.*, 2015, **82**, 187–202.
21 R. Amorati and L. Valgimigli, *Free Radic. Res.*, 2015, **49**, 633–649.
22 The inhibition rate constant for Ar2NH is in excellent agreement with reported values for 4,4′-dialkylated diphenylamines in other substrates. For example, values of 1.8 and 2.0 × 105 M−1 s−1 have been determined at 37 °C for n-octyl and t-butyl substituted diphenylamines by the peroxyl radical clock and STY-BODIPY/dioxane co-autoxidation methodologies, respectively. See ref. 37 and R. Shah , K. D. Margison and D. A. Pratt , *ACS Chem. Biol*., 2017, **12** , 2538
23 The CBS-QB3-calculated N–H BDE in 2,2,6,6,-tetramethylpiperidine and diphenylamine are 96.2 and 86.4 kcal mol−1, respectively. Although there are no reliable experimental values with which the former can be compared, there are ample experimental values for the latter. See, e.g., ref. 24 which yields 85.8 kcal mol^{-1} after the revision in ref. 25
24 D. A. Pratt, G. A. DiLabio, L. Valgimigli, G. F. Pedulli and K. U. Ingold, *J. Am. Chem. Soc.*, 2002, **124**, 11085–11092.
25 P. Mulder, H. G. Korth, D. A. Pratt, G. A. DiLabio, L. Valgimigli, G. F. Pedulli and K. U. Ingold, *J. Phys. Chem. A*, 2005, **109**, 2647–2655.
26 R. Amorati, G. F. Pedulli, D. a Pratt and L. Valgimigli, *Chem. Commun. (Camb).*, 2010, **46**, 5139–5141.
27 J. Cedrowski, G. Litwinienko, A. Baschieri and R. Amorati, *Chem. - A Eur. J.*, 2016, **22**, 16441–16445.
28 J. A. Howard and K. U. Ingold, *Can. J. Chem.*, 1967, **45**, 785–792.
29 L. R. Mahoney, G. D. Mendenhall and K. U. Ingold, *J. Am. Chem. Soc.*, 1973, **95**, 8610–8614.
30 M. Lucarini, G. F. Pedulli and M. Cipollone, *J. Org. Chem.*, 1994, **59**, 5063–5070.
31 J. A. Montgomery, M. J. Frisch, J. W. Ochterski and G. A. Petersson, *J. Chem. Phys.*, 1999, **110**, 2822–2827.

32 Litwinienko and Amorati[27] estimated that the analogous rate constant for the reaction of $HOO^{\cdot}$ and the phenoxyl radical derived from PMC is ca. 109 M^{-1} s^{-1} based upon competition with hydroperoxyl addition to the ring, for which they estimated that the rate constant was the same as for an alkylperoxyl radical (ca. 108 M^{-1} s^{-1}). It is likely that $HOO^{\cdot}$ addition is faster than alkylperoxyl radical addition, and that HAT between $HOO^{\cdot}$ and phenoxyl radicals is also diffusion-controlled.

33 V. Vaidya, K. U. Ingold and D. A. Pratt, *Angew. Chemie - Int. Ed.*, 2009, **48**, 157–160.

34 Z. Zielinski, N. Presseau, R. Amorati, L. Valgimigli and D. A. Pratt, *J. Am. Chem. Soc.*, 2014, **136**, 1570–1578.

35 J. P. R. Chauvin, M. Griesser and D. A. Pratt, *J. Am. Chem. Soc.*, 2017, **139**, 6484–6493.

36 L. Valgimigli, R. Amorati, S. Petrucci, G. F. Pedulli, D. Hu, J. J. Hanthorn and D. A. Pratt, *Angew. Chemie - Int. Ed.*, 2009, **48**, 8348–8351.

37 J. J. Hanthorn, L. Valgimigli and D. A. Pratt, *J. Am. Chem. Soc.*, 2012, **134**, 8306–8309.

38 E. M. Pliss, V. A. Machtin, A. M. Grobov, R. E. Pliss and A. V Sirick, *Int. J. Chem. Kinet.*, 2017, **49**, 173–181.

39 D. G. Hendry and D. Schuetzle, *J. Am. Chem. Soc.*, 1975, **97**, 7123–7127.

40 T. Ohta, *Int. J. Chem. Kinet.*, 1984, **16**, 1495–1503.

41 F. Berho and R. Lesclaux, *Phys. Chem. Chem. Phys.*, 2001, **3**, 970–979.

42 E. C. Tuazon, S. M. Aschmann, M. V. Nguyen and R. Atkinson, *Int. J. Chem. Kinet.*, 2003, **35**, 415–426.

43 E. Estupiñán, E. Villenave, S. Raoult, J. C. Rayez, M. T. Rayez and R. Lesclaux, *Phys. Chem. Chem. Phys.*, 2003, **5**, 4840–4845.

44 J. W. Taylor, G. Ehlker, H. H. Carstensen, L. Ruslen, R. W. Field and W. H. Green, *J. Phys. Chem. A*, 2004, **108**, 7193–7203.

45 It must be acknowledged that computations of such a process – should it exist – would likely require a multi-determinantal approach and dynamic considerations.

46 F. Agapito, P. M. Nunes, B. J. C. Cabral, R. M. B. Dos Santos and J. A. M. Simões, *J. Org. Chem.*, 2007, **72**, 8770–8779.

47 B. Ruscic, R. E. Pinzon, M. L. Morton, N. K. Srinivasan, M. C. Su, J. W. Sutherland and J. V. Michael, *J. Phys. Chem. A.*, 2006, **110**, 6592–6601.

48 W. Suprun and J. Opeida, *Chemie Ing. Tech.*, 2005, **77**, 753–762.

49 F. R. Mayo, *J. Am. Chem. Soc.*, 1958, **80**, 2465–2480.

50 R. G. Naick, W. Pritzkow and J. Rasche, *J. für Prakt. Chemie*, 1977, **319**, 785–789.

51 E. A. Lazurin, V. V Voronenkov and Y. G. Osokin, *Russ. Chem. Rev.*, 1977, **46**, 915–924.

52 D. E. Van Sickle, F. R. Mayo and R. M. Arluck, *J. Am. Chem. Soc.*, 1965, **87**, 4824–4832.

53 K. Blau, U. Müller, W. Pritzkow, W. Schmidt-Renner and Z. Sedshaw, *J. für Prakt. Chemie.*, 1980, **322**, 915–932.

54 G. Czapski, *Annu. Rev. Phys. Chem.*, 1971, **22**, 171–208.

55 It should be noted that the addition of MeOH to styrene/chlorobenzene enhances the activity of the nitroxides but does so far more so for TEMPO than for Ar_2NO; compare n = 26.3 ± 1.0 and 22.0 ± 1.0 in the presence of MeOH to n = 9.3 ± 0.9 and 10.6 ± 0.2 in its absence, respectively.

56 It must be acknowledged that computations of such a process – should it exist – would likely require a multi-determinantal approach and dynamic considerations.

57 The acid-catalyzed reaction of the nitroxide (as in Figure 2.1C) can also be excluded since little acid is formed in hexadecene autoxidations because intermolecular propagation is greatly preferred over the intramolecular propagation that is chiefly responsible for acid formation. See: R. Shah and D. A. Pratt, *J. Org. Chem.*, 2016, **81**, 6649.

58 E. Abuin, M. V Encina, S. Diaz and E. A. Lissi, *Int. J. Chem. Kinet.*, 1978, **10**, 677–686.

59 S. Goldstein and A. Samuni, *J. Phys. Chem. A.*, 2007, **111**, 1066–1072.

60 Styrene/STY-BODIPY co-autoxidations were also carried out in the presence of an H-bond accepting solvent, 2-octanone (see Supporting Information for the data). Again, the initial (inhibited) rate increased and the duration of the inhibited period decreased, consistent with

the intervention of H-bond donating H-atom donors (i.e. hydroxylamines) as the RTAs formed from the nitroxides *in situ*.

61 M. C. Krishna, D. a Grahame, a Samuni, J. B. Mitchell and a Russo, *Proc. Natl. Acad. Sci. U. S. A.*, 1992, **89**, 5537–5541.

62 J. Zádor, C. A. Taatjes and R. X. Fernandes, *Prog. Energy Combust. Sci.*, 2011, **37**, 371–421.

63 J. C. Rienstra-Kiracofe, W. D. Allen and H. F. Schaefer, *J. Phys. Chem. A.*, 2000, **104**, 9823–9840.

64 E. W. Kaiser, *J. Phys. Chem. A*, 2002, **106**, 1256–1265.

65 J. D. Savee, E. Papajak, B. Rotavera, H. Huang, A. J. Eskola, O. Welz, L. Sheps, C. A. Taatjes, J. Zádor and D. L. Osborn, *Science (80-.).*, 2015, **347**, 643–645.

66 E. G. Estupiñán, J. D. Smith, A. Tezaki, S. J. Klippenstein and C. A. Taatjes, *J. Phys. Chem. A*, 2007, **111**, 4015–4030.

67 Although they contribute to the propagation of autoxidation, it is unlikely that reactions of hydroperoxyl and/or alkoxyl radicals with the hydroxylamines are relevant under the reaction conditions. Since both alkoxyl radicals and hydroperoxyl radicals are more reactive than alkylperoxyl radicals, they are less selective for hydroxylamine over the substrate. For example, alkoxyl radicals add/abstract from olefins with $k \sim 10^6\ M^{-1}\ s^{-1}$ and react with hydroxylamines with $k \sim 108\ M^{-1}\ s^{-1}$ (E. Abuin , M. V. Encina , S. Diaz and E. A. Lissi , *Intl. J. Chem. Kinet*., 1978, **10** , 677), whereas alkylperoxyl radicals add/abstract from olefins with $k \sim 1\ M^{-1}\ s^{-1}$, but react with hydroxylamines with $k > 10^6\ M^{-1}\ s^{-1}$. Given the concentration difference (μM vs. M), only the latter competition will be important.

68 L. A. Farmer, E. A. Haidasz, M. Griesser and D. A. Pratt, *J. Org. Chem.*, 2017, **82**, 10523–10536.

69 Since the calculations predict that nitroxide + HOO˙ is diffusion-controlled, inhibition results from the successful competition between the intramolecular 1,4-HAT in the precursor to HOO˙, which is predicted to take place with k ∼ 1 to 10 s−1 depending on the substrate, and hydroxylamine + ROO˙, which we measure to take place with k ∼ 10^6 M−1 s−1. Although the rate constant for the latter is faster, it depends on [nitroxide] which is 2 μM – suggesting that the elimination is competitive under the reaction conditions

70 R. T. Skodje, D. G. Truhlar and B. C. Garrett, *J. Phys. Chem.*, 1981, **85**, 3019–3023.

71 H. Lindlar, *Helv. Chim. Acta.*, 1952, **35**, 446–450.

2.7.1. Supporting Information

2.7.2. General

Reagents were purchased from commercial suppliers and used without further purification unless otherwise indicated. TEMPOH,[1] Ar_2NH,[2] Ar_2NO,[3] Ar_2NOH,[4] Ar_2NOR,[5] TEMPOR,[5] 1-bromocyclooctene[6], 1-cyclooctyne[7], STY-BODIPY[8] and PBD-BODIPY[8] were synthesized using literature procedures. Column chromatography was carried out using flash silica gel (40−63 μm, 230−400 mesh). UV−vis spectra and kinetics were measured on a Cary 100 UV−vis spectrophotometer equipped with a temperature controller unit and a thermostated 6 × 6 multicell holder. ^{1}H and ^{13}C NMR spectra were recorded on Bruker AVANCE spectrometers at 400 and 100 MHz, respectively. ^{1}H and ^{13}C (with ^{1}H decoupling) NMR resonances are referenced to $CHCl_3/CDCl_3$ (7.26 and 77 ppm, respectively). High resolution mass spectra were obtained on a Kratos Concept Tandem mass spectrometer. All synthesized compounds were > 95% pure as determined by ^{1}H NMR.

Cumene and styrene were each extracted three times with NaOH (1M), washed with brine, dried with $MgSO_4$, filtered, distilled under reduced pressure and percolated through a silica column. The purified material could be kept at -20 °C under nitrogen for up to 5 days. Immediately before use, the distilled material was percolated again through a column with silica/basic alumina (1:2). Ethylbenzene and 1-hexadecene were percolated through a column with silica/basic alumina (1:2) immediately before use. Cyclooctene was distilled under reduced pressure (50 mbar/80 °C) and the purified material could be kept at -20 °C under nitrogen for up to 5 days. Norbornene was distilled at atmospheric pressure (120 °C) through a short distillation path and the purified material could be kept at -20 °C under nitrogen for up to 5 days. Dioxane was used directly without prior purification.

2.7.3. Co-autoxidations of Styrene at Lower Temperatures

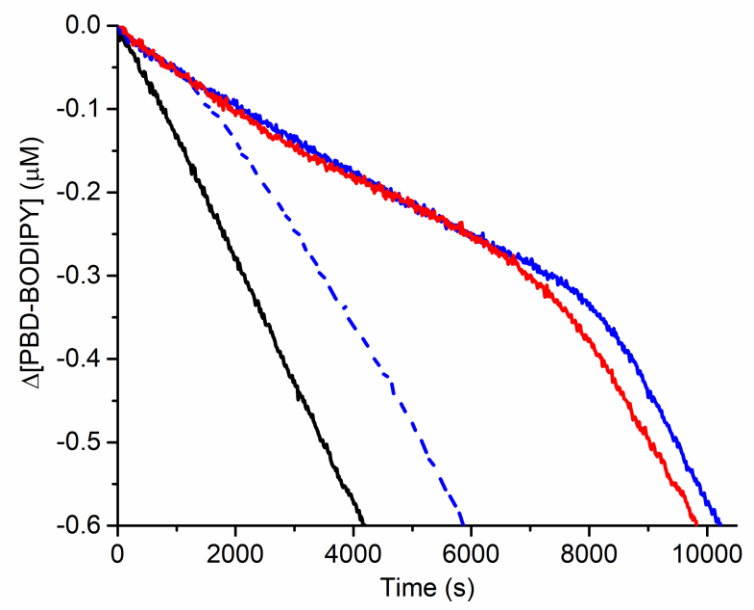

Figure S1: Co-autoxidation of styrene (4.3 M) and PBD-BODIPY (10 μM) in PhCl initiated with AIBN (6 mM) at 37 ºC (black) inhibited by 2 μM of Ar_2NH (blue dashed line), Ar_2NO (blue line), and TEMPO (red line). Reaction progress was monitored at 591 nm (ε = 139,000 $M^{-1}cm^{-1}$).

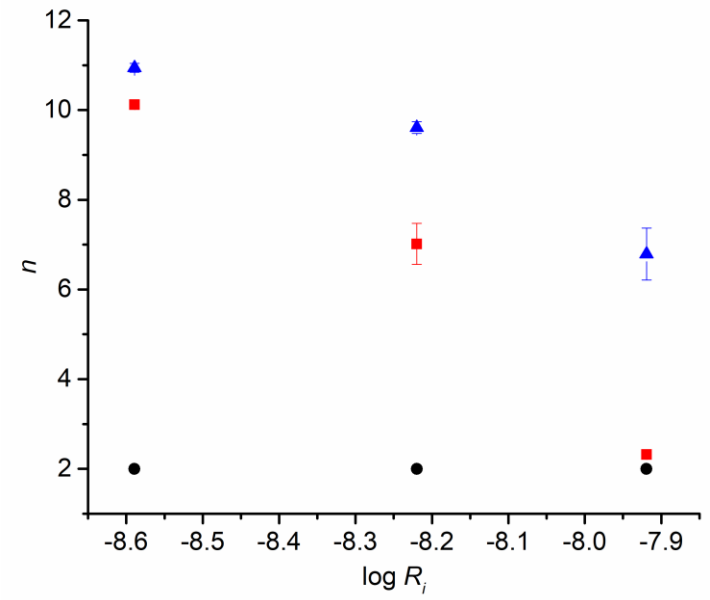

Figure S2: Stoichiometry of peroxyl radical-trapping by Ar_2NO (blue), TEMPO (red) and PMC (black) as a function of rate of initiation of styrene (4.3 M) and PBD-BODIPY (10 μM) co-autoxidations initiated by AIBN (6, 15, and 30 mM) at 37 °C. Reaction progress was monitored at 591 nm (ε = 139,000 M^{-1} cm^{-1}).

2.7.4. Co-autoxidations of Cumene and Styrene under Thomas' Conditions

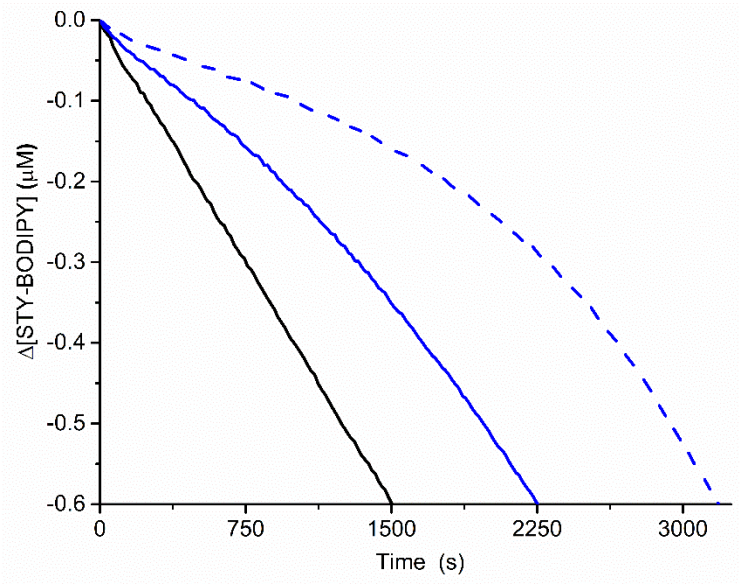

Figure S3. Co-autoxidation of cumene (0.29 M) and STY-BODIPY (10 μM) in PhCl initiated with AIBN (1 mM) at 70 °C (black) inhibited by 50 μM of Ar_2NO (blue) and Ar_2NH (blue dash). Reaction progress was monitored at 570 nm (ε = 122,213 M^{-1} cm^{-1}).

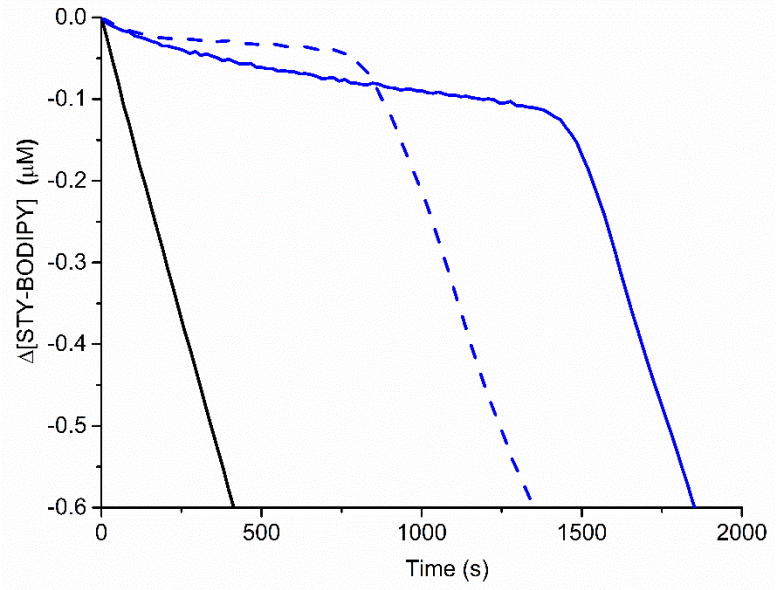

Figure S4. Co-autoxidation of styrene (3.5 M) and STY-BODIPY (10 μM) in PhCl initiated with AIBN (1 mM) at 70 °C (black) inhibited by 50 μM of Ar_2NO (blue) and Ar_2NH (blue dash). Reaction progress was monitored at 571 nm (ε = 97,235 M^{-1} cm^{-1}).

2.7.5. UV-vis Spectra and Extinction Coefficients for STY-BODIPY and PBD-BODIPY

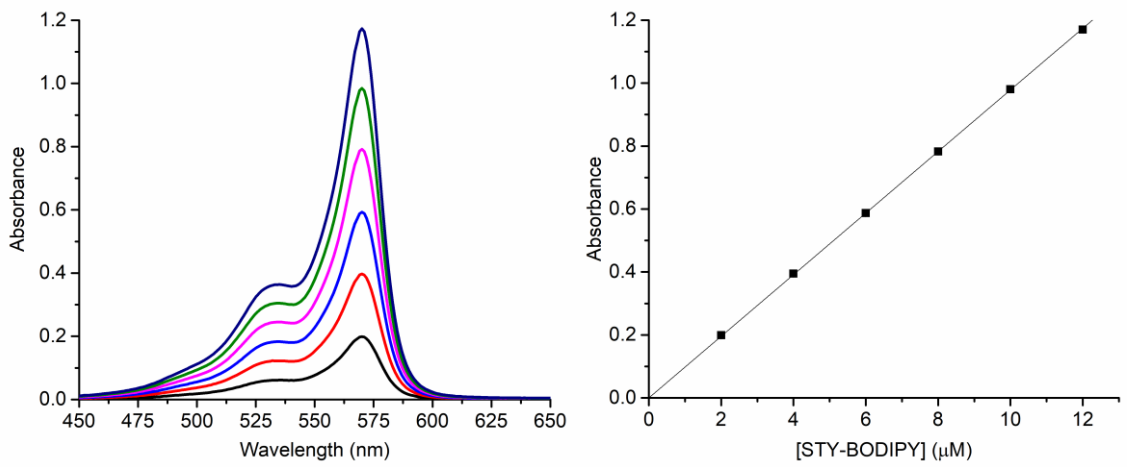

Figure S5. UV-vis spectra for STY-BODIPY (2-12 μM) in 40% v/v styrene/PhCl (left). Extinction coefficient determined for λ_{max} = 571 nm of ε = 97,235 M^{-1} cm^{-1} (right). Average of three measurements (error bars are too small to be resolved from the data points).

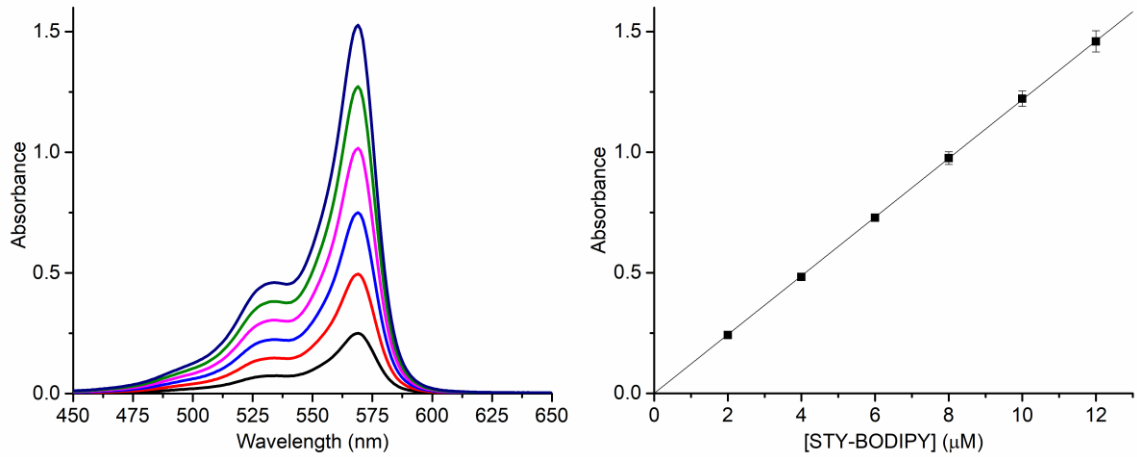

Figure S6. UV-vis spectra for STY-BODIPY (2-12 μM) in 40% v/v cumene/PhCl (left). Extinction coefficient determined for λmax = 570 nm of ε = 112,213 M^{-1} cm^{-1} (right). Average of three measurements (error bars are too small to be resolved from the data points).

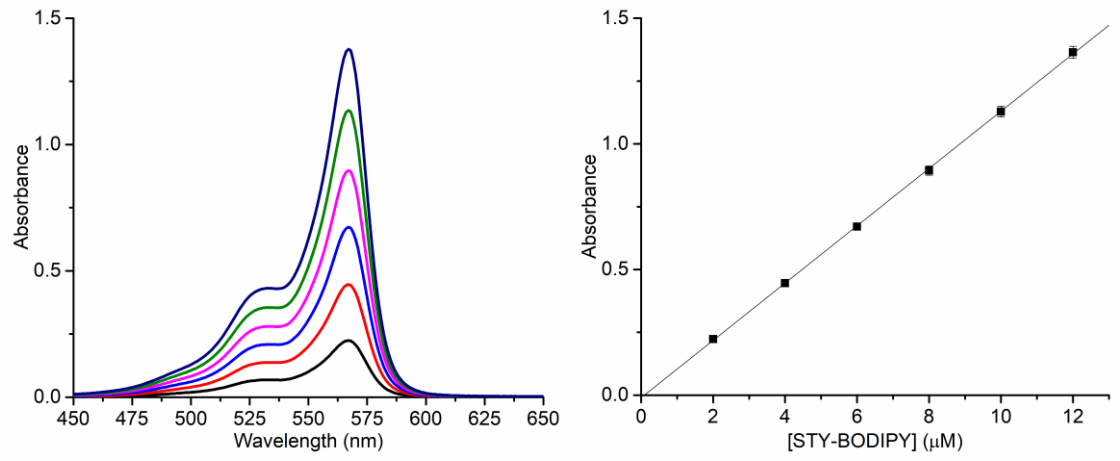

Figure S7. UV-vis spectra for STY-BODIPY (2-12 μM) in 40% v/v dioxane/PhCl (left). Extinction coefficient determined for λ_{max} = 568 nm of ε = 113,982 M^{-1} cm^{-1} (right). Average of three measurements (error bars are too small to be resolved from the data points).

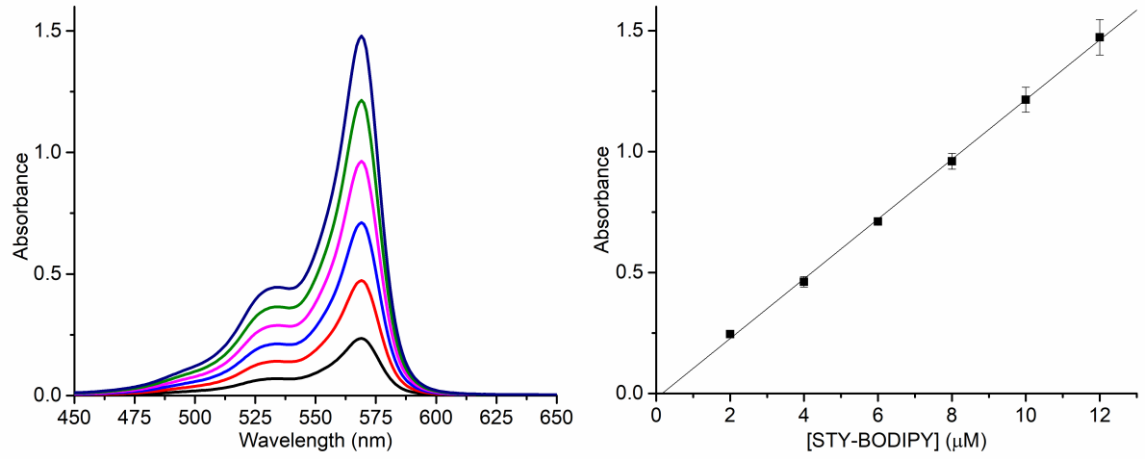

Figure S8. UV-vis spectra for STY-BODIPY (2-12 μM) in 40% v/v ethylbenzene/PhCl (left). Extinction coefficient determined for λmax = 569 nm of ε = 123,481 M^{-1} cm^{-1} (right). Average of three measurements (error bars are too small to be resolved from the data points).

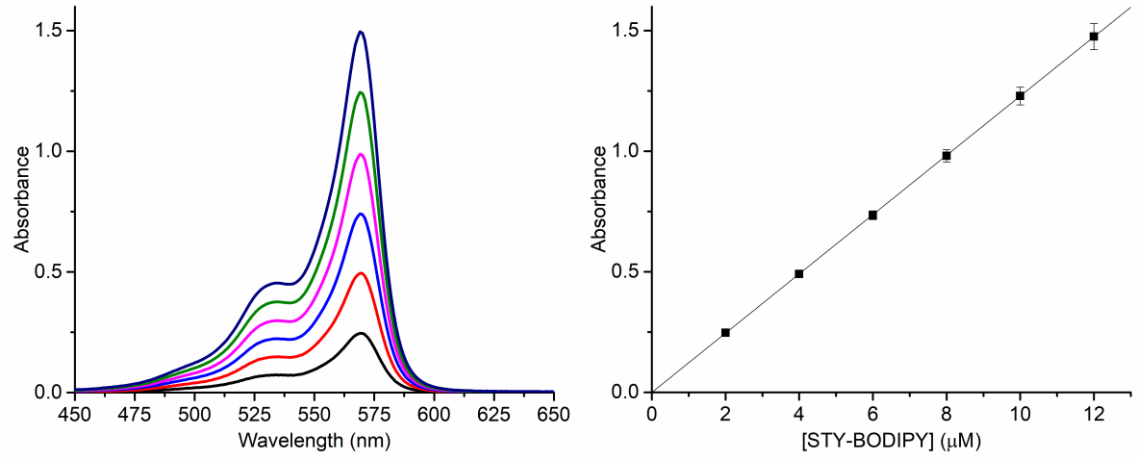

Figure S9. UV-vis spectra for STY-BODIPY (2-12 μM) in 1 M norbornene in PhCl (left). Extinction coefficient determined for λ_{max} = 569 nm of ε = 122,873 M^{-1} cm^{-1} (right). Average of three measurements (error bars are too small to be resolved from the data points).

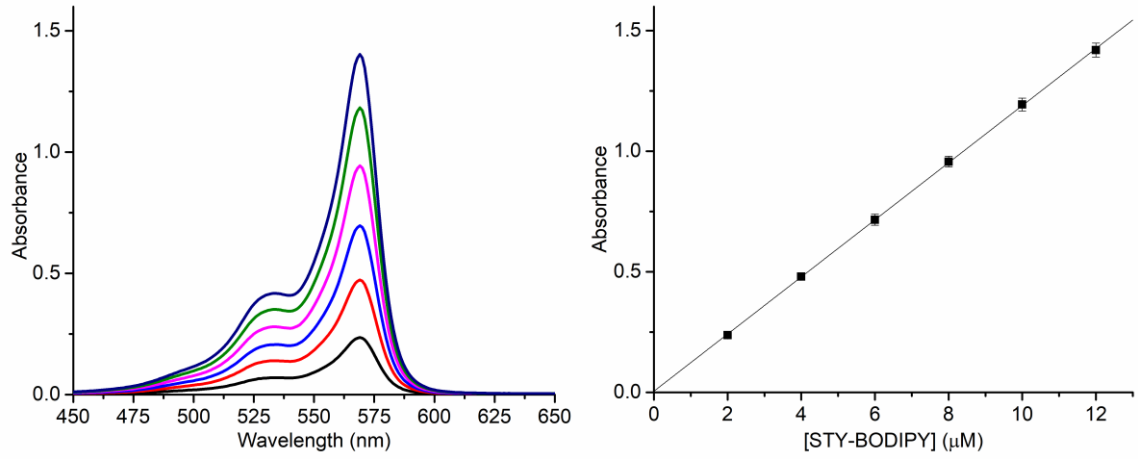

Figure S10. UV-vis spectra for STY-BODIPY (2-12 μM) in 40% v/v cyclooctene/PhCl (left). Extinction coefficient determined for λmax = 568 nm of ε = 118,405 M^{-1} cm^{-1} (right). Average of three measurements (error bars are too small to be resolved from the data points).

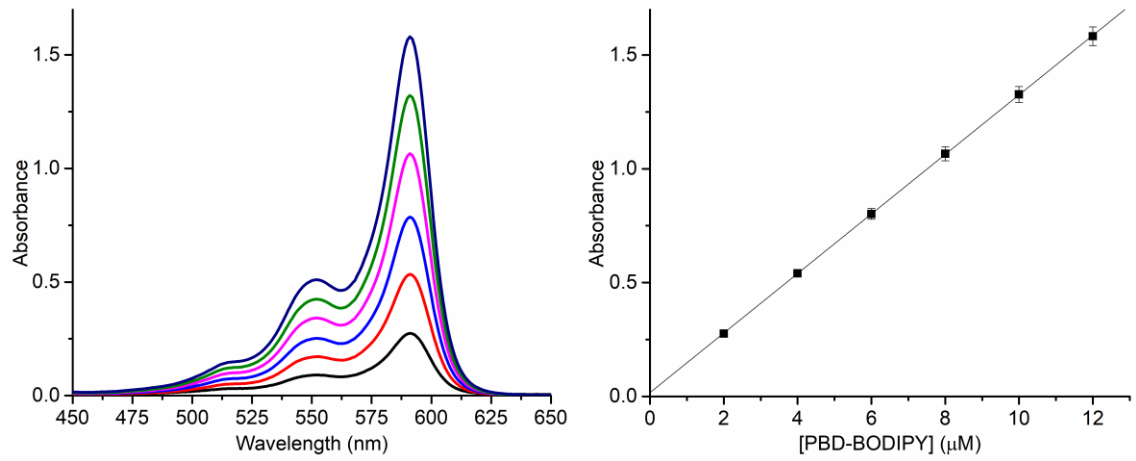

Figure S11. UV-vis spectra for PBD-BODIPY (2-12 μM) in 2.5% v/v 1,4-cyclohexadiene/PhCl (left). Extinction coefficient determined for λ_{max} = 591 nm of ε = 130,797 M^{-1} cm^{-1} (right). Average of three measurements (error bars are too small to be resolved from the data points).

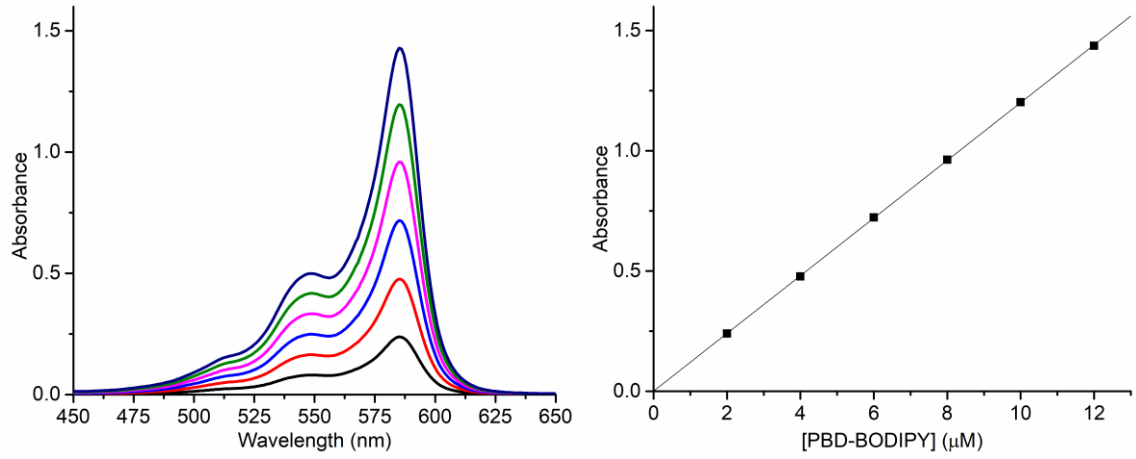

Figure S12. UV-vis spectra for STY-BODIPY (2-12 μM) in 80% v/v 1-hexadecene/PhCl (left). Extinction coefficient determined for λmax = 591 nm of ε = 119,166 M^{-1} cm^{-1} (right). Average of three measurements (error bars are too small to be resolved from the data points).

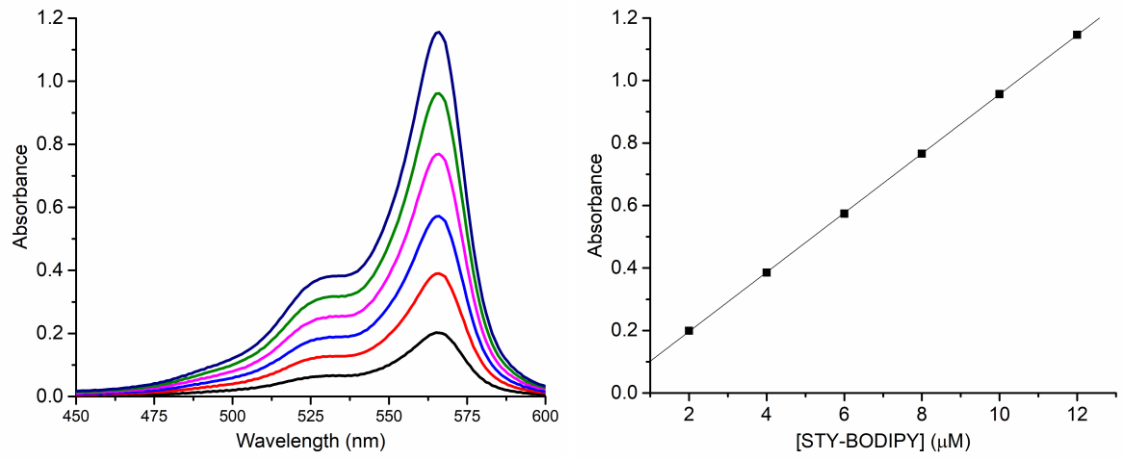

Figure S13. UV-vis spectra for STY-BODIPY (2-12 μM) in 40% v/v styrene/2-octanone (left). Extinction coefficient determined for λ_{max} = 566 nm of ε = 94,876 M^{-1} cm^{-1} (right). Average of three measurements (error bars are too small to be resolved from the data points).

2.7.6. Rate of Initiation Determination by the Inhibitor Method

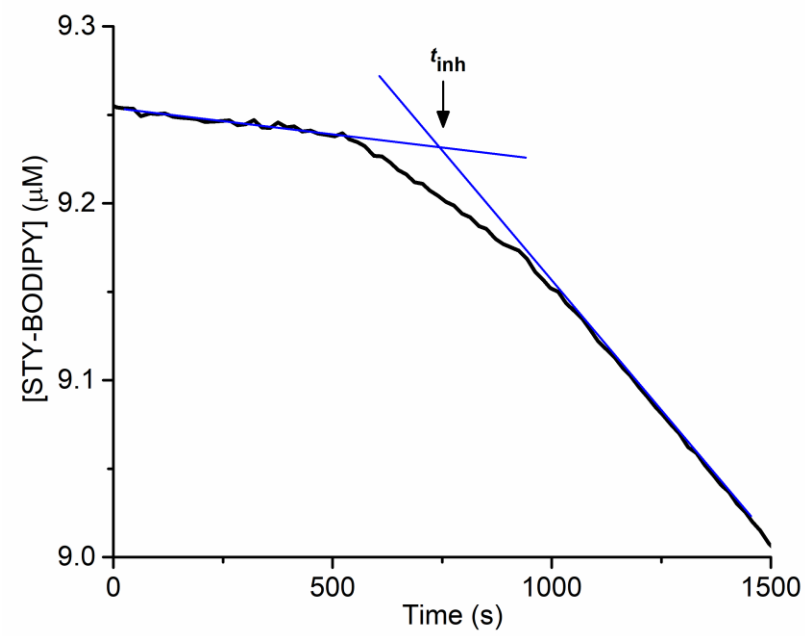

Figure S14. Identification of the inhibited period from a representative co-autoxidation of styrene (3.5 M) and STY-BODIPY (10 μM) in PhCl initiated with di-*tert*-butylperoxide (218 mM) at 70 °C inhibited by PMC (4.0 μM). Reaction progress was monitored by absorbance at 571 nm (ε = 97,235 $M^{-1}cm^{-1}$). From the average of three measurements t_{inh} = 884 s and R_i = 4.5 ± 0.3 × 10^{-9} M s^{-1} was calculated from 2[PMC]/t_{inh}.

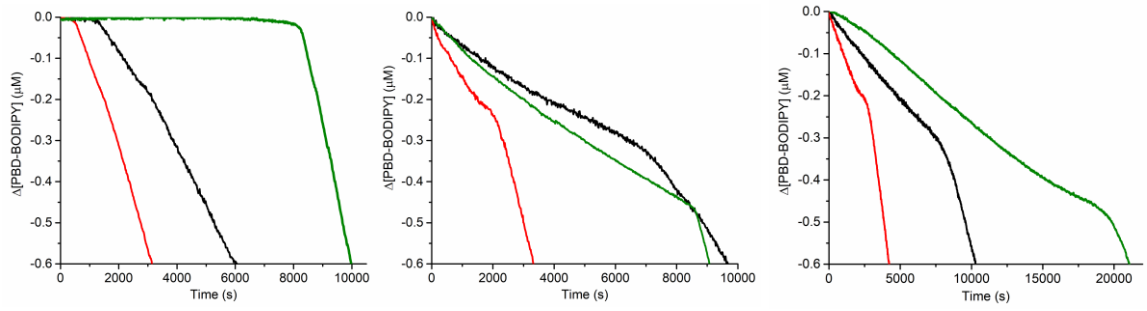

Figure S15. Representative co-autoxidation of styrene (4.3 M) and PBD-BODIPY (10 μM) in PhCl at 37 °C, initiated with AIBN (6 (black), 15 (red) mM) inhibited by 2.0 μM of PMC (left) or 2.0 μM TEMPO (middle) and 2.0 μM of Ar_2NO (right) or initiated with 30 mM AIBN (green) inhibited by 50 μM PMC (left), TEMPO (middle) or Ar_2NO (right). Reaction progress was monitored at 591 nm (ε = 139,000 M^{-1} cm^{-1}).

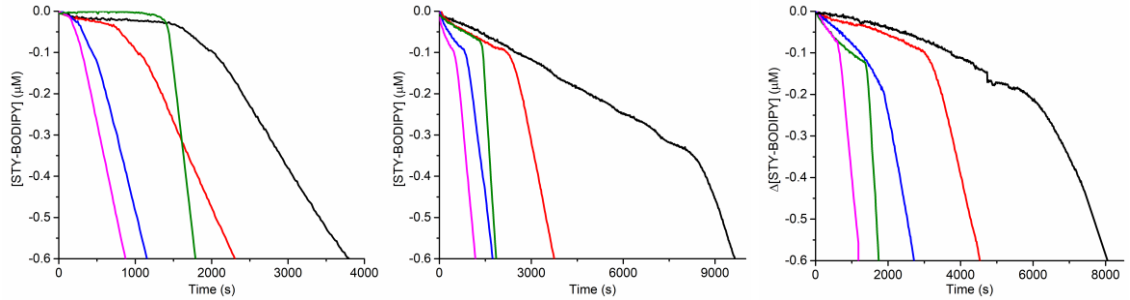

Figure S16. Representative co-autoxidation of styrene (3.5 M) and STY-BODIPY (10 μM) in PhCl at 70 °C, initiated with AIBN (62.5 (black), 125 (red), 250 (blue), 375 (magenta) μM) inhibited by 4.0 μM of PMC (left) or 2.0 μM TEMPO (middle) and 2.0 μM of Ar_2NO (right) or initiated with 1 mM AIBN (green) inhibited by 50 μM PMC (left), TEMPO (middle) or Ar_2NO (right). Reaction progress was monitored at 571 nm (ε = 97,235 M^{-1} cm^{-1}).

Table 2.1. Rates of Initiation Obtained from PMC-Inhibited Autoxidations Under Various Conditions.

substrate	T (°C)	solvent	initiator	[initiator] (mM)	R_i (s^{-1})
styrene	37	PhCl	AIBN	6	$2.6 \pm 0.2 \times 10^{-9}$
styrene	37	PhCl	AIBN	15	$6.0 \pm 0.2 \times 10^{-9}$
styrene	37	PhCl	AIBN	30	$1.2 \pm 0.4 \times 10^{-8}$
styrene	70	PhCl	^{t}BuOO^{t}Bu	218	$4.5 \pm 0.3 \times 10^{-9}$
styrene	70	2-octanone	^{t}BuOO^{t}Bu	218	$4.2 \pm 0.2 \times 10^{-9}$
styrene	70	PhCl	AIBN	6.25×10^{-3}	$3.7 \pm 0.3 \times 10^{-9}$
styrene	70	PhCl	AIBN	1.25×10^{-2}	$7.2 \pm 0.2 \times 10^{-9}$
styrene	70	PhCl	AIBN	2.50×10^{-2}	$1.4 \pm 0.1 \times 10^{-8}$
styrene	70	PhCl	AIBN	3.75×10^{-2}	$1.9 \pm 0.2 \times 10^{-8}$
styrene	70	PhCl	AIBN	1	$6.1 \pm 0.1 \times 10^{-8}$
cumene	70	PhCl	AIBN	1	$6.1 \pm 0.3 \times 10^{-8}$
1,4-dioxane	70	PhCl	^{t}BuOO^{t}Bu	218	$5.6 \pm 0.1 \times 10^{-9}$
ethylbenzene	70	PhCl	^{t}BuOO^{t}Bu	87	$3.0 \pm 0.1 \times 10^{-9}$
norbornene	70	PhCl	^{t}BuOO^{t}Bu	218	$7.5 \pm 0.4 \times 10^{-9}$
cyclooctene	70	PhCl	^{t}BuOO^{t}Bu	218	$4.5 \pm 0.2 \times 10^{-9}$
1-hexadecene	70	PhCl	^{t}BuOO^{t}Bu	87	$1.1 \pm 0.1 \times 10^{-9}$
1-hexadecene	100	PhCl	dicumyl peroxide	1	$4.6 \pm 0.4 \times 10^{-9}$
1,4-cyclohexadiene	30	PhCl	^{t}BuOO^{t}Bu	218	N/A

2.7.7. Propagation Rate Constant Determination for STY-BODIPY and PBD-BODIPY Under Various Conditions

Co-autoxidations for determination of propagation rate constants for reactions of alkylperoxyl radicals with STY-BODIPY/PBD-BODIPY. Freshly purified substrate: styrene, cumene, ethylbenzene, dioxane, cyclooctene, norbornene or1-hexadecene was loaded into a 3 mL cuvette and diluted in PhCl to a final volume of 2.5 mL. The cuvette was placed into the thermostated sample holder of a UV−vis spectrophotometer and allowed to equilibrate to 70-100 °C. A small aliquot (2.5 μL, 5.0 μL, 7.5 μL, 10.0

μL, 12.5 μL, 15.0 μL) of a 2.0 mM solution of the BODIPY probe in 1,2,4-trichlorobenzene was added to each cuvette, followed by initiator, and the solution was thoroughly mixed. The absorbance at either 586-591 nm (PBD-BODIPY) or 566-571 nm (STY-BODIPY) was monitored.

$$\frac{-\partial[\text{PBD-BODIPY}]}{\partial t} = \frac{k_{\text{PBD-BODIPY}}}{\sqrt{2k_t}}\sqrt{R_i}\,[\text{PBD-BODIPY}]$$

A plot of the rate of dye consumption versus the dye concentration yields a line where the slope is given by a combination of k_p, R_i, and $\sqrt{2k_t}$. The rate of initiation for the exact reaction conditions of each system can be determined from the times of inihibition of an inhibited autoxidation with an RTA of known concentration and stoichiometric number. The mechanism of PMC-inhibited autoxidations is well-established and as such PMC was chosen to determine R_i for these systems. Despite multiple termination pathways being feasible for termination, the rate of termination is largely dictated by the radical-radical reaction of two substrate-derived alkylperoxyl radicals.

Using these values of k_t and R_i, the rate constant for the reaction between STY-BODIPY/PBD-BODIPY and peroxyl radicals can be calculated for each of the given co-autoxidations.

$$\frac{k_{t1}}{k_{t2}} = \frac{Ae^{\frac{-E_a}{RT_1}}}{Ae^{\frac{-Ea}{RT_2}}}$$

Literature values for rates of termination at 30 °C were determined by the rotating sector method by Howard and Ingold[9,10,11] and extrapolated to 70 °C using the ratio of Arrhenius equations shown above. Where rates of termination could not be located, the value for styrene was used seeing as the nature of the terminating radical in all cases studied was secondary and styrene offered the best approximation for the end reaction. The k_p determination for styrene/PBD-BODIPY co-autoxidations at 37 °C was previously reported by Haidasz et al.[8] The E_a value of sec-butyl peroxyl Russell termination (2.3 kcal mol^{-1}) was used to simulate the nature of chain terminating reactions of secondary alkylperoxyls from the work of Lee et al.[12]

Table 2.2. Summary of termination rate constants (k_t) derived from rotating sector experiments and extrapolated to higher temperatures using a k_1/k_2 ratio of the Arrhenius equation

substrate	T (°C)	k_{t30}	k_t at T(°C)
styrene	70	2.1 x 10^7 $M^{-1}s^{-1}$	3.4 x 10^7 $M^{-1}s^{-1}$
1,4-dioxane	70	2.5 x 10^7 $M^{-1}s^{-1}$	3.9 x 10^7 $M^{-1}s^{-1}$
ethylbenzene	70	1.6 x 10^7 $M^{-1}s^{-1}$	2.5 x 10^7 $M^{-1}s^{-1}$
norbornene[a]	70	2.1 x 10^7 $M^{-1}s^{-1}$	3.4 x 10^7 $M^{-1}s^{-1}$
cyclooctene[a]	70	2.1 x 10^7 $M^{-1}s^{-1}$	3.4 x 10^7 $M^{-1}s^{-1}$

1-hexadecene[b]	70	1.3 x 10^8 $M^{-1}s^{-1}$	2.0 ± 10^8 $M^{-1}s^{-1}$
1-hexadecene[b]	100	1.3 x 10^8 $M^{-1}s^{-1}$	2.7 ± 10^8 $M^{-1}s^{-1}$

[a]k_t of secondary styrylperoxyls at 30 °C used in place of shown substrate

[b]k_t of 1-octene derived secondary peroxyls at 30 °C used in place of shown substrate

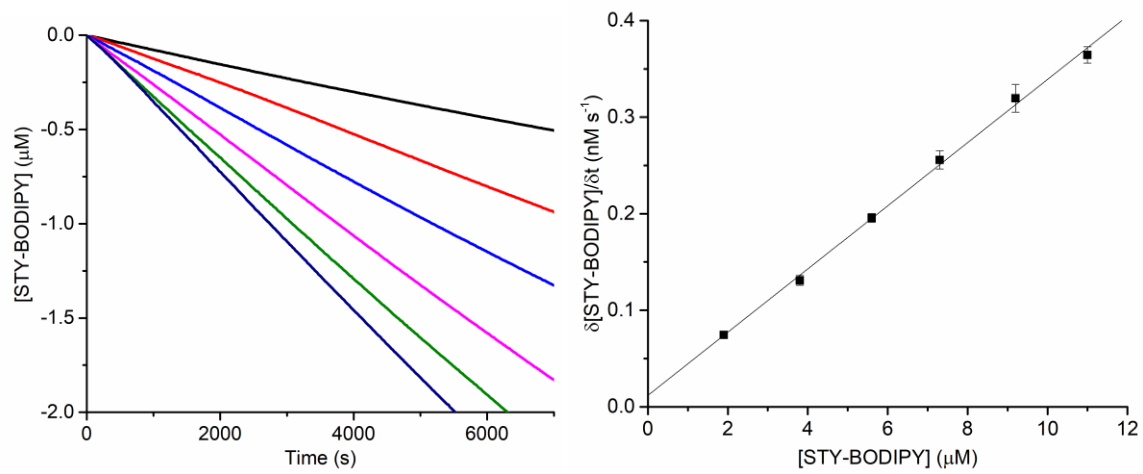

Figure S17. Co-autoxidation of STY-BODIPY and styrene (3.5 M) in PhCl at 70 °C initiated by di-*tert*-butylperoxide (218 mM) as a function of STY-BODIPY concentration (left). Reaction progress was monitored by absorbance at 571 nm (ε = 97,235 M^{-1} cm^{-1}), and the observed rates were plotted as a function of STY-BODIPY concentration (right) to yield k_p = 4012 ± 96 M^{-1} s^{-1}.

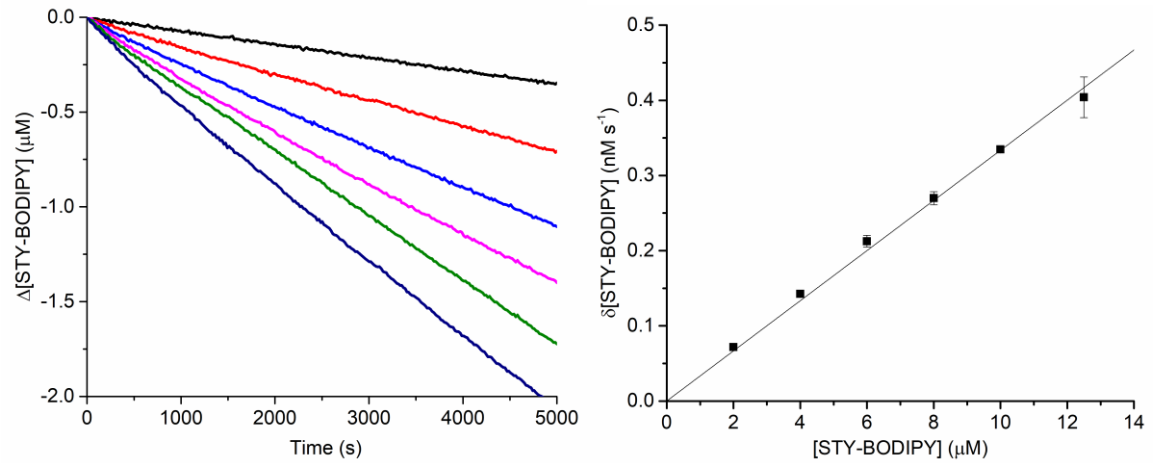

Figure S18. Co-autoxidation of STY-BODIPY and styrene (3.5 M) in 2-octanone at 70 °C initiated by di-*tert*-butylperoxide (218 mM) as a function of STY-BODIPY concentration (left). Reaction progress was monitored by absorbance at 566 nm (ε = 94,876 M^{-1} cm^{-1}), and the observed rates were plotted as a function of STY-BODIPY concentration (right) to yield k_p = 4004 ± 264 M^{-1} s^{-1}.

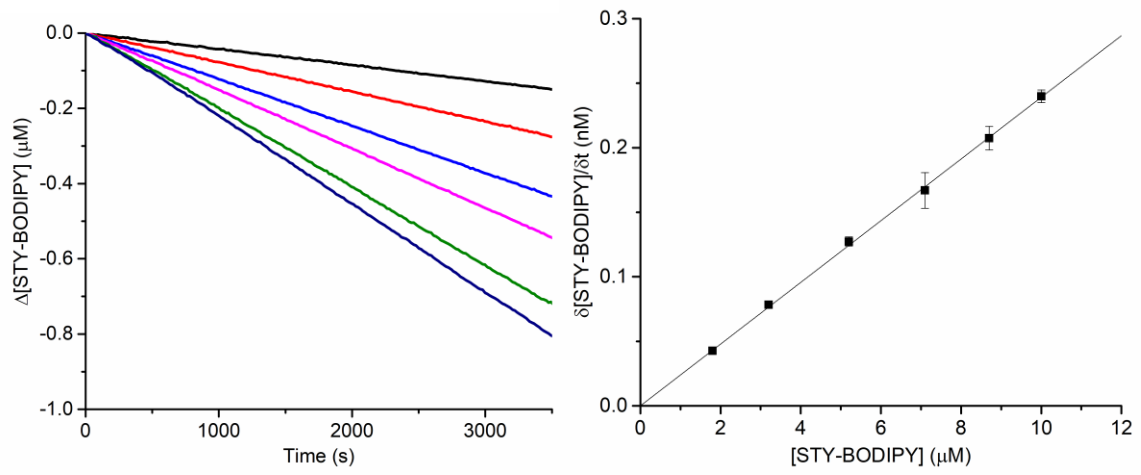

Figure S19. Co-autoxidation of STY-BODIPY and cyclooctene (3.1 M) in PhCl at 70 °C initiated by di-*tert*-butylperoxide (218 mM) as a function of STY-BODIPY concentration (left). Reaction progress was monitored by absorbance at 568 nm (ε = 118,405 M^{-1} cm^{-1}), and the observed rates were plotted as a function of STY-BODIPY concentration (right) to yield k_p = 2689 ± 134 M^{-1} s^{-1}.

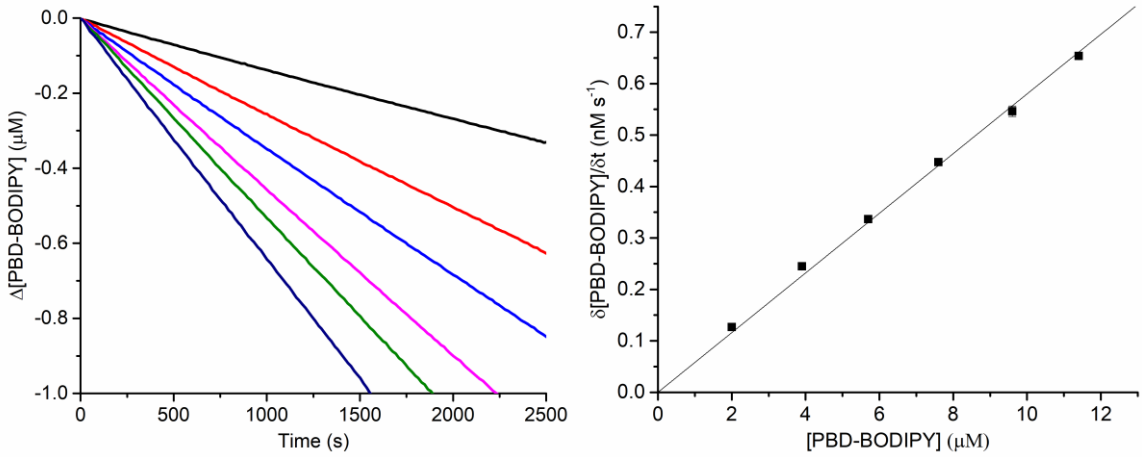

Figure S20. Co-autoxidation of PBD-BODIPY and 1-hexadecene (2.8 M) in PhCl at 100 °C initiated by dicumylperoxide (1 mM) as a function of PBD-BODIPY concentration (left). Reaction progress was monitored by absorbance at 586 nm (ε = 119,166 M^{-1} cm^{-1}), and the observed rates were plotted as a function of PBD-BODIPY concentration (right) to yield k_p = 17, 802 ± 414 M^{-1} s^{-1}.

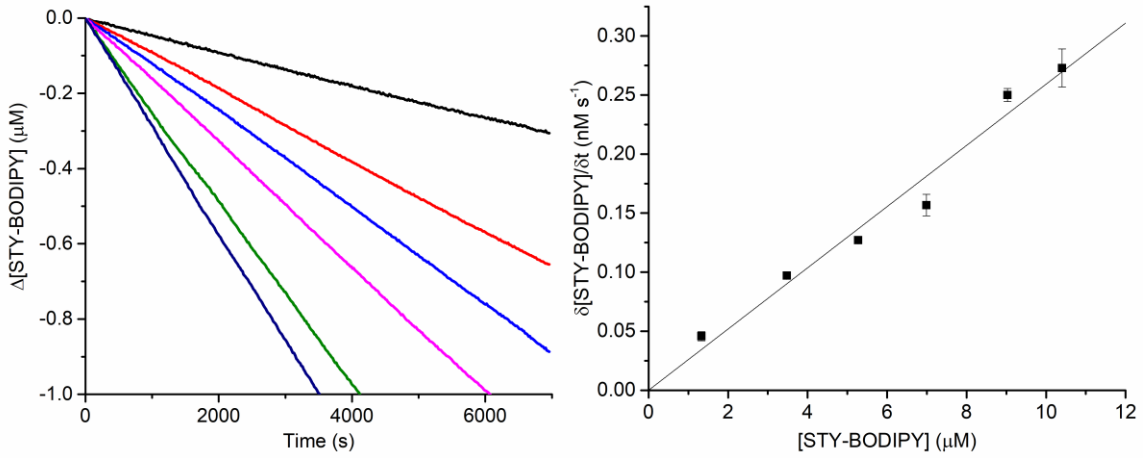

Figure S21. Co-autoxidation of STY-BODIPY and ethylbenzene (3.3 M) in PhCl at 70 °C initiated by di-*tert*-butylperoxide (87 mM) as a function of STY-BODIPY concentration (left). Reaction progress was monitored by absorbance at 569 nm (ε = 123,481 M^{-1} cm^{-1}), and the observed rates were plotted as a function of STY-BODIPY concentration (right) to yield k_p = 3402 ± 195 M^{-1} s^{-1}.

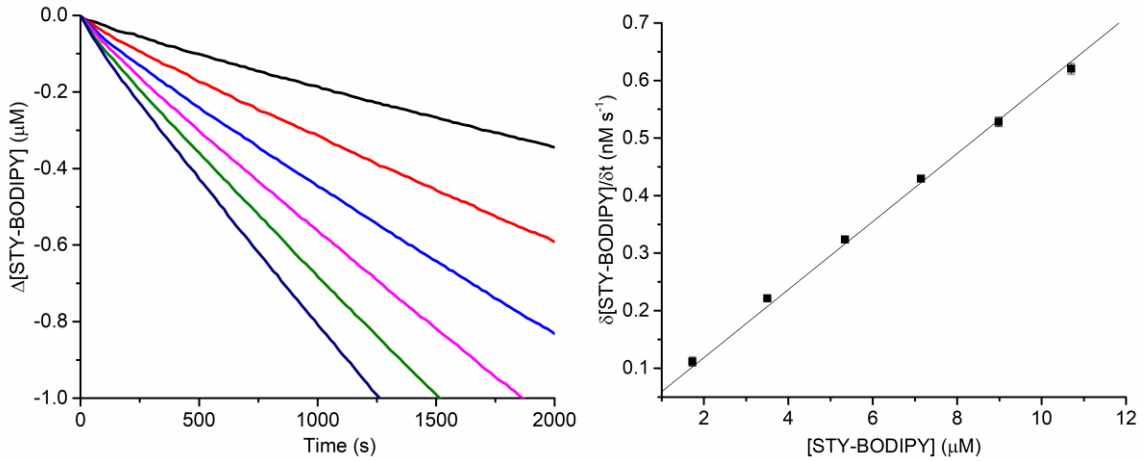

Figure S22. Co-autoxidation of STY-BODIPY and 1,4 dioxane (2.9 M) in PhCl at 70 °C initiated by di-*tert*-butylperoxide (218 mM) as a function of STY-BODIPY concentration (left). Reaction progress was monitored by absorbance at 568 nm (ε = 113,982 M^{-1} cm^{-1}), and the observed rates were plotted as a function of STY-BODIPY concentration (right) to yield k_p = 6707 ± 44 M^{-1} s^{-1}.

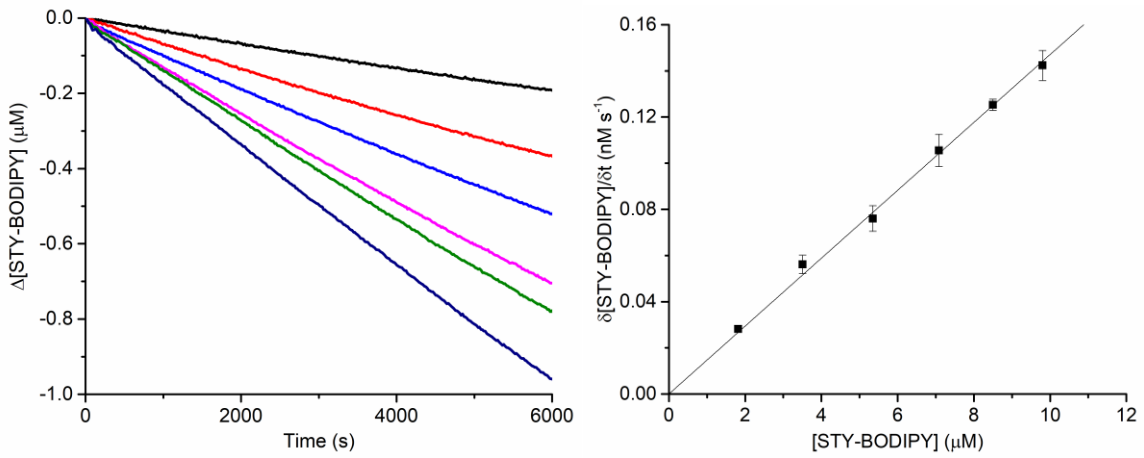

Figure S23. Co-autoxidation of STY-BODIPY and norbornene (1.0 M) in PhCl at 70 °C initiated by di-*tert*-butylperoxide (218 mM) as a function of STY-BODIPY concentration (left). Reaction progress was monitored by absorbance at 569 nm (ε = 122,873 M^{-1} cm^{-1}), and the observed rates were plotted as a function of STY-BODIPY concentration (right) to yield k_p = 1358 ± 47 M^{-1} s^{-1}.

2.7.8. Supplemental Data for KIE and KSE Determinations

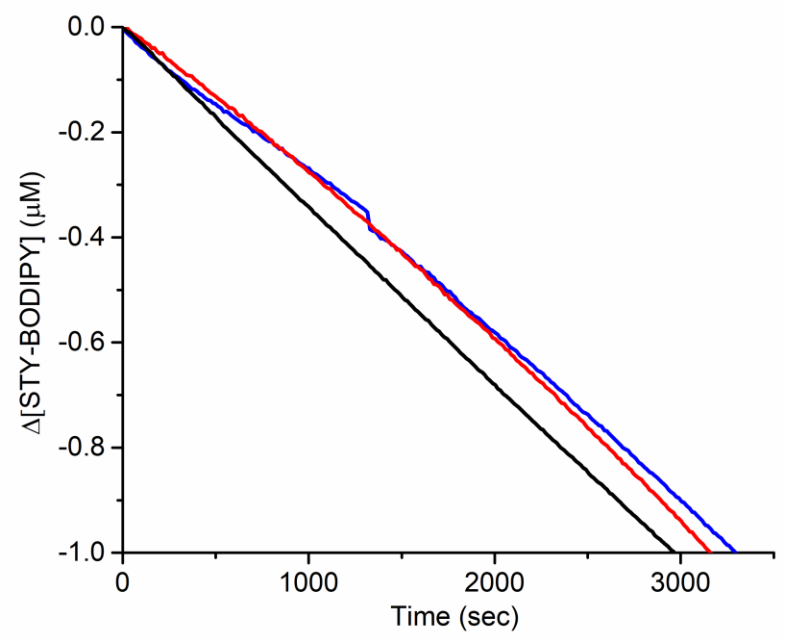

Figure S24: Representative co-autoxidations of styrene (3.5 M) and STY-BODIPY (10 μM) in PhCl (black) with 1% MeOH (blue) or 1% MeOD (red) initiated with di-*tert*-butylperoxide (218 mM) at 70 °C. Reaction progress was monitored at 571 nm (ε = 97,235 M^{-1} cm^{-1}).

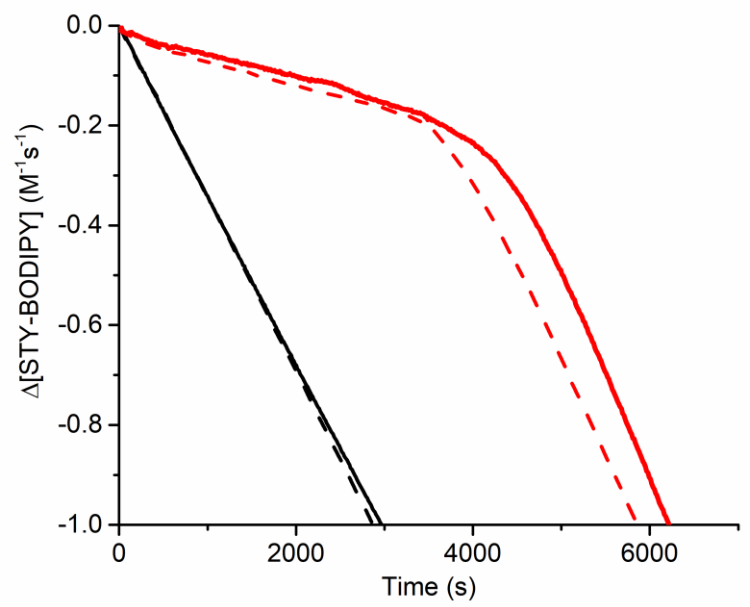

Figure S25. Representative co-autoxidations of styrene (3.5 M) and STY-BODIPY (10 μM) in PhCl (solid) or 2-octanone (dashed) initiated with di-*tert*-butylperoxide (218 mM) at 70 °C (black) inhibited by TEMPO (red). Reaction progress was monitored at 571 nm (ε = 97,235 M^{-1} cm^{-1}) for PhCl or 566 nm (ε = 94,876 M^{-1} cm^{-1}) for 2-octanone.

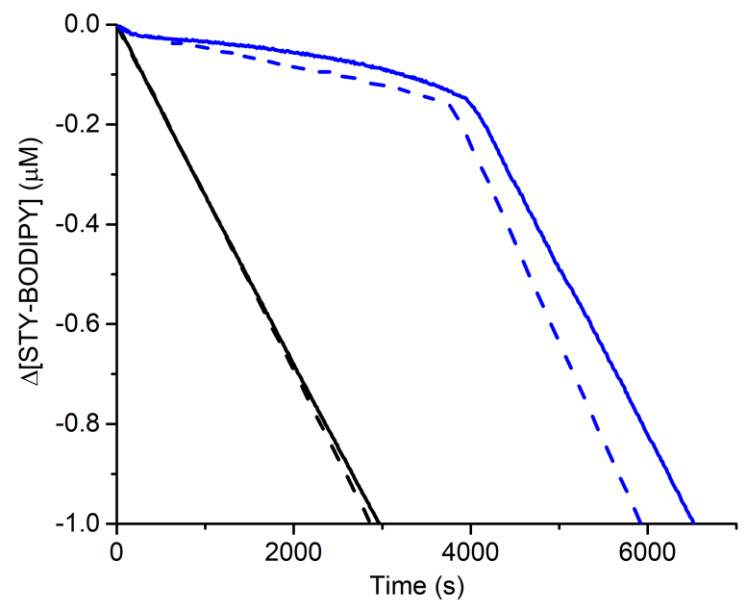

Figure S26. Representative reaction progress curves for the co-autoxidation of styrene (3.5 M) and STY-BODIPY (10 μM) in PhCl (solid) or 2-octanone (dashed) initiated with di-*tert*-butylperoxide (218 mM) at 70 ºC (black) inhibited by Ar_2NO (blue). Reaction progress was monitored at 571 nm (ε = 97,235 M^{-1} cm^{-1}) for PhCl or 566 nm (ε = 94,876 M^{-1} cm^{-1}) for 2-octanone.

2.7.9. Monitoring of Nitroxide Formation from Diarylamine during Autoxidations

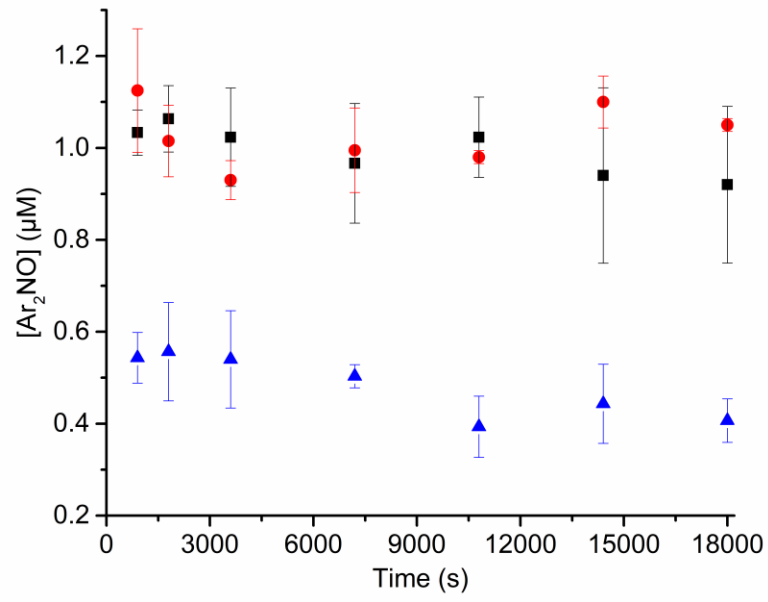

Figure S27. Concentration of Ar_2NO determined by EPR during Ar_2NH-inhibited autoxidations. Cyclooctene (3.1 M, black), norbornene (1.0 M, blue) and 1-hexadecene (2.7 M, red) in PhCl initiated with di-*tert*-butylperoxide (218 mM) inhibited by 2.0 μM of Ar_2NH.

2.7.10. Autoxidations of Deuterated Cyclooctene

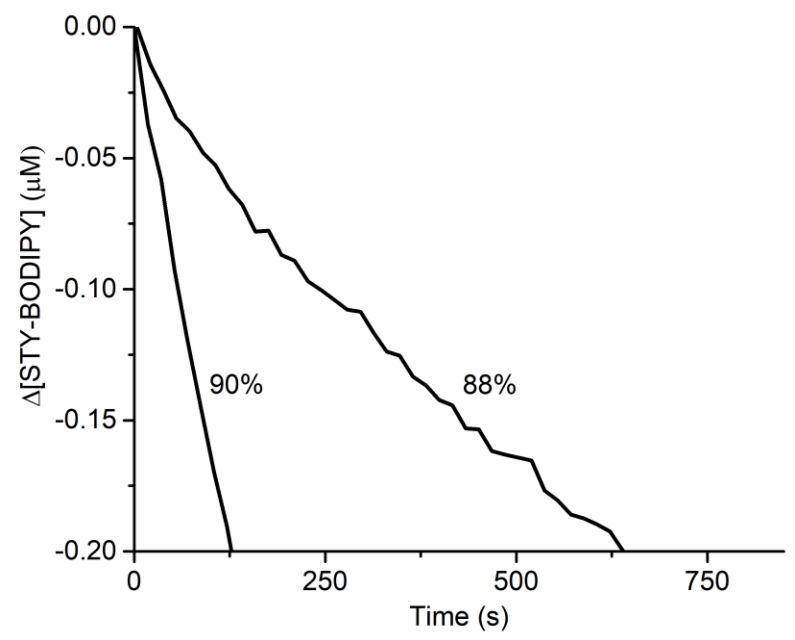

Figure S28 Co-autoxidation of 1,2-d_2-cyclooctene (88 and 90% deuterium incorporation) (3.1 M) and STY-BODIPY (10 μM) in PhCl initiated with di-*tert*-butylperoxide (218mM) at 70 °C. Reaction progress was monitored at 568 nm (ε =118,405 M^{-1} cm^{-1}).

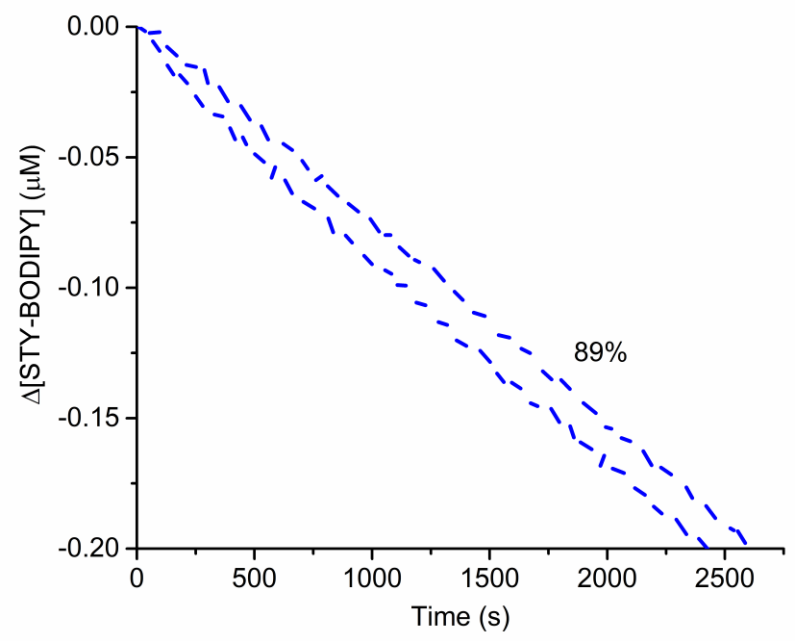

Figure S29. Co-autoxidation of 1,2-d_2-cyclooctene (89% deuterium incorporation) (3.1 M) and STY-BODIPY (10 μM) in PhCl initiated with di-*tert*-butylperoxide (218 mM) inhibited by DTBNH (blue dash). Reaction progress was monitored at 568 nm (ε =118,405 M^{-1} cm^{-1}).

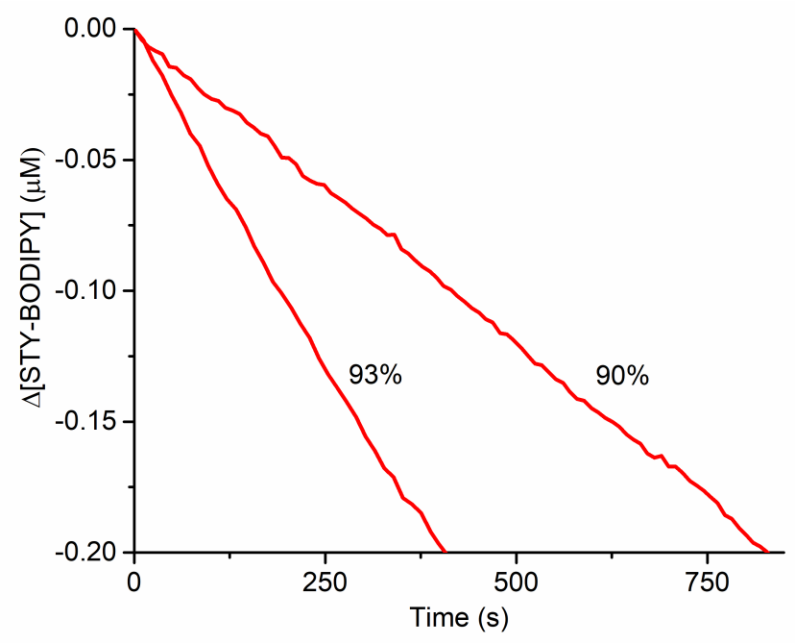

Figure S30. Co-autoxidation of 1,2-d_2-cyclooctene (90 and 93% deuterium incorporation) (3.1 M) and STY-BODIPY (10 μM) in PhCl initiated with di-*tert*-butylperoxide (218 mM) inhibited by TEMPO (red). Reaction progress was monitored at 568 nm (ε =118,405 M^{-1} cm^{-1}).

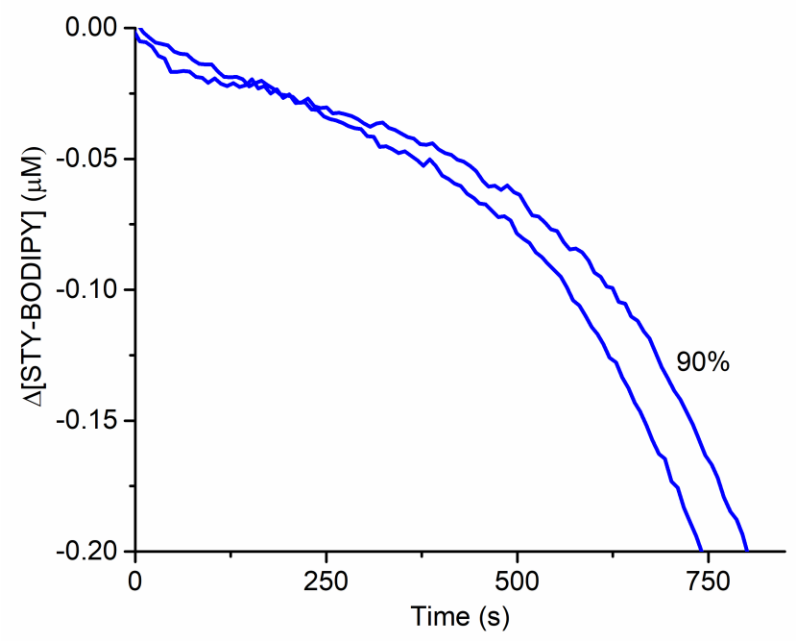

Figure S31. Co-autoxidation of 1,2-d_2-cyclooctene (90% deuterium incorporation) (3.1 M) and STY-BODIPY (10 μM) in PhCl initiated with di-*tert*-butylperoxide (218 mM) inhibited by Ar_2NO (blue) Reaction progress was monitored by absorbance at 568 nm (ε =118,405 M^{-1} cm^{-1}).

Table S3. Summary of inhibition rate constants (k_{inh}) and stoichiometries (n) derived from co-autoxidations of various substrates inhibited by nitroxides and their precursors.

RTA	k_{inh} (M^{-1} s^{-1})	n
styrene in PhCl, 37 °C, 2 μM RTA, ε = 139,000 M^{-1} cm^{-1}		
AIBN (6mM) R_i =2.8 × 10^{-9} s^{-1}, k_t = 3.4 × 10^7 M^{-1} s^{-1}, k_p = 2720 M^{-1} s^{-1}		
DTBNH	5.2± 0.6 × 10^5	3.1 ± 0.1
DTBNO	7.3 ± 0.7 × 10^5	10.9 ± 0.1
TEMPO	7.1 ± 0.4 × 10^5	10.1 ± 0.1
styrene in PhCl, 37 °C, 2 μM RTA, ε = 139,000 M^{-1} cm^{-1}		
AIBN (6, 15, and 30 mM) R_i =2.6 × 10^{-9} s^{-1}, k_t = 2.3 × 10^7 M^{-1} s^{-1}, k_p = 2720 M^{-1} s^{-1}		
TEMPO, AIBN 6 mM	7.1 ± 0.4 × 10^5	10.1 ± 0.1
TEMPO, AIBN 15 mM	-	7.0 ± 0.4
TEMPO (50 μM), AIBN 30 mM	-	2.3 ± 0.1
DTBNO, AIBN 6 mM	7.3 ± 0.7 × 10^5	10.9 ± 0.1
DTBNO, AIBN 15 mM	-	9.6 ± 0.1
DTBNO (50 μM), AIBN 30 mM	-	6.8 ± 0.6
styrene in PhCl, 70 °C, 2 μM RTA, ε = 97,235 M^{-1} cm^{-1}		
AIBN (0.0625, 0.125, 0.250, 0.375, and 1 mM)		
TEMPO, AIBN 62.5 μM	-	21.9 ± 1.4
TEMPO, AIBN 125 μM	-	10.7 ± 1.1
TEMPO, AIBN 250 μM	-	9.8 ± 0.4
TEMPO, AIBN 375 μM	-	7.6 ± 1.0
TEMPO (50 μM), AIBN 1 mM	-	2.1 ± 0.1
DTBNO, AIBN 62.5 μM	-	18.3 ± 0.5
DTBNO, AIBN 125 μM	-	12.4 ± 0.7
DTBNO, AIBN 250 μM	-	10.1 ± 0.2
DTBNO, AIBN 375 μM	-	5.9 ± 0.6
DTBNO (50 μM), AIBN 1 mM	-	1.9 ± 0.2
styrene in PhCl, 70 °C, 2 μM RTA, ε = 97,235 M^{-1} cm^{-1}		
^{t}BuOO^{t}Bu (218 mM), R_i =4.5 × 10^{-9} s^{-1}, k_t = 3.4 × 10^7 M^{-1} s^{-1}, k_p = 4012 M^{-1} s^{-1}		
DTBNH	7.9 ± 1.0 × 10^5	2.1 ± 0.2

DTBNO	$7.9 \pm 0.7 \times 10^6$	10.6 ± 0.2
DTBNOH	$8.5 \pm 1.3 \times 10^6$	11.6 ± 0.1
TEMPH	$4.6 \pm 0.5 \times 10^5$	1.9 ± 0.1
TEMPO	$2.1 \pm 0.7 \times 10^6$	9.3 ± 0.9
TEMPOH	$3.0 \pm 0.7 \times 10^6$	10.0 ± 0.2
DTBNO (MeOD)	$3.3 \pm 1.3 \times 10^6$	10.4 ± 0.5
TEMPO (MeOD)	$1.3 \pm 0.4 \times 10^6$	8.9 ± 0.2
DTBNO (MeOH)	$1.1 \pm 0.3 \times 10^7$	22.0 ± 1.0
TEMPO (MeOH)	$5.5 \pm 0.6 \times 10^6$	26.3 ± 1.0
styrene in 2-octanone, 70 °C, 2 μM RTA, ε = 94,876 M^{-1} cm^{-1}		
^{t}BuOO^{t}Bu (218 mM), $R_i = 4.2 \times 10^{-9}$ s^{-1}, $k_t = 3.4 \times 10^7$ M^{-1} s^{-1}, $k_p = 4004$ M^{-1} s^{-1}		
DTBNO	$2.8 \pm 0.3 \times 10^6$	8.6 ± 0.2
TEMPO	$1.8 \pm 0.5 \times 10^6$	8.5 ± 0.3
styrene in PhCl, 70 °C, 50 μM RTA, ε = 97,235 $M^{-1}cm^{-1}$		
1mM AIBN (1 mM), $R_i = 6.1 \times 10^{-8}$ s^{-1}, $k_t = 3.4 \times 10^7$ M^{-1} s^{-1}, $k_p = 4012$ M^{-1} s^{-1}		
DTBNH	$1.2 \pm 0.5 \times 10^6$	0.8 ± 0.2
DTBNO	$2.2 \pm 0.3 \times 10^5$	1.8 ± 0.2
cumene in PhCl, 68.5 °C, 50 μM RTA, ε = 122,213 M^{-1} cm^{-1}		
AIBN (1 mM), $R_i = 6.1 \times 10^{-8}$ s^{-1}, $k_t = 1.9 \times 10^4$ M^{-1} s^{-1}		
DTBNH	-	2.3 ± 0.1
DTBNO	-	1.1 ± 0.1
norbornene in PhCl, 70 °C, 2 μM RTA, ε = 122,873 M^{-1} cm^{-1}		
^{t}BuOO^{t}Bu (218 mM), $R_i = 7.5 \times 10^{-9}$ s^{-1}, $k_t = 3.4 \times 10^7$ M^{-1} s^{-1}, $k_p = 1358$ M^{-1} s^{-1}		
DTBNO	$2.2 \pm 0.3 \times 10^6$	56.3 ± 1
TEMPO	$1.6 \pm 0.4 \times 10^6$	21.8 ± 2
cyclooctene in PhCl, 70 °C, 2 μM RTA, ε = 118,405 M^{-1} cm^{-1}		
^{t}BuOO^{t}Bu (218 mM), $R_i = 4.5 \times 10^{-9}$ s^{-1}, $k_t = 3.4 \times 10^7$ M^{-1} s^{-1}, $k_p = 2689$ M^{-1} s^{-1}		
DTBNH	$2.5 \pm 0.2 \times 10^6$	15.8 ± 0.2
DTBNO	$1.7 \pm 0.1 \times 10^7$	9.9 ± 0.1
TEMPO	$2.6 \pm 0.2 \times 10^7$	8.9 ± 0.1
1-hexadecene in PhCl 70 °C, 2 μM RTA, ε = 131,972 M^{-1} cm^{-1}		
^{t}BuOO^{t}Bu (87 mM), $R_i = 1.1 \times 10^{-9}$ M^{-1} s^{-1}, $k_t = 2.0 \times 10^8$ M^{-1} s^{-1}, $k_p = 7633$ M^{-1} s^{-1}.		

DTBNO	$1.1 \pm 0.2 \times 10^6$	-
DTBNH	$1.1 \pm 0.2 \times 10^6$	-
TEMPO	$1.1 \pm 0.2 \times 10^6$	-

1-hexadecene in PhCl 100 °C, 2 µM RTA, ε = 119,166 M^{-1} cm^{-1}		
dicumyl peroxide (1 mM), $R_i = 4.6 \times 10^{-9}$ M^{-1} s^{-1}, $k_t = 2.6 \times 10^8$ M^{-1} s^{-1}, $k_p = 8283$ M^{-1} s^{-1}.		
DTBNO	$3.4 \pm 0.4 \times 10^6$	117 ± 7
DTBNH	$6.2 \pm 0.4 \times 10^5$	23 ± 3
TEMPO	$3.2 \pm 0.1 \times 10^6$	-
ethylbenzene in PhCl, 70 °C, 2 µM RTA, ε = 123,481 M^{-1} cm^{-1}		
^{t}BuOO^{t}Bu (87 mM), $R_i = 3.0 \times 10^{-9}$ s^{-1}, $k_t = 2.5 \times 10^7$ M^{-1} s^{-1}, $k_p = 3402$ M^{-1} s^{-1}		
DTBNH	$4.6 \pm 0.7 \times 10^5$	2.3 ± 0.1
dioxane in PhCl, 70 °C, 2 µM RTA, ε = 113,982 M^{-1} cm^{-1}		
^{t}BuOO^{t}Bu (218 mM), $R_i = 5.6 \times 10^{-9}$ s^{-1}, $k_t = 3.9 \times 10^7$ M^{-1} s^{-1}, $k_p = 6707$ M^{-1} s^{-1}		
DTBNH	$3.3 \pm 0.2 \times 10^5$	1.8 ± 0.1

2.7.11. Autoxidations of 1-hexadecene at Various Temperatures

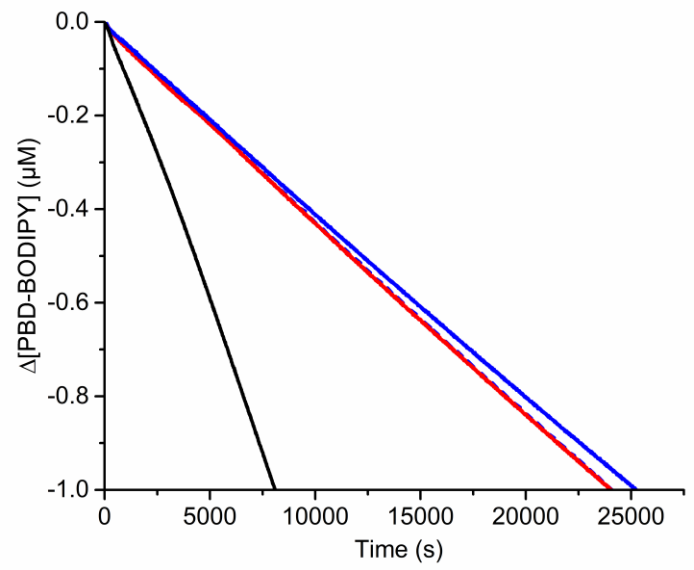

Figure S32: Co-autoxidation of 1-hexadecene (2.7 M) and PBD-BODIPY (10 μM) in PhCl initiated with di-*tert*-butylperoxide (87 mM) at 70 °C (black) inhibited by 2 μM of Ar_2NH (blue dashed line), Ar_2NO (blue line), and TEMPO (red line). Reaction progress was monitored at 587 nm (ε = 131,972 $M^{-1}cm^{-1}$).

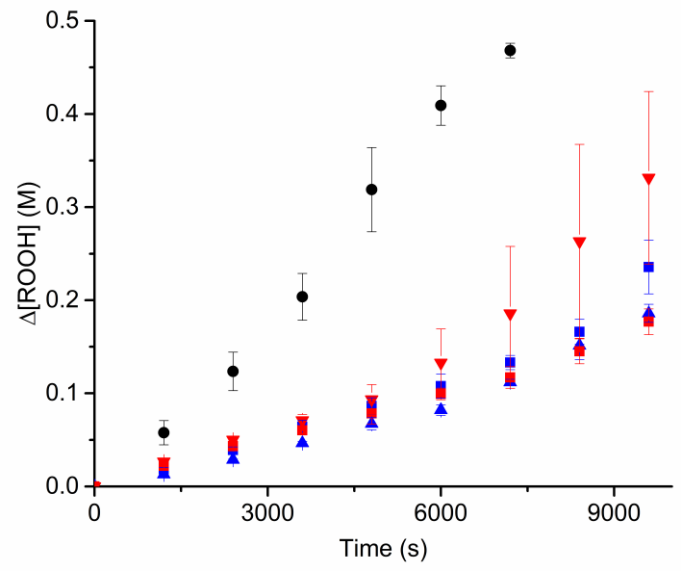

Figure S33: Autoxidation of neat 1-hexadecene (3.5M) at 130 °C initiated with dicumylperoxide (6mM) (black circle) inhibited by 200 μM of Ar_2NH (blue triangle), Ar_2NO (blue square), TEMPH (red triangle), TEMPO (red square). Aliquots were taken at 20 min intervals over a 3 h time course. Hydroperoxide concentration was measured using a fluorogenic phosphine dye read on a microplate reader.[12]

2.7.12. Representative NMR Spectra of Deuterated Cyclooctene

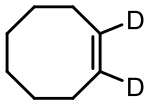

in $CDCl_3$

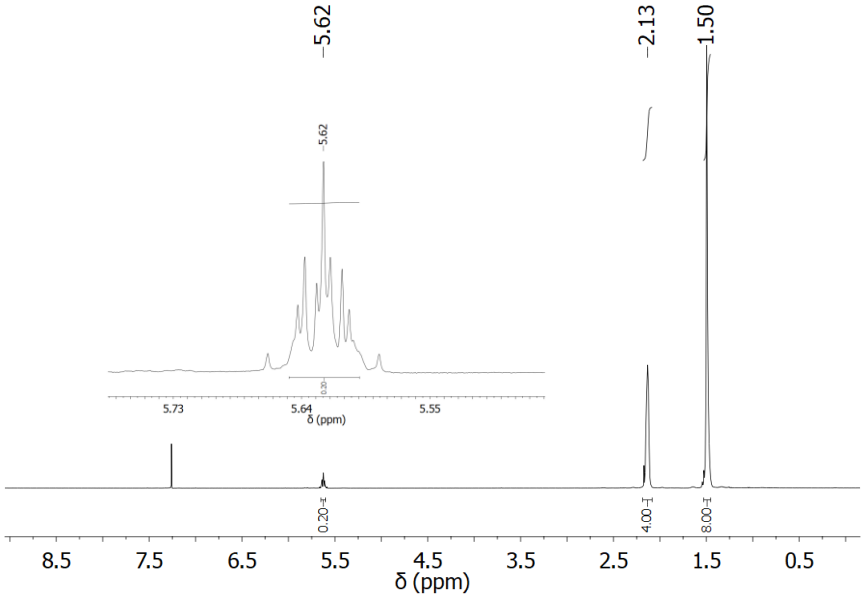

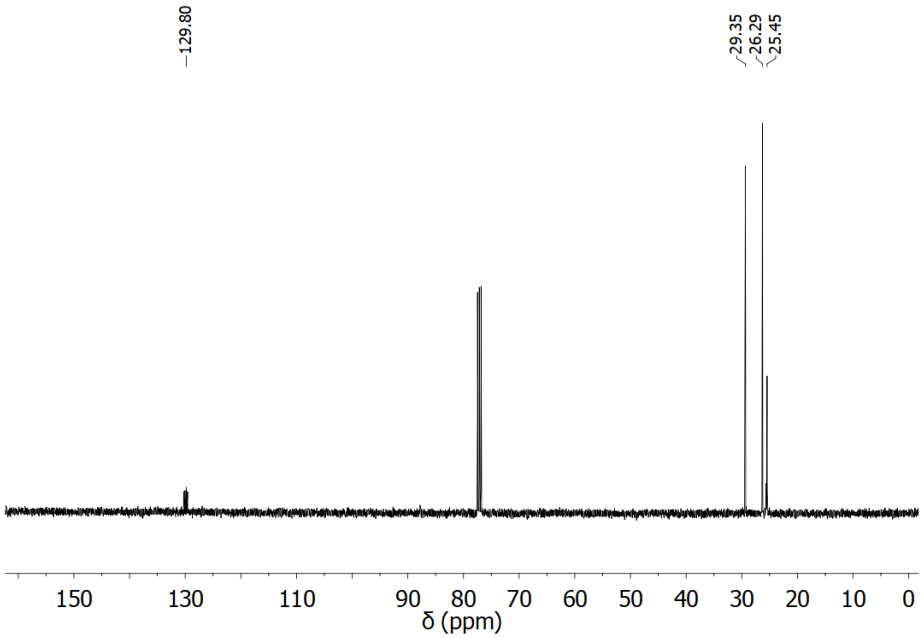

2.8.1. Supplementary References

1 A. J. McGrath, G. E. Garrett, L. Valgimigli, D. A. Pratt, *J. Am. Chem. Soc*., 2010, **132**, 16759 −16761

2 J. J. Hanthorn, L. Valgimigli, D. A. Pratt, *J. Org. Chem.*, 2012, **77**, 6908–6916.

3 V. A. Golubev, V. D. Sen', *Russ. J. Org. Chem*., 2013, **49**, 555–558.

4 V. A. Golubev, V. V. Tkachev, V. D. Sen', Russ. *J. Org. Chem.* 2014, **50**, 678–684.

5 J. Willenbacher, K. N. R. Wuest, J. O. Mueller, M. Kaupp, H. Wagenknecht, C. BarnerKowollik, *ACS Macro Lett.*, 2014, **3**, 574–579.

6 J. Garcia-Hartjes, J. Dommerholt, T. Wennekes, F. L.van Delft, and H. Zuilhof, *Eur. J. Org. Chem.,* **2013**, 3715.

7 L. Brandsma, H. D. Verkruijsse, *Synthesis.*, 1978, **4**, 290.

8 E. A. Haidasz, A. T. Van Kessel, D. A. Pratt, *J. Org. Chem.*, 2016, **81**, 737.

9 J. A. Howard, K. U. Ingold. *Can. J. Chem.*, 1966, **44**, 1119−1130.

10 J. A. Howard, K. U. Ingold. *Can. J. Chem.*, 1969, **47**, 3809-3815.

11 J. A. Howard, K. U. Ingold. *Can. J. Chem.*, 1967, **45,** 793-802.

12 R. Shah, D. A. Pratt. *J. Org. Chem*., 2016, **81**, 6649−6656.

Chapter 3

Towards a Novel Synthesis of Fluorinated Polyunsaturated Lipids

3.1. Introduction

The discovery of isoform-specific inhibitors of lipoxygenases (LOXs) would be greatly enabled by the availability of x-ray crystallographic structures depicting the active enzyme-substrate complex. Inhibitors could then be designed to exploit the structural differences responsible for the regio- and stereoselectivity of substrate dioxygenation carried out by the individual isoforms. Indeed, co-crystal structures of cyclooxygenase isoforms COX-1 and COX-2 with arachidonic acid bound in the active site guided the design of the blockbuster selective COX-2 inhibitors VIOXX (Merck) and Celebrex (Pfizer).[1,2,3,4] The co-crystal structures were made possible by substituting the peroxidase site iron-protoporyphyrin with a redox inactive cobalt-protoporphyrin to prevent enzyme turnover. No such redox cofactor swapping strategy is possible for LOXs, whose non-heme iron is integral to the structure of the protein. Therefore, in order to generate an active form LOX-substrate complex incapable of turnover, we need to alter the structure of the substrate and not the enzyme. Unnatural lipid derivatives that fit within the active site and maintain the enzyme's active conformation, while not undergoing oxidation, would be ideal candidates.

The rate-determining step of LOX-mediated arachidonic acid peroxidation is the abstraction of one of the *bis*-allylic hydrogen atoms from the substrate. If this methylene unit were replaced by a functionality that lacked labile hydrogen atoms, this reaction could no longer take place. The similarity of the van der Waals radii of hydrogen (1.2 Å) and fluorine (1.47 Å) is hypothesized to allow for entry of the substrate into the enzyme active site. In addition, the bond dissociation enthalpy (BDE) of a C-F bond (490 kJ/mol) is much greater than a C-H bond (410 kJ/mol) and should disallow enzymatic turnover of the target atom position.[5]

In the 1980's, Fried and coworkers reported the synthesis of 7,7, 10,10- and 13,13 difluoroarachidonic acids and subsequently examined their capacity to serve as substrates for cyclooxygenases and soybean lipoxygenases.[6,7] They proposed that replacing the *bis*-allylic methylene units on arachidonic acid with *gem*-difluoro methylene subunits would inhibit the *pro*-S hydrogen atom abstraction known to be involved in lipoxygenase and cyclooxygenase enzymatic turnover. The authors speculated that 7,7-difluoroarachidonic acid would inhibit 5-LOX and 10,10-difluoroarachidonic acid would inhibit 12-LOX by preventing hydroperoxyeicosatetraenoic acid (HPETE) formation. As a result,

the 7,7- and 10,10-difluoroarachidonic acids would effectively suppress the formation of downstream inflammatory mediators such as thromboxanes, leukotrienes and lipoxins. Of the three isomers which were synthesized, only 10,10-difluoroarachidonic acid was assayed for its ability to suppress COX and LOX activity.[7] The difluorinated arachidonic acids were incubated with soybean lipoxygenase in phosphate buffer and products were monitored by HPLC. To their surprise, the major products observed were the hydroxyeicosatetraenoic acids (HETEs). They rationalized this observation via S_N2' elimination of fluoride by water from either side of the *gem*-difluoro methylene. Their analysis revealed that the HPETE products were not produced but the rationale behind why these products were not observed was not explored further. (Scheme 3.1)

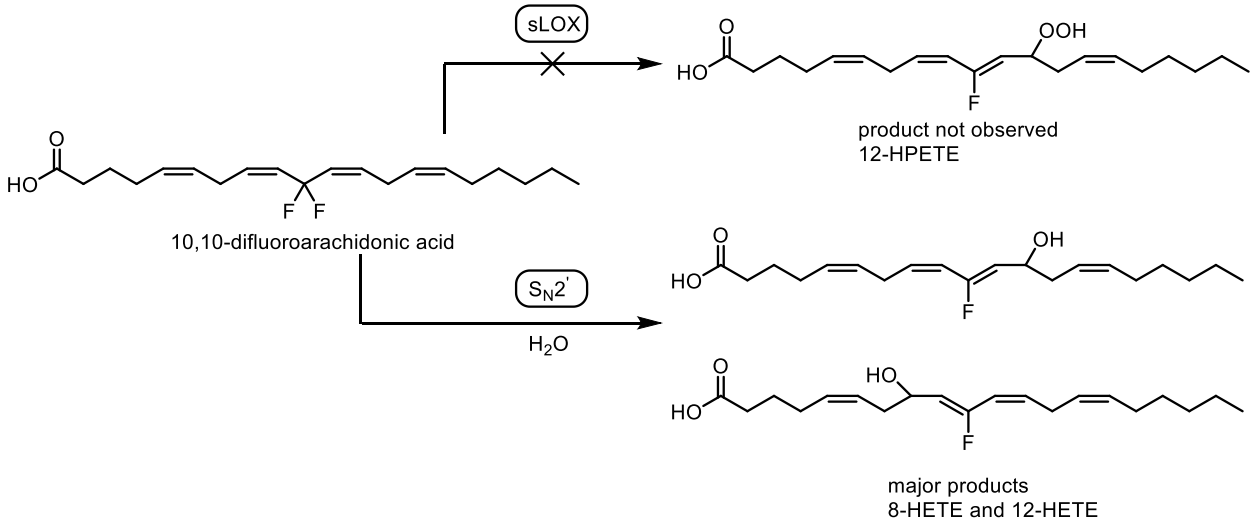

Scheme 3.1. Product distribution of 10,10-difluoroarachidonic acid incubated with soybean lipoxygenase (sLOX) in phosphate buffer.

The total synthesis of 10,10-difluoroarachidonic acid is shown below in Scheme 3.2. 7,7-Difluoroarachidonic acid and 13,13-difluoroarachidonic acid, which were synthesized by similar approaches, were reported to also be hydrolytically unstable, undergoing S_N2' reactions with water before being assayed.[7] It is unclear why the 10,10-difluoroarachidonic acid was more stable to hydrolysis. When COX-1 obtained from ram seminal vesicle microsomes was treated with 10,10-difluoroarachidonic acid, various fluorinated products were observed by HPLC.[7] These products included conjugated hydroxy acids that were indicative of typical COX enzymatic turnover, but the expected cyclized prostaglandin products were not detected. The fact that oxygenation still occurred at C11 as it does on the native substrate suggested that the subsequent reactions steps were impacted by fluorination at C10.

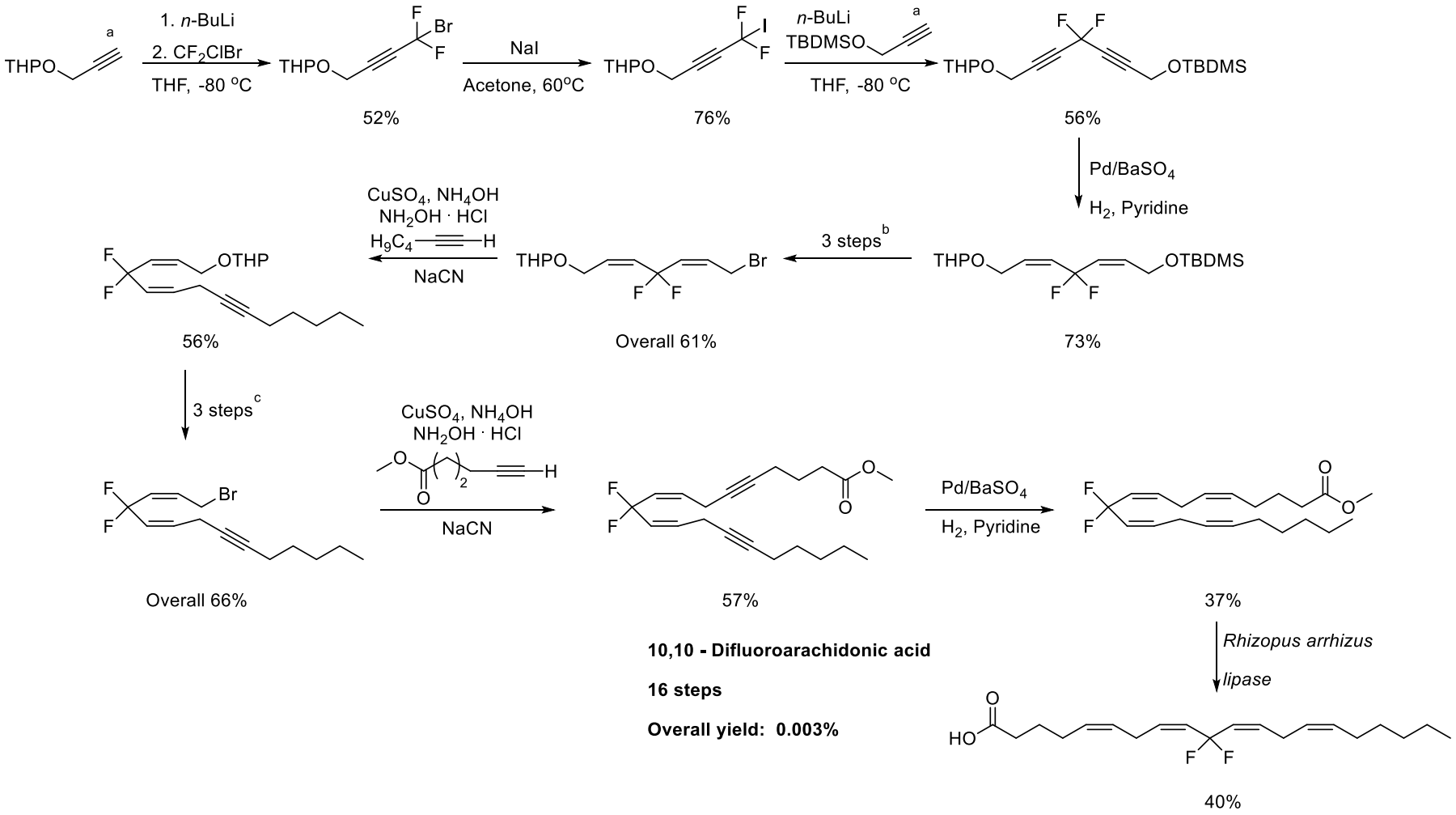

[a]Obtained from propargyl alcohol.
[b]Involved removal of TBDMS silyl protecting group, followed by mesylation and substitution with bromide.
[c]Involved removal of THP protecting group, followed by mesylation and substitution with bromide.

Scheme 3.2. Fried's total synthesis of 10,10-difluorolinoleic acid.

Given these results, it is likely that the 7,7 and 13,13-difluoro acids might block the pathway to leukotrienes that are generated from 5-LOX or 15-HPETEs generated from 15-LOX, respectively. Knowing that 5-LOX has been unequivocally linked to a variety of human diseases, it would be ideal to examine specific inhibitors of this enzyme. The 7,7-difluoroarachidonic acid should act as a selective inhibitor for 5-LOX but not 12 or 15-LOX and would provide more insight into the mechanism of action and leukotriene cascade process. Although these compounds are reported they were never tested and have not been revisited, presumably due to the arduous nature of the synthesis as well as their alleged hydrolytic instability.

The works of Stockwell, Pratt and Dixon strongly suggest that supplementation of cells with non-oxidizable unsaturated fatty acids confers resistance to ferroptiosis.[8,9,10] Stockwell and Pratt *et* al showed that linoleate and arachidonate analogues, respectively, which contain deuterium atoms at the prominent *bis*-allylic sites, suppress ferroptosis.[8,10] The deuterated PUFAs are resistant to (auto)oxidation due to a significant kinetic isotope effect. Dixon *et* al employed monounsaturated fatty acids such as oleic acid, completely forgoing a highly oxidizable *bis*-allylic moiety for a less oxidizable allylic moiety.[9] The propagation rate constants measured for autoxidation of oleic acid (k_p = 0.9 M^{-1} s^{-1}), linoleic acid (k_p = 62 M^{-1} s^{-1}) or arachidonic acid (k_p = 201 M^{-1} s^{-1}) underlie this observation (Figure 3.1).[11] We wondered if fluorinated polyunsaturated fatty acids, such as those synthesized by Fried and which may serve as isoform-selective inhibitors of lipoxygenase, would also confer ferroptosis resistance to cells.

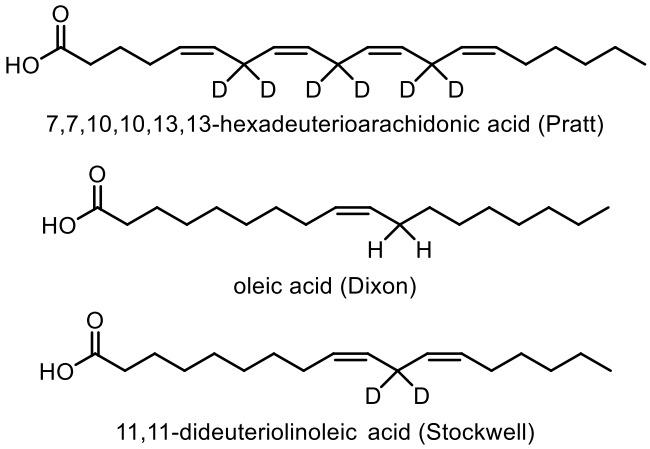

Figure 3.1. Unsaturated lipid substrates resistant to enzyme-mediated lipid peroxidation.

Although Fried and coworkers were able to successfully synthesize these fluorinated PUFAs and confirm the activity of one of them as a substrate for COX/LOX, the synthesis would be difficult for us to replicate. The haloalkane from which the key *gem*-difluoro methylene is derived, bromochloro-

difluoromethane (CF_2ClBr), is prohibited from sale or use in Canada because of its ozone-depleting properties. As a result, other viable CF_2 equivalents that are admissible to Canada were considered. We considered ethyl bromodifluoroacetate (EDFA), which could be coupled to a prefunctionalized alkynyl electrophile using Reformasky-type conditions.[12] The newly formed difluoroalkyne ester could then be decarboxylatively coupled to a second alkenyl subunit that would furnish the core functionalities of the target compound. We also considered direct deoxofluorination of an appropriately substituted ketone using reagents such as DAST and Deoxofluor.[12] The two approaches are depicted below in Scheme 3.3.

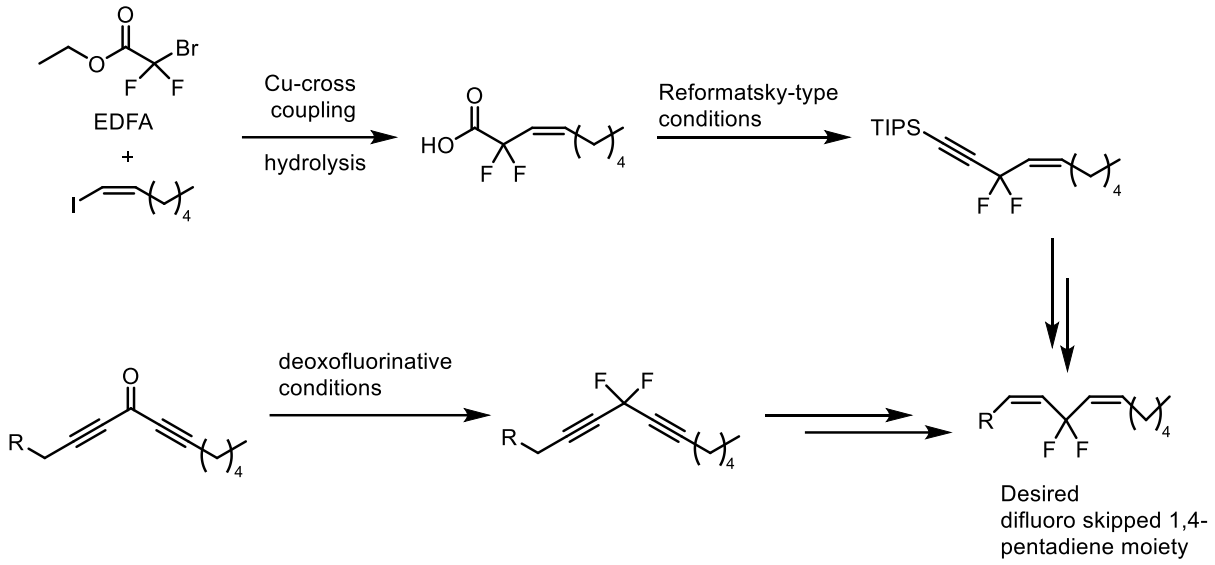

Scheme 3.3. Novel synthetic route options toward building blocks for fluorinated unsaturated fatty acids.

With each of these approaches in mind, we set out to prepare the simpler fatty acid analogue 11,11-difluorolinoleic acid and determine its activity as an inhibitor of soybean lipoxygenase L-1, which utilizes linoleic acid as its native substrate. The synthesis of 11,11-difluorolinoleic acid would serve as a proof-of-principle towards the goal of synthesizing the various fluorinated analogues of arachidonic acid as substrate analogs (inhibitors) for (of) mammalian lipoxygenases. Previously, a former member of the Pratt group Meghan Haycock and current member Ron Shah had tackled the challenging synthesis of 11,11-difluorolinoleic acid using the approach shown below (Scheme 3.4).

Their approach made use of a convergent approach to build up to the 18-carbon backbone of linoleic acid, utilizing ethyl bromodifluoroacetate as the source of the key germinal difluoride moiety. It was coupled to (*Z*)-1-iodohept-1-ene using incredibly delicate reaction conditions consisting of activated copper and anhydrous DMSO.[13] The resultant compound was subsequently hydrolyzed to the free carboxylic acid and then subjected to a silver-catalyzed decarboxylative alkynylation using a TIPS acetylene derived from

a modified Togni reagent.[14] Concurrently, ethyl 8-bromooctanoate was synthesized in four steps from commercially available 1,8-octanediol to serve as an electrophile for the latent terminal alkyne of the fluorinated synthon. Unfortunately, Meghan, Ron and I all failed to remove the TIPS protecting group to furnish the free alkyne in a clean and efficient manner.

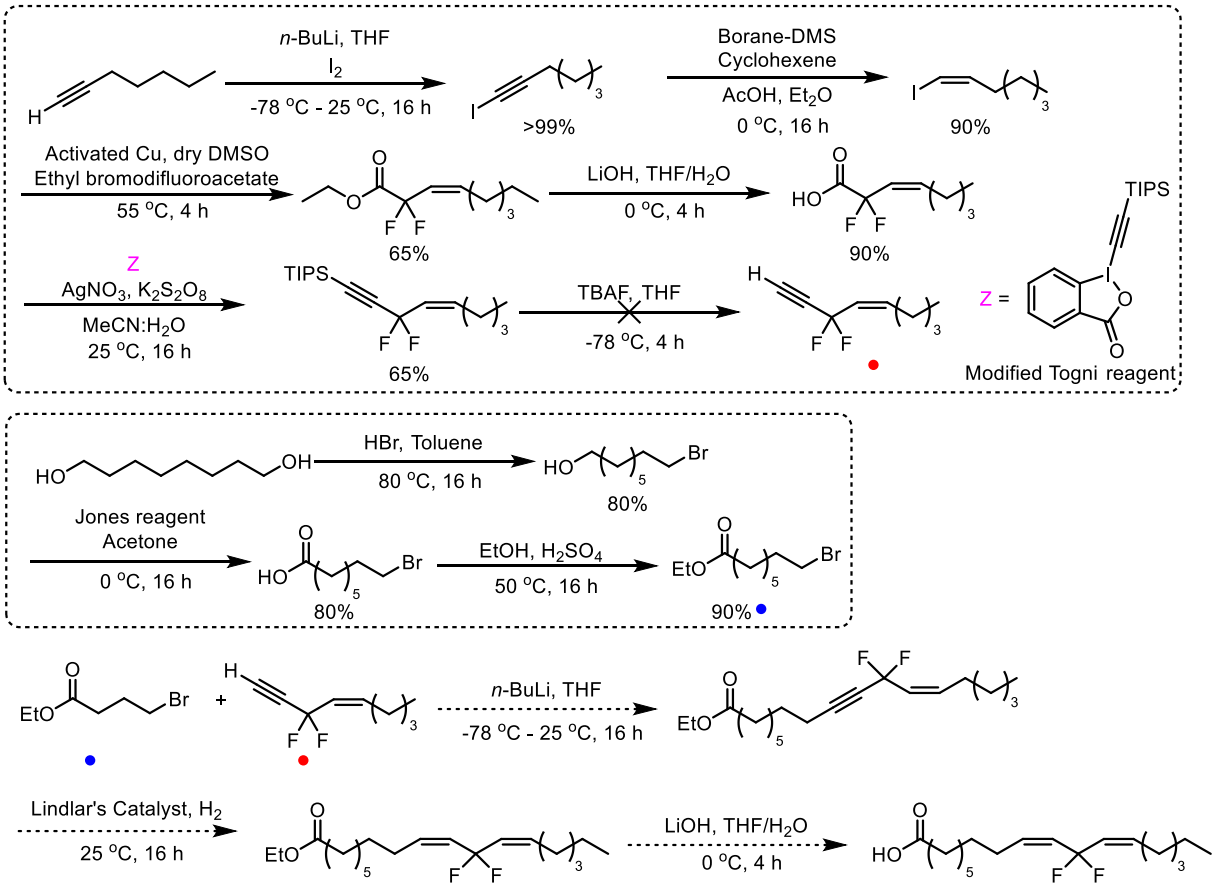

Scheme 3.4. Attempted synthesis of 11, 11-difluorolinoleic acid via radical decarboxylation.

Herein, I describe my efforts to develop a new method to access 11,11-difluorolinoleic acid via a deoxofluorinative approach (Scheme 3.5). It was envisioned that the 1,4-pentadiene moiety could be installed by hydrogenation of a 1,4-pentadiyne featuring the key difluoro functionality at the bis-propargylic position, which would result from deoxyfluorination of the corresponding ketone. The fatty acid backbone could be derived from nucleophilic attack of a terminally protected decynol synthon onto 2-octynal that could be later oxidized at the central alcohol to the *bis*-alkynyl ketone. The protected decynol synthon could be generated from any commercially available isomer of decynol and 2-octynal can be furnished in one step from DMF and 1-heptyne.

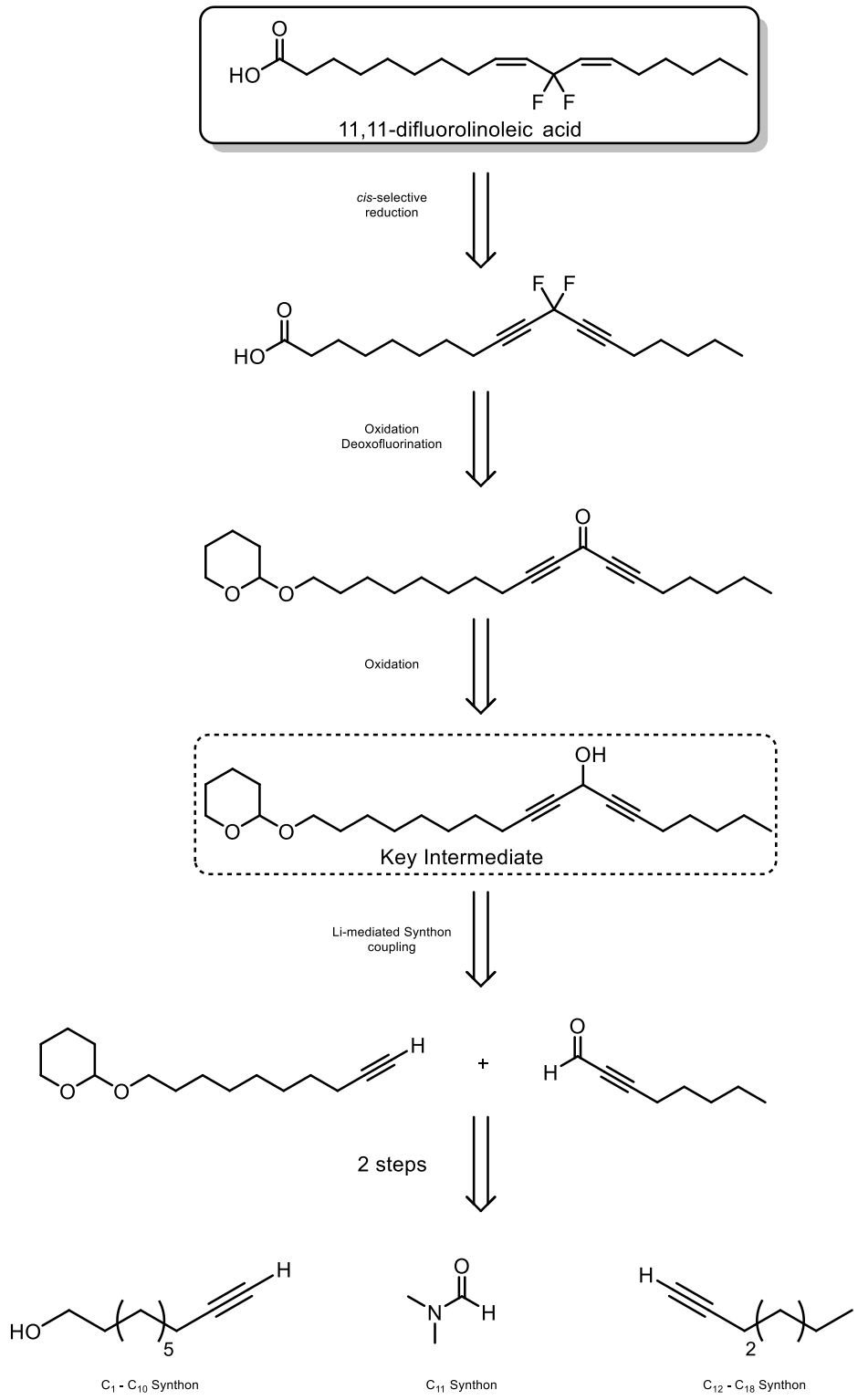

Scheme 3.5. Retrosynthetic analysis to furnish (9*Z*,12*Z*)-11, 11-difluorooctadeca-9,12-dienoic acid.

3.2. Results

3.2.1. Efforts Toward 11,11-Difluorolinoleic Acid

Assembly of the key intermediate shown above was made possible in 3 steps starting from commercially available starting materials dec-3-yn-1-ol, *N*, *N*-dimethylformamide and 1-hepytne.

3.2.1.1 Synthesis of the C1 – C10 Synthon

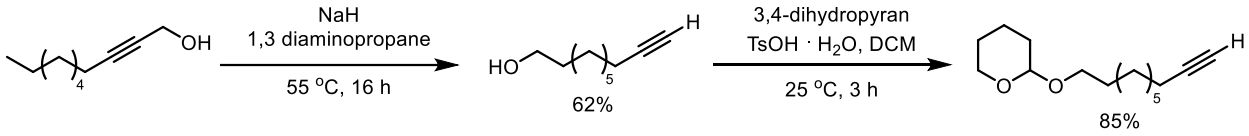

The head of the linoleate backbone requires an oxygenated carbon at C1 and an embedded alkene precursor at C9-C10. The simplest route that we envisioned began from a decanol fragment terminated with an alkyne unit. A quick scan from various suppliers indicated that the desired dec-9-yn-1-ol would be monetarily prohibitive to purchase directly, but several decyn-1-ol derivatives with internal alkynes were readily available. This synthesis employs dec-3-yn-1-ol as the cheapest option, but dec-2-yn-1-ol and dec-5-yn-1-ol have also been tested. A simple alkyne zipper reaction using excess sodium hydride in 1,3-diaminopropane afforded the isomerized dec-9-yn-1-ol product in 62% yield. Next, the C1 alcohol was protected in 85% yield using the tetrahydropyran ether protecting group, preceding the critical lithium mediated alkyne-aldehyde coupling. This protecting group has been successfully featured in numerous lipid derivative syntheses and is suitably robust to highly basic reaction conditions.

3.2.1.2 Synthesis of the C11 – C18 Synthon

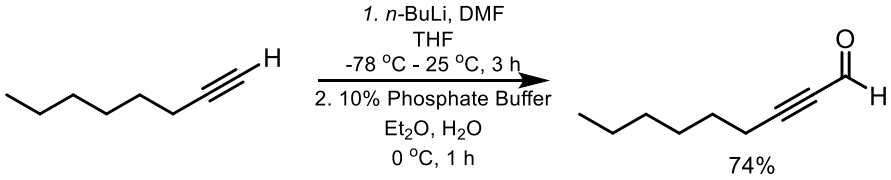

The C11 – C18 synthon is comprised of a simple alkyl chain that contains a functional group handle at C11 to convert to the desired fluoro group attached to an alkynyl unit from carbons 12-14. Concurrent to the head group synthon synthesis, commercially available 1-heptyne was lithiated and then formylated with dimethylformamide. The reaction afforded the 2-octynal in 81% yield with careful

quenching of the excess *n*-Buli with a buffered biphasic solution of KH_2PO_4 and diethyl ether. It was noted that this quenching protocol significantly boosted the isolated yield from ~50% to ~74%.

3.2.1.3. C1 – C18 Synthon Assembly and Functionalization

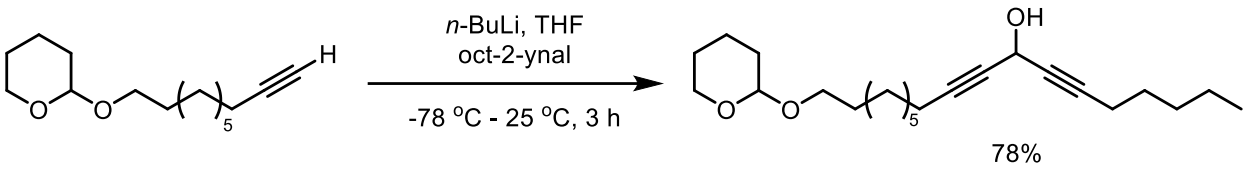

With the C1-C10 and C11-C18 synthons in hand, the full linoleic acid carbon back bone could be assembled by addition of the lithium-acetylinide of the THP protected decynol to oct-2-ynal. The reaction was similarly quenched with a buffered KH_2PO_4/Et_2O solution to afford the key intermediate complete with the critical skipped 1,4 diynyl alcohol unit in 78% yield.

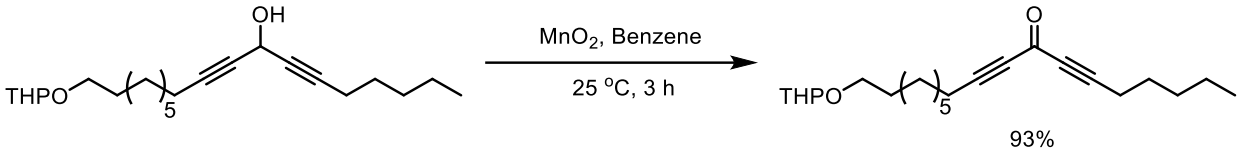

The key intermediate alcohol was readily oxidized over excess manganese dioxide in benzene to afford the diynyl ketone in excellent yields of 93%.

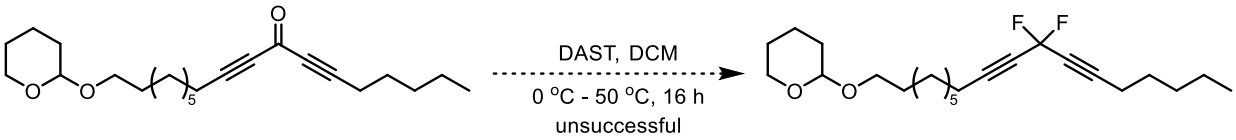

Unfortunately, the key ketone intermediate showed unexpected resistance to deoxofluorination. It is known that ketones require higher equivalents of fluorinating reagent and temperatures compared to alcohols when considering deoxofluorination techniques. However, crude samples consistently showed little progress toward the desired product when following previously reported protocols.[28] This persisted after adding additional equivalents of fluorinating reagent and refluxing the reaction for several days. At this stage, the difluorinated linoleic acid route was halted until alternative methods could be explored.

3.2.2. Efforts Toward 11-Fluorolinoleic Acid

Despite the intermediate ketone being an unsuitable substrate for deoxofluorination, its precursor alcohol proved to be amenable to the reaction conditions. The monofluorinated linoleic acid was also to be a useful compound to test our hypothesis and we sought to explore this pathway further. A retrosynthetic

analysis highlighting the approach towards the monofluorinated analogue of linoleic acid is depicted below (Scheme 3.6).

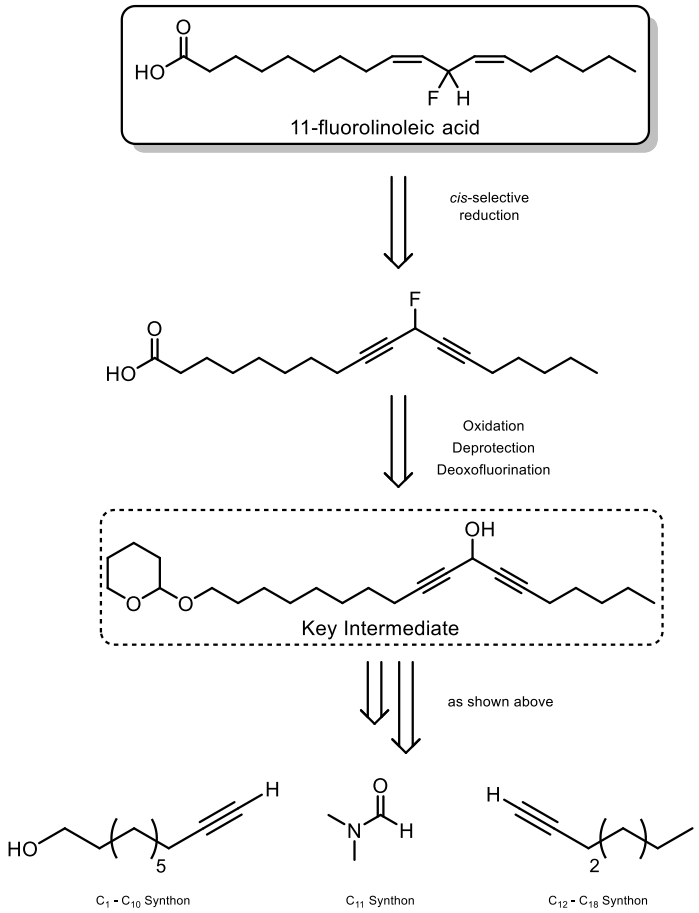

Scheme 3.6. Retrosynthetic analysis to furnish (9*Z*,12*Z*)-11-fluorooctadeca-9,12-dienoic acid.

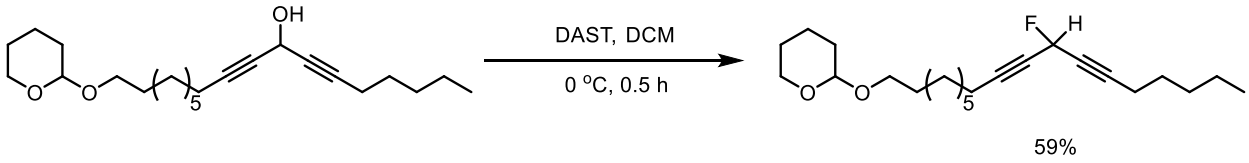

This diynyl alcohol was treated with diethylamino sulfur trifluoride (DAST), a common dexoxofluorinating agent to generate the necessary skipped 1,4 diynyl fluoride in 59% yield. With the fluoride in hand, the final steps were taken to generate the fully functionalized analogue to linoleic acid.

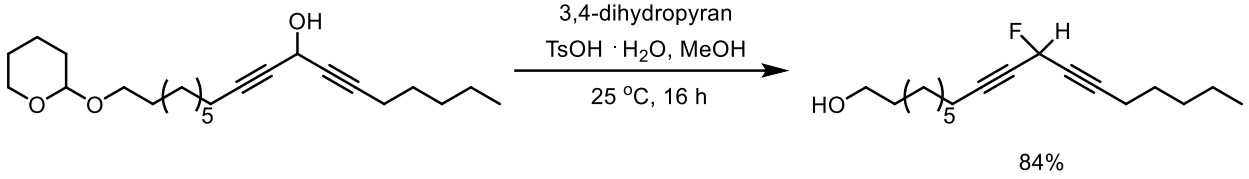

The THP protecting group was cleaved using 10% tosyic acid monohydrate in methanol with an 84% yield.

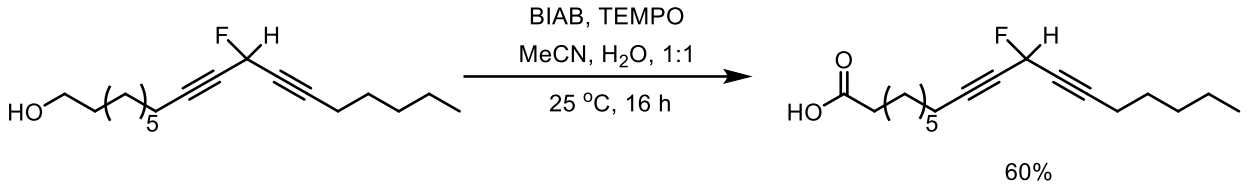

The free alcohol at C1 required a two-stage oxidation at C1 which proved more difficult than originally envisioned. Simple Jones oxidation ruined the starting material and led to multiple fluorinated side products observable by ^{19}F NMR. Gentler oxidation to the aldehyde was viable using typical Swern conditions but oxidation of this pendant aldehyde using Oxone in DMF often gave poor, and inconsistent yields. After several screens suitable conditions were found using an iodobenzene diacetate/TEMPO system in an acetonitrile:water solvent mixture. The oxidation cleanly afforded the C1 carboxylic acid in 60% yield free of any significant by-products. Finally, the last reaction required a double cis-selective reduction of the acetylenic bonds of the skipped 1,4 diyne unit about the fluorine installation. The table given below outlines the protocols employed to overcome this hurdle (Table 3.1).

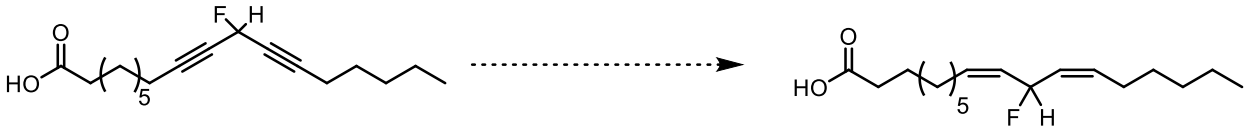

Table 3.1. Hydrogenation protocols used to effect double hydrogenation of 11-fluorooctadeca-9,12-diynoic acid. Reaction volumes were maintained at 0.1 M of substrate in solvent with any additives include at 1 w.t.% unless otherwise indicated.

Entry	Catalyst (w.t.%)	Solvent/Additive	Outcome
1[a]	Lindlar's catalyst: $Pd/CaCO_3/Pb$ (50)	Toluene/Quinoline	N.R. – SM recovered
2[a]	Lindlar's catalyst: $Pd/BaSO_4/Pb$ (50)	Toluene/Quinioline	N.R. – SM recovered
3[a]	Lindlar's catalyst: $Pd/CaCO_3/Pb$ (50)	Toluene/N.A.	N.R. – SM recovered
4[a]	Lindlar's catalyst: $Pd/CaCO_3/Pb$ (50)	Toluene/3,6-dithia-1,8-octandiol	N.R. – SM recovered
5[b]	Lindlar's catalyst: $Pd/CaCO_3/Pb$ (50)	Toluene/Quinioline	Multiple (5) fluorinated products
6[b]	Lindlar's catalyst: $Pd/CaCO_3/Pb$ (5)	Toluene/3,6-dithia-1,8-octandiol	Multiple (5) fluorinated products
7[c]	Lindlar's catalyst: $Pd/CaCO_3/Pb$ (50)	Toluene/3,6-dithia-1,8-octandiol	N.R. – S.M. recovered
8[d]	P2-Nickel Boride: $Ni(OAc)_2$, $NaBH_4$, (0.5eq)	$EtOH:H_2O$ $Pd(NO_3)_2$, 1,3-diaminopropane	Multiple non-fluorinated products.
9[d]	N/A	Et_2O, Borane-DMS, Cyclohexene, Acetic acid	Numerous fluorinated products

[a]Reaction Time: 24 h, Reaction Temperature: 40 °C, atmospheric pressure.
[b]Reaction Time: 24 h, Reaction Temperature: 40 °C, 600 psi.
[c]Reaction Time: 96 h, Reaction Temperature: 60 °C, atmospheric pressure.
[d]Reaction Time: 24 h, Reaction Temperature: 25 °C, atmospheric pressure.

Numerous attempts to catalyze these hydrogenations using various forms of Lindlar's catalyst and additives proved unsuccessful. Inspired by the works of Fried and coworkers, atypically high catalyst loadings were employed to effect hydrogenative reduction of the double bonds as seen in entries 1-4 (Table 3.1).[6] Surprisingly, no reaction of any kind was observed upon NMR analysis of the reaction using various forms of Lindlar's catalyst and additives. 1,3-Dithia-1,8-octandiol was used as a substitute to quinoline as recommended by Dubois to better favour reactivity as shown in entries 4,6 and 7.[15] Unfortunately, this additive also proved ineffective in this reaction. Lastly, Lindlar's hydrogenation was attempted in a high-pressure bomb. While conversion was observed, the reaction yielded a mixture of fluorinated products by ^{19}F NMR without any strong correlation to a predominant olefinic product in the corresponding ^{1}H NMR. This indicates a drastic loss in selectivity usually observed with Lindlar's catalyst and presumably the products observed are a mixture of *trans* and *cis* olefins as well as alkanes and unreacted alkynes.

Considering the lack of useable material obtained from Lindlar's reduction, we moved towards other protocols. Entry 8 highlights a Brown's catalytic hydrogenation using P2-nickel boride (Ni_2B generated from $Ni(OAc)_2$ and $NaBH_4$ in ethanol).[16] This protocol did prove effective in converting starting material to olefinic product; however, the crude material showed a lack of fluorinated material. Presumably, the basic solution of sodium borohydride in ethanol and water led to S_N2' hydrolytic side-reactions that destroyed the starting material. Lastly, hydrogenation was attempted using dicyclohexylborane in anhydrous diethyl ether using a preparation optimized by Woodcock.[17] Our group had initially used this preparation to reduction 1-iodoheptyne to 1-iodoheptene with near quantitative conversion. Borane-complexed to dimethyl sulfide in anhydrous diethyl ether was treated with cyclohexene for 1 hour before the substrate acid was added. This reaction yielded the poorest results with complete scattering of proton signals in the ^1H NMR and several indiscernible fluorinated products. The optimizations made for terminal alkynes were not transferable to the target substrate. To our surprise, the fluorine atom at the skipped diyne structure seems to inhibit the reduction of the flanking triple bonds to a staggering degree. More work needs to be done to be to improve the reactivity of any catalyst system to be employed in the future on the diyne acid penultimate intermediate.

3.3. Discussion

LOX enzymes share many similarities to COX enzymes in their ability to metabolize fatty acid substrates into a host of lipid hydroperoxides and inflammatory mediators implicated in a wide variety of diseases. Critical discoveries into the understanding of COXs were made possible due to obtaining substrate-enzyme co-crystal structures of their active conformational form. To date, no such substrate-enzyme co-crystal structure of native LOXs with a substrate bound in the active site has been obtained. The motivation behind synthesizing fluorinated analogues of linoleic acid was to dock the active site of a native LOX enzyme with a substrate of similar sterics but inert to enzymatic turnover. Analogues of linoleic acid were the substrates of choice due to their simpler functional group composition compared to arachidonic acid derivatives. The synthesis of these fluorinated linoleic acid analogues and docking into soybean lipoxygenases (sLOXs) would serve as a proof of principle before applying successful techniques to fluorinated arachidonic acid synthesis and docking experiments with mammalian lipoxygenases. In addition, it was anticipated that these molecules may enable the elucidation of the mechanisms by which non-oxidizable fatty acids suppress ferroptotic cell death.

Our efforts toward fluorinated linoleic acid analogues have come tantalizingly close to fruition, stopping short at the penultimate fluorinated 1,4-skipped diyne intermediate. There are several reaction conditions and protocols left to explore in order to facilitate the double hydrogenative step envisioned above. Frustratingly, Lindlar's catalyst[15] and Brown's catalyst[16], both routinely used to convert alkynes to alkenes and avoiding over-reduction, proved untenable in facilitating the desired reduction of the alkyne subunits.

Alternative methods left to explore for conversion of the alkynes to *cis*-alkenes include diimide $(NH)_2$, which can be generated *in situ* from acid-catalyzed decarboxylation of potassium azodicarboxylate or copper catalyzed oxidation of hydrazine. It is known to be a clean, stoichiometric hydrogen transfer agent capable of reducing alkynes in the presence of several functional groups not tolerated by traditional metal catalysts including peroxides, alkyl halides and thiols.[18] A possible drawback of this approach is that diimide isn't especially known to halt reduction at the alkene and can over-reduce to the alkane. This could be further complicated by the fact that there are two alkynes that need to be reduced in this approach and would require excess equivalents of the diimide precursor. However, it is known that diimide reacts preferentially with alkynes and strained alkenes.[18] With careful monitoring, the two alkynes may be reduced first based on their higher reactivity versus the desired alkenes and the reaction could be quenched before over-reduction becomes an issue. Lastly, recent advances in electrochemical methods have enabled concerted *cis*-selective reduction of alkynes with a high tolerance to fluorine atoms adjacent to the reduction

sites.[19] These methods source hydrogen from the solvent and palladium nanoparticles serve as a surface for the electrochemical reaction to take place.

Once complete, there are several avenues to consider with respect to the efficacy of the synthetic analogues developed. As previously discussed, LOX enzymes are known to perform the conversion of fatty acids into lipid hydroperoxides via successive hydrogen atom abstraction from the *bis*-allylic position followed by oxygenation of the fatty acid *antarafacial* to the hydrogen atom abstraction position. For example, sLOX is known to only abstract the pro-(*S*) hydrogen atom during its fatty acid metabolism.[20] As a result, the racemic monofluorinated linoleic acid analogue mixture is expected to be less effective than the difluorinated linoleic acid assuming only half of the enzymatically susceptible hydrogen atoms will have been replaced with inactive fluorine atoms (Scheme 3.7).

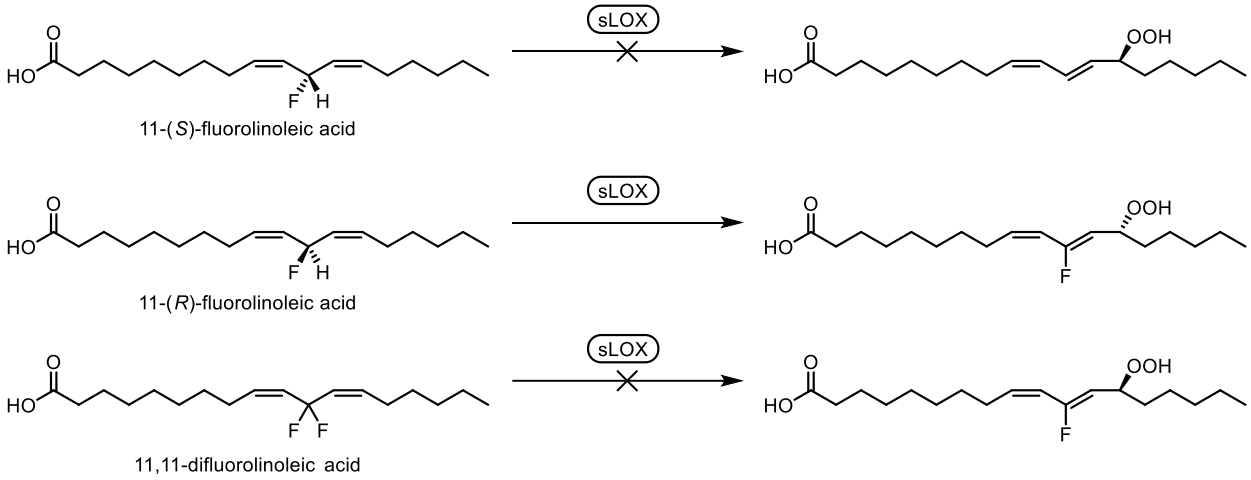

Scheme 3.7. Expected reactivity profiles of fluorinated linoleic acid analogues by the initial reaction catalyzed by soybean lipoxygenase (sLOX).

With the expectation that the racemic 11-fluorolinoleic acid can be achieved from the skipped 1,4-diyne acid, stereospecific analogues could be achieved through modulation of a previous step. We envisioned that the synthesis of the 'key intermediate' i.e. the 1,4-skipped diyne alcohol could be made stereoselective using asymmetric alkynylation approaches by Mukaiyama and Pu.[21,22] These works employ titanium-based or zinc-based Lewis acids coordinated with various chiral ligands to influence the pendant alkoxide after the lithium acetylinide nucleophilically attacks the aldehyde (Scheme 3.8).

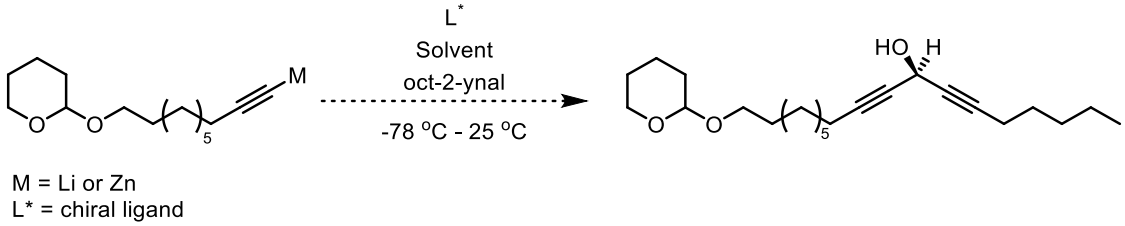

Scheme 3.8. Proposed enantioselective synthesis of the 1,4-skipped diyne alcohol intermediate.

From this enantioenriched material, the remainder of the initially proposed monofluorinated synthesis could be reused without the risk of racemizing the chiral center. The only point to consider would be the deoxofluorination with DAST which proceeds via an S_N2 mechanism where the incoming fluoride displaces the hydroxide anion with an inversion of stereochemistry (Scheme 3.9).

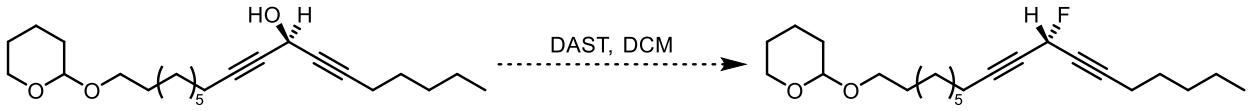

Scheme 3.9. Stereoinversion of the chiral alcohol using fluoride derived from DAST.

If any of the undesired racemate is left in the isolated material, it is feasible that the enantiomers could be separable by chiral column through preparative HPLC to furnish the enantiopure product.

Stereochemically pure fluorinated lipids may also prove useful in probing the extent to which the chiral nature of the cellular milieu influences non-enzymatic lipid autoxidation.[23] There is a possibility that the cell is predisposed to influence how fatty acids are oxidized without the intervention of LOXs being necessary. The exquisite positional control of lipoxygenase enzyme active site activity and the unexplored space of membrane enclosed lipid peroxidation sparks the notion that the synthesis of monofluorinated fatty acids could be revisited in a stereospecific manner.

3.4. Conclusions and Future Work

The synthesis of 11-fluorolinoleic acid and 11,11-difluorolinoleic acid have proven to be a considerable challenge. Although the synthesis of the 11,11-difluorolinoleic acid stalled prior at the deoxyfluorination stage, significant progress has been toward 11-fluorolinoleic acid, with only the penultimate step remaining to be optimized. The final synthetic scheme towards (9*Z*,12*Z*)-11-fluorooctadeca-9,12-dienoic acid is depicted in Scheme 3.10 including the future extension towards esterification onto lysophotidylcholine (lyso-PC) to afford a fluorinated phospholipid analogue to be used in experiments in phospholipid bilayers.

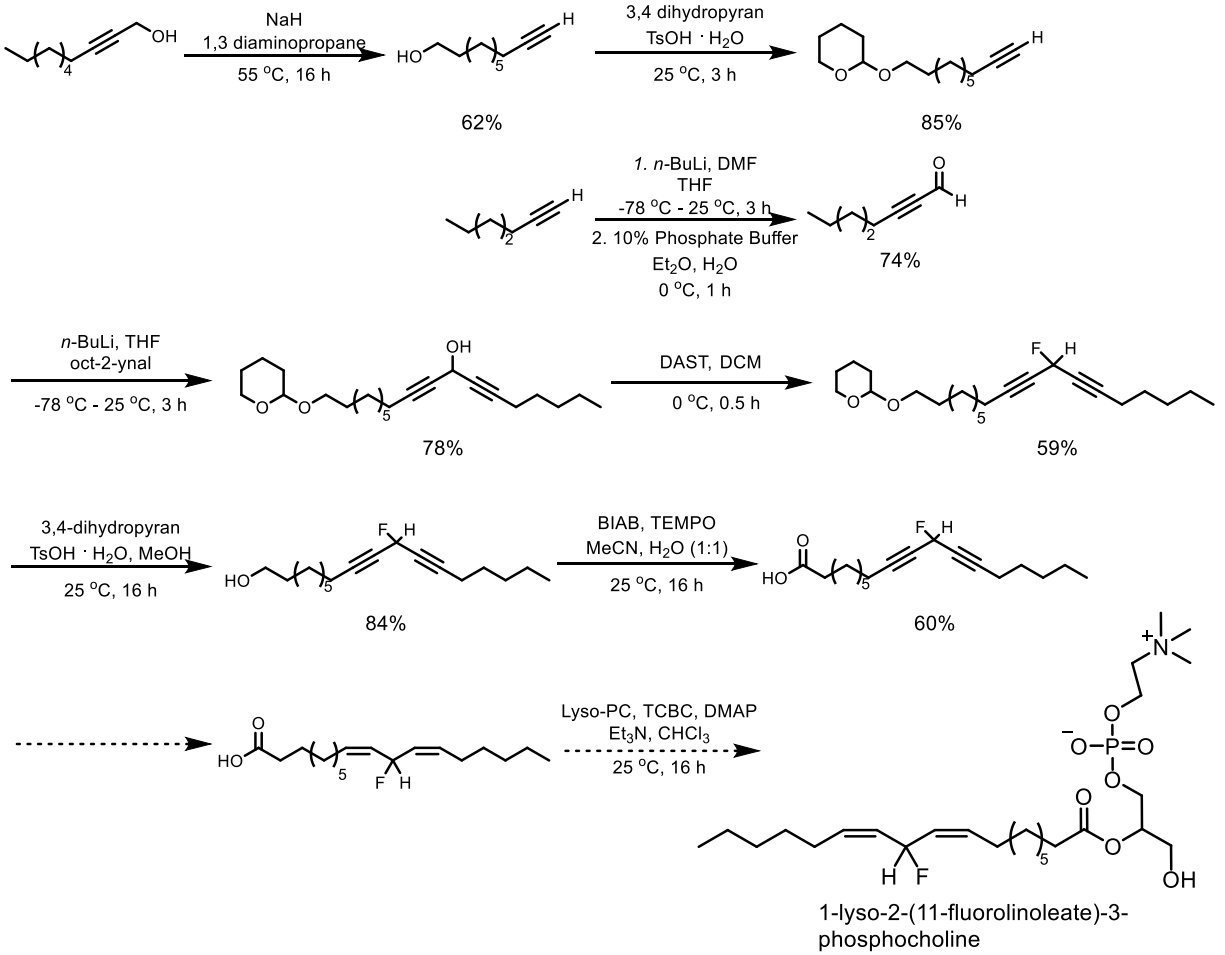

Scheme 3.10. Progress toward (9*Z*,12*Z*)-11-fluorooctadeca-9,12-dienoic acid and its incorporation into a phosphotidylcholine phospholipid.

The synthesis of the penultimate product leading to the free monofluorinated fatty acid is a seven-step endeavour that makes use of a single protecting group as the precursor to the fatty acid head group. The synthesis invokes a convergent approach where the C1-C10 head fragment can be cleanly joined to the C11-C18 tail fragment to introduce the alcohol functionality necessary to elicit the key deoxofluorination. Each step of the synthesis afforded moderate to excellent isolated yields. A few avenues to explore would be to freshly prepare Lindlar's catalyst from palladous chloride, calcium carbonate and lead acetate to see if there is a boost in reactivity compared to commercial sources.[24] Alternative additives could be explored branching away from quinoline and 3,6-dithia-1,8-octandiol that attenuate the catalyst less but still confer the desired *cis*-selectivity. Diimide is also an attractive option outside of the previously explored metal catalysts due to its high functional group tolerance and selectivity toward alkynes.

First and foremost, the free acid could be incubated with soybean lipoxygenase to dock the unnatural substrate analogue in the native active site and obtain a substrate-enzyme crystal complex. This co-crystal structure could provide critical insights into how to most effectively inhibit lipoxygenase enzymes chemically using key peptide interactions with the substrate analogue within the active site. These interactions offer the best potential to be translated to mammalian lipoxygenases and aid in the structure-activity relationships of small molecule inhibitors with key peptide residues in the active site. Crucially, the synthetic methods employed in the successful synthesis of the linoleate analogues could be used towards the arachidonate analogues due to the similarities found between the native substrates. In addition, the free fluorinated linoleic acid could be esterified to lysophosphotidylcholine to generate a phospholipid with an embedded fluorinated fatty acid side chain. This phospholipid could then be supplemented in liposome and cell assays to see how the central fluorine atom potentially inhibits lipid peroxidation versus natural linoleic acid. Results from these data could be compared to previous works that used deuterated and monounsaturated fatty acids. A structure-activity relationship could be explored to explain the phenomena that surround perturbations of polyunsaturated fatty acids and their subsequent autoxidations.

3.5. Experimental Procedures

Reagents were purchased from commercial suppliers and used without further purification. Column chromatography was carried out using flash silica gel (40−63 μm, 230−400 mesh). Proton, carbon, and fluorine magnetic resonance spectra (^{1}H, ^{13}C and ^{19}F NMR) were recorded on a Bruker AVANCE spectrometer at 400, 100 and 376 MHz, respectively, unless specified otherwise. Chemical shifts for protons are reported in parts per million and are referenced to residual protium in solvent (^{1}H NMR: $CDCl_3$ at 7.26 ppm). Chemical shifts for carbons are reported in parts per million and are referenced to the carbon resonances of the residual solvent peak (^{13}C NMR: $CDCl_3$ at 77.0 ppm). Chemical shifts for fluorine are reported in parts per million and are referenced to $PhCF_3$ (δ -63.72 ppm) as the external standard. NMR data are represented as follows: chemical shift, multiplicity (s = singlet, bs = broad singlet, d = doublet, dd = doublet of doublet, t = triplet, q = quartet, m = multiplet), coupling constants (Hz), and integration. High-resolution mass spectra were obtained on a Kratos Concept Tandem mass spectrometer.

3.5.1. Oct-2-ynal

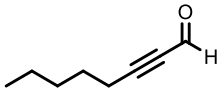

A 250 mL round bottomed flask was equipped with a magnetic stirrer and flame-dried under reduced pressure. The flask was backfilled with desiccated nitrogen gas and fitted with a rubber septum

under a balloon filled with nitrogen gas. The flask was charged with 1-heptyne (3.0 g, 31.2 mmol, 1.0 eq.) in anhydrous THF (78 mL). The solution was chilled to -78 ºC in a dry ice/acetone bath for 5 min then charged dropwise with a room temperature solution of 2.5 M *n*-butyllithium in hexanes (13.7 mL, 34.3 mmol, 1.1 eq) over a 5 min period with a stainless-steel needle/Luer lock syringe. Once the addition was complete, the lithium acetylinide solution was stirred at -78 ºC for 40 min and then charged dropwise with DMF (4.8 mL, 62.2 mmol, 2.0 eq). The reaction was stirred -78 ºC for 1 h then allowed to warm to room temperature over a 90 min period. Once complete (determined by TLC analysis based on SM consumption) the reaction was quenched by pouring into an ice-cold solution of 10 % $KH_2PO_{4\,(aq)}$ (164 mL) in Et_2O (156 mL). The quenched solution was stirred for 30 min then extracted using a separatory funnel. The aqueous phase was extracted with diethyl ether (100 mL) three times and the organic phases were collected. The organics were washed once with water (100 mL) to remove any trace salts then brine (30 mL). The organics were dried over magnesium sulphate anhydrous, filtered and the filtrate concentrated under reduced pressure. The crude residue was purified using flash column chromatography on a gradient of 0-5% ethyl acetate:hexanes.[25]

Yield 2.9 g (23.0 mmol) = 74%, ^{1}H NMR (400 MHz, $CDCl_3$) δ 9.16 (s, 1H), 2.39 (t, J=8.0 Hz, 2H), 1.55 – 1.63 (m, 2H), 1.29 – 1.43 (m, 4H), 0.90 (t, J=8.0 Hz, 3H); ^{13}C NMR (100 MHz, $CDCl_3$) δ 177.4, 99.5, 81.8, 31.1, 27.3, 22.2, 19.2, 14.0; HRMS (EI) calculated for $C_7H_{11}^+$ (loss of formyl group at C1 from $C_8H_{12}O$) $C_7H_{11}^+$ 95.0855, found 95.0864

3.5.2. Dec-9-yn-1-ol

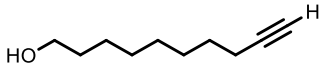

A 250 mL round bottomed flask was equipped with a magnetic stirrer and flame-dried under reduced pressure. The flask was backfilled with desiccated nitrogen gas and fitted with a rubber septum under a balloon filled with nitrogen gas. The flask was charged with 1,3-diaminopropane (110 mL) and heated to 60 ºC in a hot mineral oil bath monitoring with a temperature probe. Separately, sodium hydride (NaH) (5.2 g, 130 mmol, 8.0 eq) (60% dispersed in mineral oil) was briefly washed free of its mineral oil dispersion with hexanes (50 mL) via suction filtration. The gray solid NaH was deftly added to the heated 1,3-diaminopropane portionwise over a 10 min period via spatula. The flask was sufficiently vented with a needle to expel the produced hydrogen gas. After 1 hour, the dark brown solution was charged dropwise with dec-3-yn-1-ol (2.5 g, 16.2 mmol, 1.0 eq). The isomerization reaction was maintained at 60 ºC and allowed to proceed for 24 h. Once complete (determined by TLC analysis based on SM consumption) the reaction was quenched by pouring into an ice-cold solution of water (250 mL) and extracted with ethyl

acetate three times (100 mL). The organics were collected and washed twice with water (50 mL) to remove trace salts and remove the 1,3-diaminopropane then once more with brine (30 mL). The organics were dried over magnesium sulphate anhydrous, filtered and concentrated under reduced pressure. The crude residue was purified by flash column chromatography with a solvent system of 0-10% ethyl acetate:hexanes.[26]

Yield 1.5 g (9.7 mmol) 62% ^{1}H NMR (400 MHz, $CDCl_3$) δ 3.62 (t, J=8.0 Hz, 2H), 2.14 – 2.19 (m, 2H), 1.92 – 1.94 (t, J = 8.0 Hz, 1H), 1.47 – 1.58 (m, 5H), 1.32 – 1.42 (m, 8H); ^{13}C NMR (100 MHz, $CDCl_3$) δ 84.5, 67.9, 62.8, 32.5, 29.1, 28.8, 28.5, 28.2, 25.5, 18.2 ; HRMS (EI) calculated for $C_9H_{15}^+$ (loss of C_2H_2OH from $C_{10}H_{18}O$) 123.1168 found 123.1177

3.5.3. 2-(dec-9-yn-1-yloxy)tetrahydro-2*H*-pyran

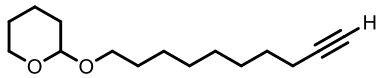

A round bottomed flask was equipped with a magnetic stirrer and flame-dried under reduced pressure. The flask was backfilled with desiccated nitrogen gas and fitted with a rubber septum under a balloon filled with nitrogen gas. The flask was charged with dec-9-yn-1-ol (1.5 g, 9.7 mmol) in DCM (20 mL) followed by 3,4-dihydro-(*2H*)-pyran (0.9 mL, 11.6 mmol, 1.2 eq) and tosyic acid monohydrate (0.2 g, 1.0 mmol, 0.1 eq). The reaction mixture was stirred for 4 h at room temperature. Once complete (determined by TLC analysis based on SM consumption), the reaction mixture was diluted in ethyl acetate (40 mL) and water (30 mL). The aqueous phase was extracted three times with ethyl acetate (40 mL) and the organics were collected. The organics were washed once with water (20 mL) and brine (10 mL). The organics were then dried over magnesium sulphate anhydrous, filtered and concentrated under reduced pressure. The crude residue was purified via flash column chromatography with a solvent gradient of 0-10% diethyl ether:petroleum ether.[27]

Yield: 2.0 g (8.2 mmol) 85% ^{1}H NMR (400 MHz, $CDCl_3$) δ 4.57 (s, 1H), 3.84 – 3.89 (m, 1H), 3.69 – 3.73 (m, 1H), 3.48 – 3.52 (m, 1H), 3.34 – 3.47 (m, 1H), 2.15 – 2.19 (m, 1H), 1.92 – 1.94 (t, J=8.0 Hz, 2H), 1.79 – 1.84 (m, 1H), 1.68 – 1.74 (1H), 1.50 – 1.60 (m, 8H), 1.32 – 1.42 (m, 8H); ^{13}C NMR (100 MHz, $CDCl_3$) δ 99.0, 84.9, 68.2, 67.8, 62.5, 30.9, 29.8, 29.5, 29.2, 28.8, 28.6, 26.3, 25.6, 19.8, 18.5; HRMS (EI) calculated for $C_{15}H_{25}O_2^+$ (from loss of H^+ from $C_{15}H_{26}O_2$) 237.1849 found 237.1822

3.5.4. 18-((tetrahydro-2*H*-pyran-2-yl)oxy)octadeca-6,9-diyn-8-ol.

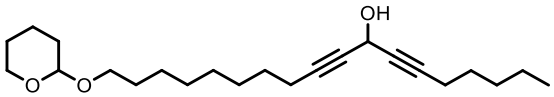

A 25 mL round bottomed flask was equipped with a magnetic stirrer and flame-dried under reduced pressure. The flask was backfilled with desiccated nitrogen gas and fitted with a rubber septum under a balloon filled with nitrogen gas. The flask was charged with 2-(dec-9-yn-1-yloxy)tetrahydro-2*H*-pyran (1.3 g, 5.4 mmol, 1.3 eq) in anhydrous THF (6mL) and cooled to -78 °C in a dry ice/acetone bath. The solution was chilled to -78 °C in a dry ice/acetone bath for 5 min then charged dropwise with a room temperature solution of 2.5 M *n*-butyllithium in hexanes (2.4 mL, 6.0 mmol, 1.4 eq) over a 5 min period with a stainless-steel needle/Luer lock syringe. Once the addition was complete, the lithium acetylinide solution was stirred at -78 °C for 40 min and then charged dropwise with oct-2-ynal (0.5 g, 4.2 mmol, 1.0 eq) in anhydrous THF (6 mL) over a 10 min period. The reaction was stirred at -78 °C for 1 h then the cooling bath removed and warmed to room temperature for an additional 3 h. Once complete (determined by TLC analysis based on SM consumption, the reaction was cooled to 0 °C in an ice-water bath and quenched with a saturated aqueous solution of ammonium chloride (20 mL). The solution was extracted with ethyl acetate (50 mL) three times and the organics were collected. The organics were washed once with water (40 mL) to remove trace salts and once more with brine (10 mL). The organics were then dried over magnesium sulphate anhydrous, filtered and concentrated under reduced pressure. The crude residue was purified via flash column chromatography using a solvent gradient of 0-10% ethyl acetate:hexanes.[27]

Yield: 1.2 g (3.2 mmol) 78% ^{1}H NMR (400 MHz, $CDCl_3$) δ 5.10 (m, 1H), 4.56 – 4.59 (m, 1H), 3.85 – 3.91 (m, 1H), 3.69 – 3.77 (m, 1H), 3.48 – 3.53 (m, 1H), 3.34 – 3.42 (m, 1H), 2.19 – 2.26 (m, 4H), 1.83 – 1.86 (m, 1H), 1.68 – 1.79 (m, 1H), 1.54 – 1.63 (m, 10H), 1.26 – 1.43 (m, 12H), 0.90 (t, , J=8.0 Hz, 3H); ^{13}C NMR (100 MHz, $CDCl_3$) δ 99.0, 67.8, 62.4, 52.7, 31.2, 30.9, 29.8, 29.4, 29.2, 28.9, 28.4, 28.2, 26.3, 25.7, 22.4, 19.9, 18.8, 14.1; HRMS (EI) calculated for (loss of THP group from THPO of $C_{23}H_{38}O_3$) $C_{18}H_{29}O_2^+$ 277.2162 found 277.2165

3.5.5. 2-((11-fluorooctadeca-9,12-diyn-1-yl)oxy)tetrahydro-2*H*-pyran

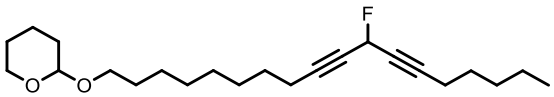

A 50 mL round bottomed flask was equipped with a magnetic stirrer and flame-dried under reduced pressure. The flask was backfilled with desiccated nitrogen gas and fitted with a rubber septum under a balloon filled with nitrogen gas. The flask was charged with 18-((tetrahydro-2*H*-pyran-2-yl)oxy)octadeca-

6,9-diyn-8-ol (3.6 g, 9.8 mmol, 1.0 eq) in dry dichloromethane (20 mL) and cooled to 0 °C in an ice-water bath. The solution was charged with diethylamino sulfur trifluoride (1.3 mL, 9.8 mmol, 1.0 eq) in one portion via syringe and left to stir at 0 °C for 15 min. Once complete (determined by TLC analysis based on SM consumption), the reaction was quenched with a saturated aqueous solution (10 mL) for 30 min then extracted with dichloromethane three times (20 mL). The organics were collected and washed once with brine (10 mL). The organics were dried over magnesium sulphate anhydrous, filtered and concentrated under reduced pressure. The crude residue was purified via flash column chromatography using a solvent gradient of 0-10% diethyl ether:hexanes.[28] Yield: 3.6 g (9.8 mmol) 59% ^{1}H NMR (400 MHz, $CDCl_3$) δ 5.61-5.74 (dt, 1H), 4.56 – 4.58 (m, 1H), 3.85 – 3.87 (m, 1H), 3.84 – 3.89 (m, 1H), 3.70 – 3.75 (m, 1H), 3.47 – 3.52 (m, 1H), 3.35 – 3.41 (m, 1H), 2.23 – 2.28 (m, 2H), 1.79 – 1.87 (m, 1H), 1.68 – 1.75 (m, 1H), 1.50 – 1.61 (m, 10H), 1.31-1.39 (m, 12H), 0.88-0.92 (t, J=8.0 Hz, 3H) ^{13}C NMR (100 MHz, $CDCl_3$) δ 98.9, 89.0-89.1, 74.7-74.8, 74.4-74.5, 71.8, 70.2, 67.6, 62.4, 31.0, 30.8, 29.7, 29.3, 29.0, 28.8, 28.1, 27.8, 26.2, 25.5, 22.1, 19.7, 18.8, 18.7, 13.9 ^{19}F NMR (376 MHz, $PhCF_3$) δ -155.90-(-156.16) (dq J = 1.0 Hz, 0.1Hz); HRMS (EI) calculated for $C_{23}H_{36}FO_2^+$ 363.2694 found 363.2712

3.5.6. 11-fluorooctadeca-9,12-diyn-1-ol

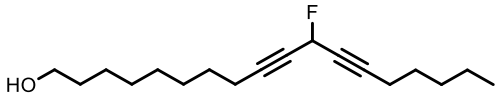

A 50 mL round bottomed flask was equipped with a magnetic stirrer and flame-dried under reduced pressure. The flask was backfilled with desiccated nitrogen gas and fitted with a rubber septum under a balloon filled with nitrogen gas. The flask was charged with 2-((11-fluorooctadeca-9,12-diyn-1-yl)oxy)tetrahydro-2*H*-pyran (1.9 g, 5.2 mmol, 1.0 eq) in methanol (35 mL) at room temperature followed by tosyic acid monohydrate (0.1 g, 0.5 mmol, 0.1 eq). The reaction was stirred for 4 h at room temperature. Once complete (determined by TLC analysis based on SM consumption), the reaction was diluted in water (20 mL) and extracted three times with ethyl acetate (40 mL). The organics were collected and washed once with brine (10 mL). The organics were dried over magnesium sulphate anhydrous, filtered and concentrated under reduced pressure. The crude residue was purified via flash column chromatography using a solvent gradient of 0-25% ethyl acetate:hexanes.[6] Yield: 1.2 g (4.4 mmol) 84% ^{1}H NMR (400 MHz, $CDCl_3$) δ 5.63-5.74 (m, 1H), 3.62-3.65 (t, J = 8.0 Hz, 2H), 3.40 (b, 1H), 2.21-2.29 (m, 4H), 1.50-1.60 (m, 6H), 1.28 – 1.42 (m, 13H), 0.88-0.92 (t, J=8.0 Hz, 3H) ^{13}C NMR (100 MHz, $CDCl_3$) δ 89.2, 74.9, 74.6, 72.0, 70.4, 63.2, 32.9, 31.1, 29.4, 29.1, 28.9, 28.2, 27.9, 25.8, 22.3, 18.9, 18.9, 14.1 ^{19}F NMR (376 MHz, $PhCF_3$) δ -155.98-(-156.17) (dq J = 0.5Hz, 0.1Hz); HRMS (EI) calculated for $C_{18}H_{28}FO^+$ 279.2119 found 279.2131

3.5.7. 11-fluorooctadeca-9,12-diynoic acid

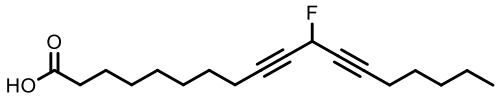

A round bottomed flask was equipped with a magnetic stirrer and flame-dried under reduced pressure. The flask was backfilled with desiccated nitrogen gas and fitted with a rubber septum under a balloon filled with nitrogen gas. The flask was charged 11-fluorooctadeca-9,12-diyn-1-ol (1.1 g, 3.9 mmol, 1.0 eq) in a 1:1 solution of acetonitrile (25 mL) and water (25 mL). The solution was then successively charged with iodobenzene diacetate (3.0 g, 9.4 mmol, 2.4 eq) and TEMPO (0.2 g, 0.9 mmol, 0.2 eq). The reaction was stirred overnight at room temperature under nitrogen gas. Once complete (determined by TLC analysis based on SM consumption), the reaction was quenched with a saturated solution of sodium thiosulphate (10 mL) and taken up in ethyl acetate (40 mL). The aqueous phase was extracted three times with ethyl acetate (40 mL). The organics were collected and washed once with brine (10 mL). The organics were dried over magnesium sulphate anhydrous, filtered and concentrated under reduced pressure. The crude residue was purified via flash column chromatography using a solvent gradient of 0-25% diethyl ether:petroleum ether.[29]

Yield: 0.5 g (1.6 mmol) 60% ^{1}H NMR (400 MHz, $CDCl_3$) δ 11.02 (b, 1H), 5.61-5.75 (m, 1H), 2.33-2.37 (t, J=8.0 Hz, 2H) 2.23-2.29 (m, 4H), 1.60-1.67 (m, 2H), 1.51 – 1.56 (m, 4H), 1.31-1.43 (m, 10H), 0.88-0.92 (t, J=8.0 Hz, 3H)^{13}C NMR (100 MHz, $CDCl_3$) δ 179.6, 89.2-89.3, 89.0-89.3, , 74.6-75.0, 71.9, 70.3, 34.0, 31.1, 29.0, 28.8, 28.7, 28.1, 27.9, 24.7, 22.3, 18.9, 18.8, 14.1 ^{19}F NMR (376 MHz, $PhCF_3$) δ -155.90-(-156.16) (dq J = 1.0Hz, 0.1Hz); HRMS (EI) calculated for $C_{18}H_{26}FO_2^+$ 293.1911 found 293.1934

3.6. References

1 M. G. Malkowski, S. L. Ginell, W. L. Smith and R. M. Garavito, *Science.*, 2000, **289**, 1933 - 1937.
2 D. Picot, P. J. Loll and R. M. Garavito, *Nature*, 1994, **367**, 243–249.
3 R. G. Kurumbail, A. M. Stevens, J. K. Gierse, J. J. McDonald, R. A. Stegeman, J. Y. Pak, D. Gildehaus, J. M. iyashiro, T. D. Penning, K. Seibert, P. C. Isakson and W. C. Stallings, *Nature*, 1996, **384**, 644–648.
4 T. D. Penning, J. J. Talley, S. R. Bertenshaw, J. S. Carter, P. W. Collins, S. Docter, M. J. Graneto, L. F. Lee, J. W. Malecha, J. M. Miyashiro, R. S. Rogers, D. J. Rogier, S. S. Yu, G. D. Anderson, E. G. Burton, J. N. Cogburn, S. A. Gregory, C. M. Koboldt, W. E. Perkins, K. Seibert, A. W. Veenhuizen, Y. Y. Zhang and P. C. Isakson, *J. Med. Chem.*, 1997, **40**, 1347–1365.
5 C. Chatalova-Sazepin, R. Hemelaere, J. F. Paquin and G. M. Sammis, *Synth.*, 2015, **47**, 2554–2569.
6 P.Y. Kwok, F. W. Muellner, C.K. Chen and J. Fried, *J. Am. Chem. Soc.*, 1987, **109**, 3684–3692.
7 P. Kwok, F. W. Muellner and J. Fried, *J. Am. Chem. Soc.*, 1987, 3692–3698.
8 R. Shah, M. S. Shchepinov and D. A. Pratt, *ACS Cent. Sci.*, 2018, **4**, 387–396.
9 L. Magtanong, P.-J. Ko, M. To, J. Y. Cao, G. C. Forcina, A. Tarangelo, C. C. Ward, K. Cho, G. J. Patti, D. K. Nomura, J. A. Olzmann and S. J. Dixon, *Cell Chem. Biol.*, 2019, **26**, 420-432.
10 W. S. Yang, K. J. Kim, M. M. Gaschler, M. Patel, M. S. Shchepinov and B. R. Stockwell, *Proc. Natl. Acad. Sci.*, 2016, **113**, 4966-4975.
11 Z. A. M. Zielinski and D. A. Pratt, *J. Org. Chem.*, 2017, **82**, 2817–2825.
12 M. J. Tozer and T. F. Herpin, *Tetrahedron*, 1996, **52**, 8619–8683.
13 K. Sato, M. Omote, A. Ando and I. Kumadaki, *J. Fluor. Chem.*, 2004, **125**, 509–515.
14 H. Huang, G. Zhang, L. Gong, S. Zhang and Y. Chen, *J. Am. Chem. Soc.*, 2014, **136**, 2280–2283.
15 R. Lindlar, H. Dubuis, *Org. Synth.*, 1966, **46**, 89.
16 C. A. Brown, *J. Chem. Soc. D Chem. Commun.*, 1969, 952.
17 S. R. Woodcock, A. J. V Marwitz, P. Bruno and B. P. Branchaud, *Org. Lett.*, 2006, **8**, 3931–3934.
18 D. J. Pasto, *Encycl. Reagents Org. Synth.*, 2001.
19 B. Li and H. Ge, *Sci. Adv.*, 2019, **5**, 2774.
20 A. Andreou and I. Feussner, *Phytochemistry.*, 2009, **70**, 1504–1510.
21 T. Mukaiyama, K. Suzuki, K. Soai and T. Sato, *Chem. Lett.*, 1979, **8**, 447–448.
22 G. Gao, D. Moore, R.-G. Xie and L. Pu, *Org. Lett.*, 2002, **4**, 4143–4146.
23 F. Eghiaian, *Biophys. J.*, 2015, **108**, 2757–2758.
24 A. Publication, *Org. Synth.*, 1966, **46**, 89.
25 K. Frimpong, J. Wzorek, C. Lawlor, K. Spencer and T. Mitzel, *J. Org. Chem.*, 2009, **74**, 5861–5870.
26 C. A. Brown and A. Yamashita, *J. Am. Chem. Soc.*, 1975, **97**, 891–892.
27 A.V. R. Rao, E. R. Reddy, G. V. M. Sharma, P. Yadagiri and J. S. Yadav, *Tetrahedron*, 1986, **42**, 4523–4532.
28 W.-H. Guo, Z.-J. Luo, W. Zeng and X. Zhang, *ACS Catal.*, 2017, **7**, 896–901.
29 M. J. Corr, R. A. Cormanich, C. N. von Hahmann, M. Bühl, D. B. Cordes, A. M. Z. Slawin and D. O'Hagan, *Org. Biomol. Chem.*, 2016, **14**, 211–219.

3.7. NMR Spectra

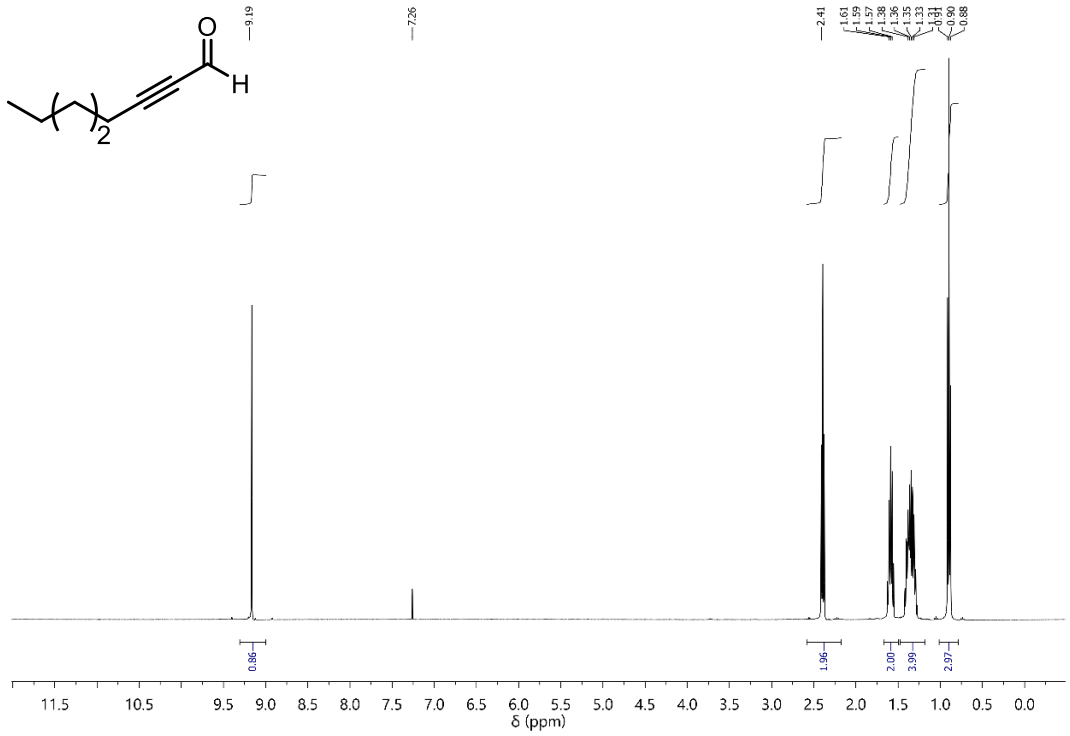

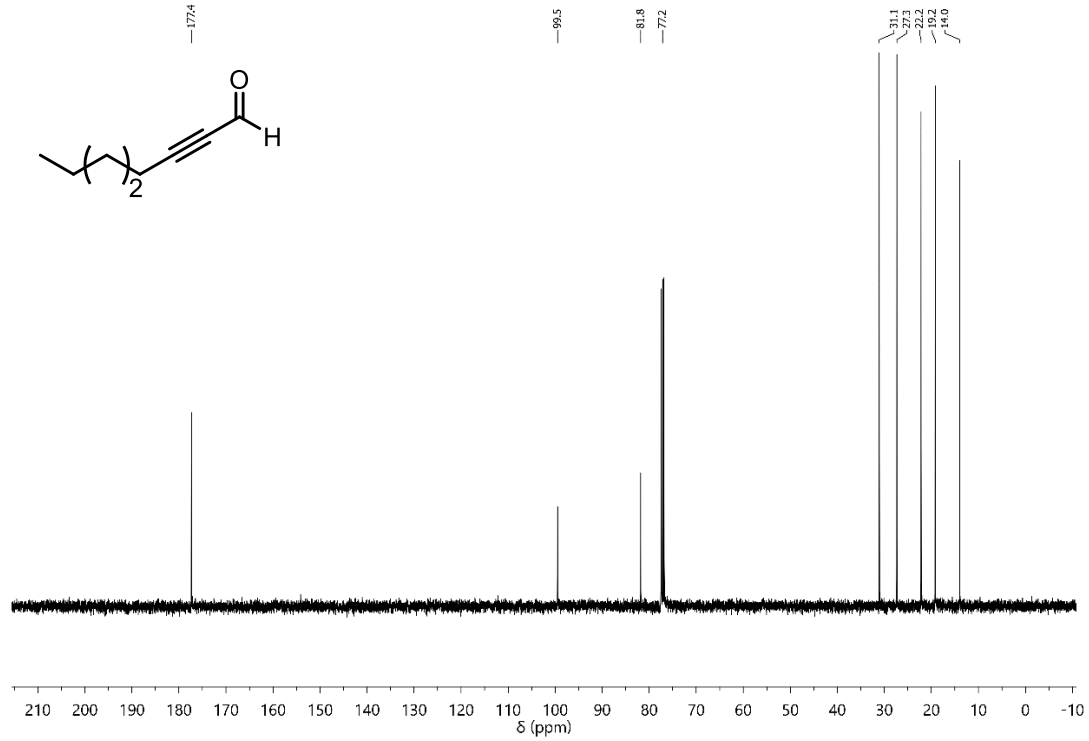

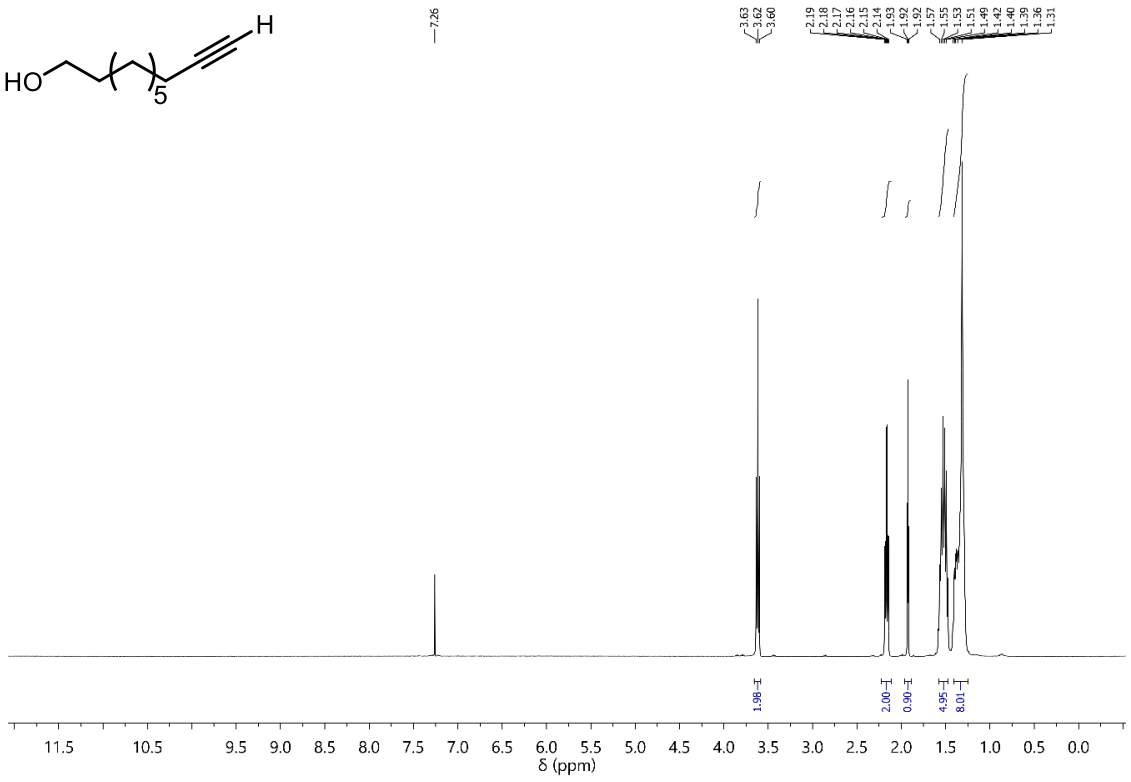
HO
H
5
7.26
3.63
3.62
3.60
2.19
2.18
2.17
2.16
2.15
2.14
1.93
1.92
1.92
1.57
1.55
1.53
1.51
1.49
1.42
1.40
1.39
1.36
1.31
1.98
2.00
0.90
4.95
8.01
δ (ppm)

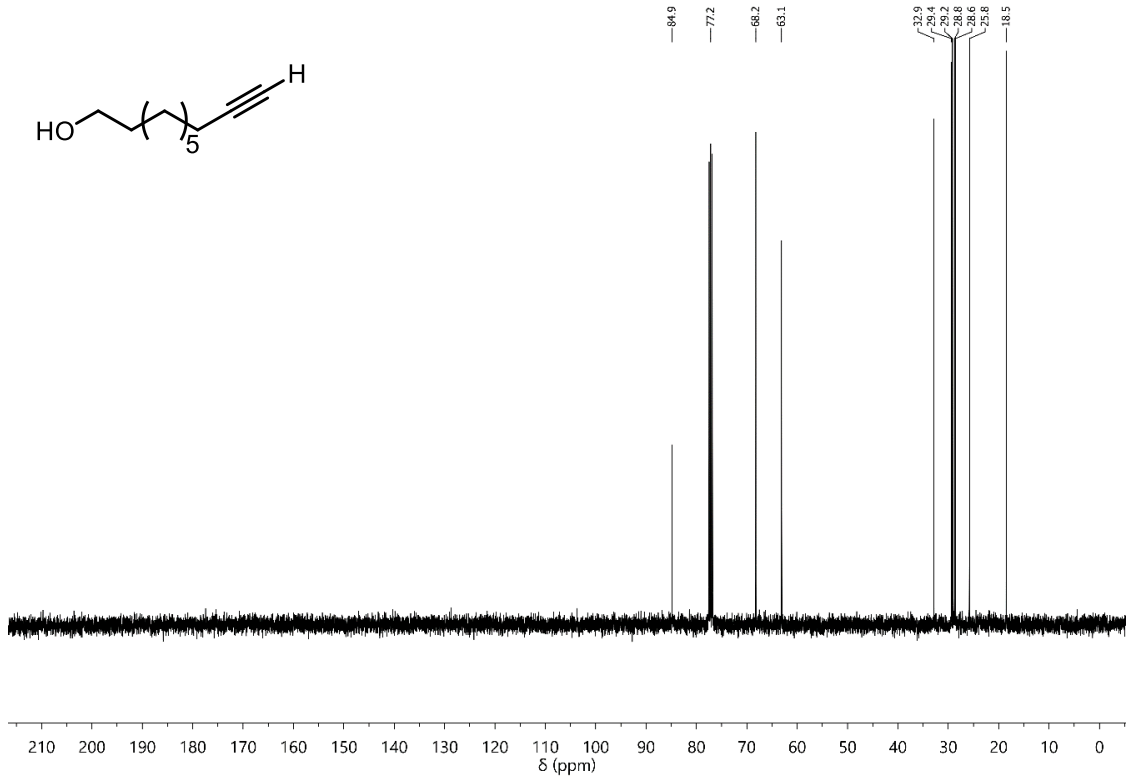
HO
H
5
84.9
77.2
68.2
63.1
32.9
29.4
29.2
28.8
28.6
25.8
18.5
δ (ppm)

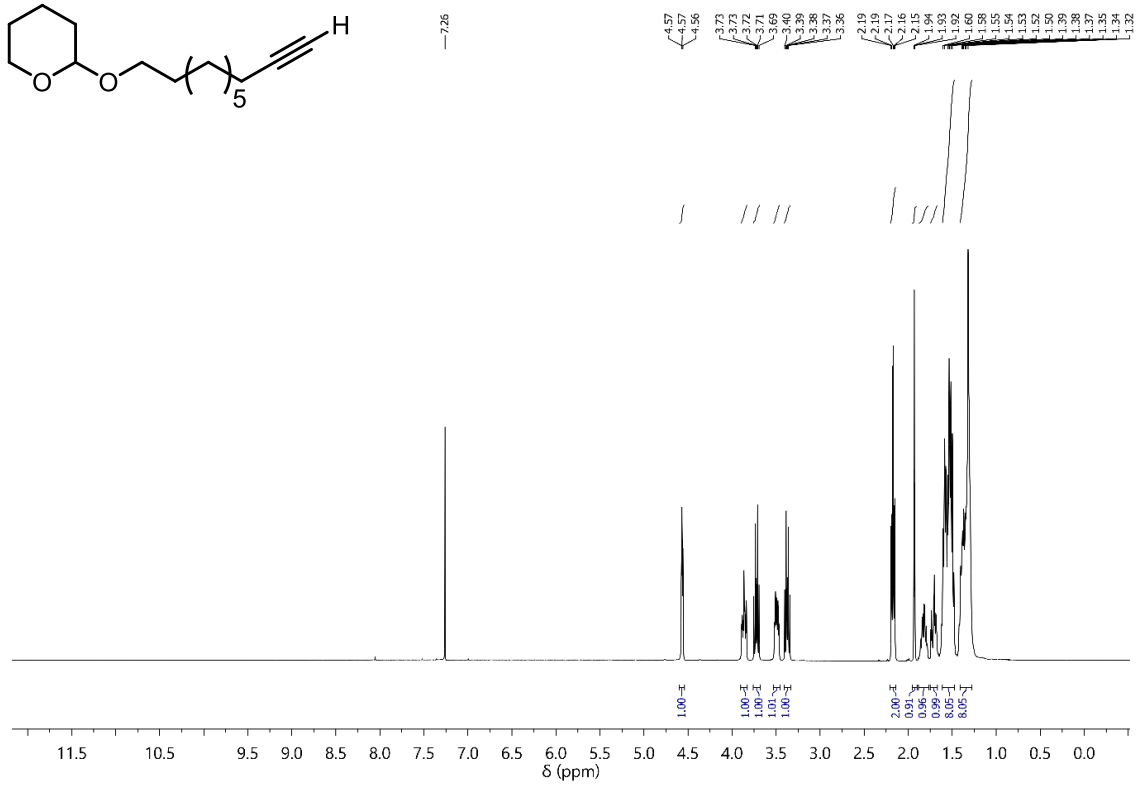
H
O
O
5
7.26
4.57
4.57
4.56
3.73
3.72
3.72
3.71
3.69
3.40
3.39
3.38
3.37
3.36
2.19
2.19
2.17
2.16
2.15
1.94
1.93
1.92
1.60
1.58
1.55
1.54
1.53
1.52
1.50
1.39
1.38
1.37
1.35
1.34
1.32
1.00
1.00
1.00
1.01
1.00
2.00
0.91
0.96
0.99
8.05
8.05
11.5
10.5
9.5
9.0
8.5
8.0
7.5
7.0
6.5
6.0
5.5
5.0
4.5
4.0
3.5
3.0
2.5
2.0
1.5
1.0
0.5
0.0
δ (ppm)

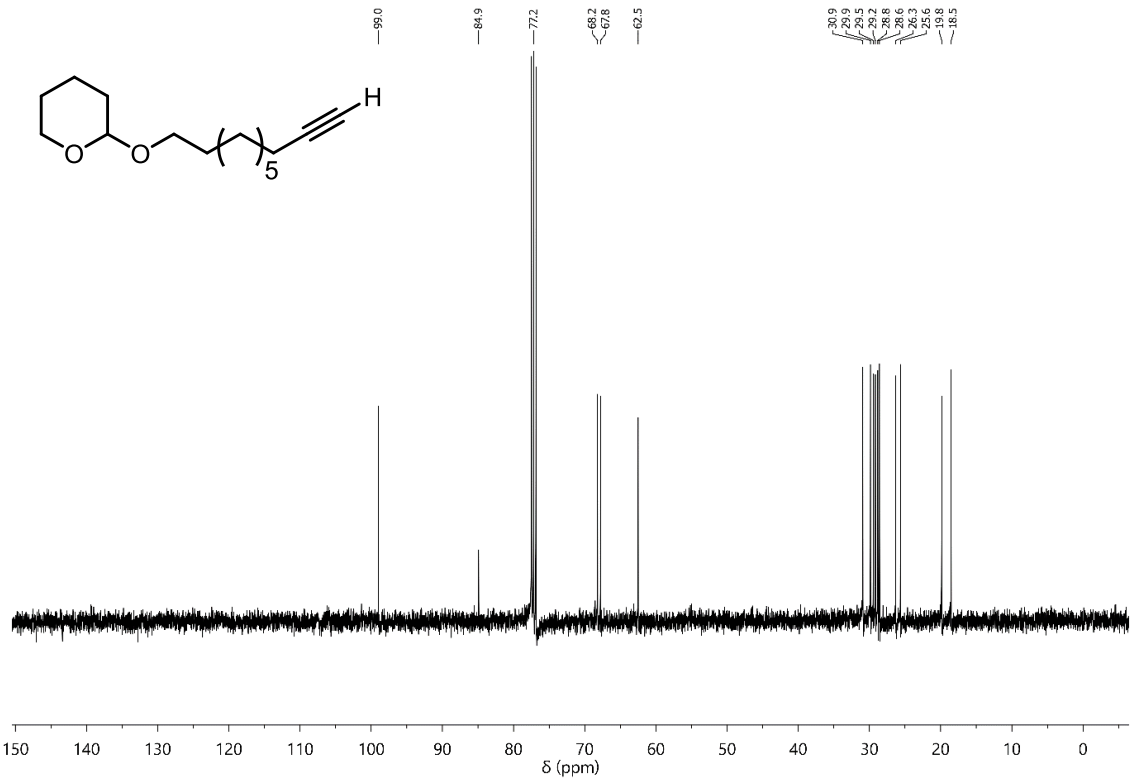
H
O
O
5
99.0
84.9
77.2
68.2
67.8
62.5
30.9
30.9
29.5
29.2
28.8
28.6
26.3
25.6
19.8
18.5
150
140
130
120
110
100
90
80
70
60
50
40
30
20
10
0
δ (ppm)

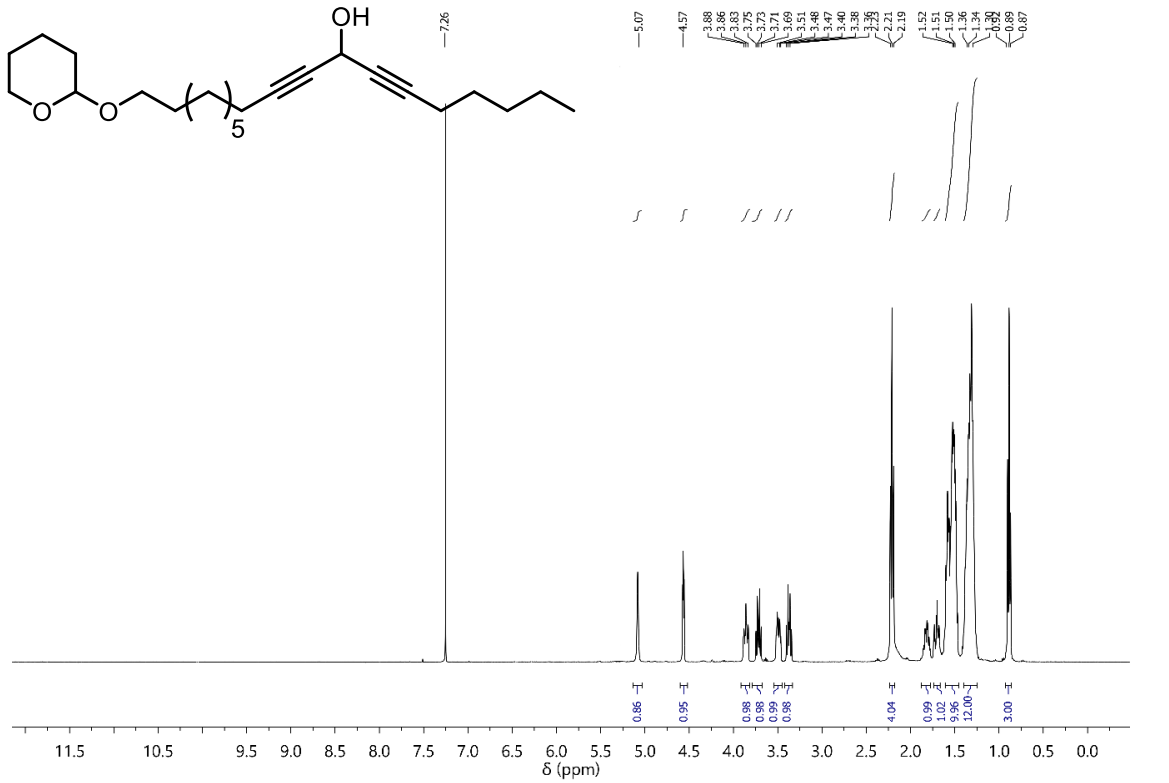
OH
O
O
5
7.26
5.07
4.57
3.88
3.86
3.83
3.75
3.73
3.71
3.69
3.51
3.48
3.47
3.40
3.38
2.21
2.19
1.52
1.51
1.50
1.36
1.34
0.89
0.87
0.86
0.95
0.98
0.98
0.99
0.98
4.04
0.99
1.02
9.96
12.00
3.00
δ (ppm)

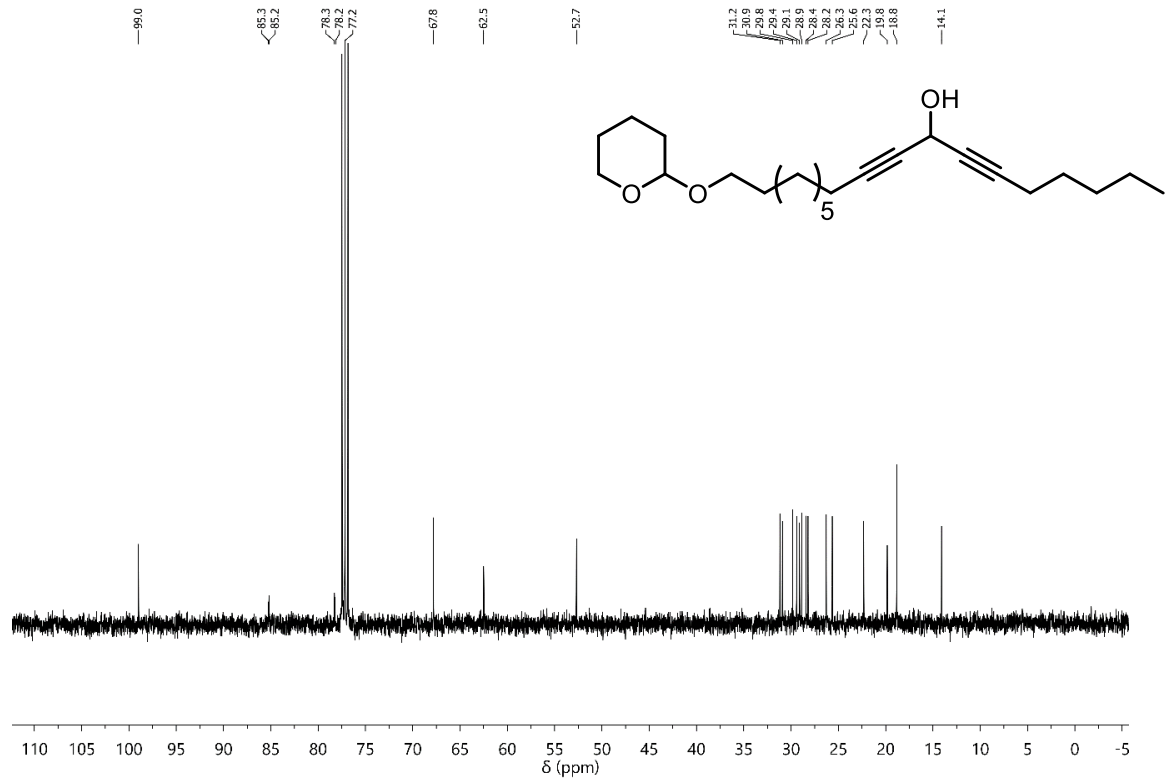
99.0
85.3
85.2
78.3
78.2
77.2
67.8
62.5
52.7
31.2
30.9
29.8
29.4
29.1
28.9
28.4
28.2
26.3
25.6
22.3
19.8
18.8
14.1
OH
O
O
5
δ (ppm)

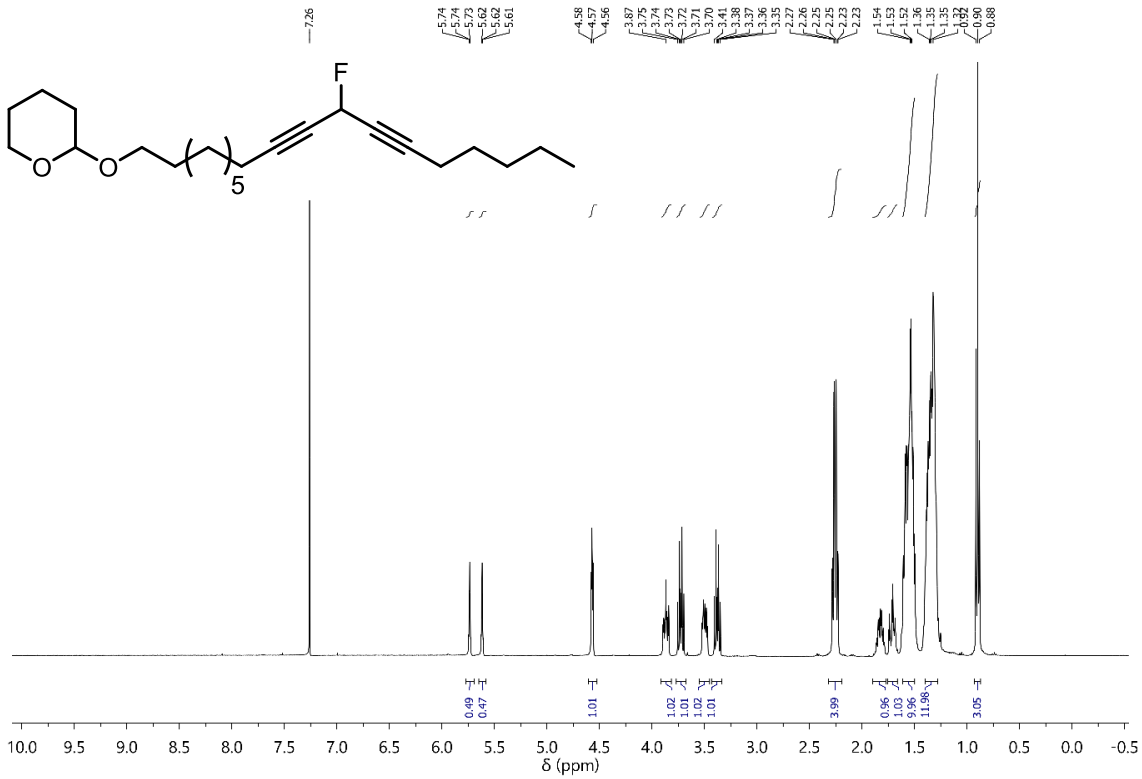
F
O
O
5
δ (ppm)

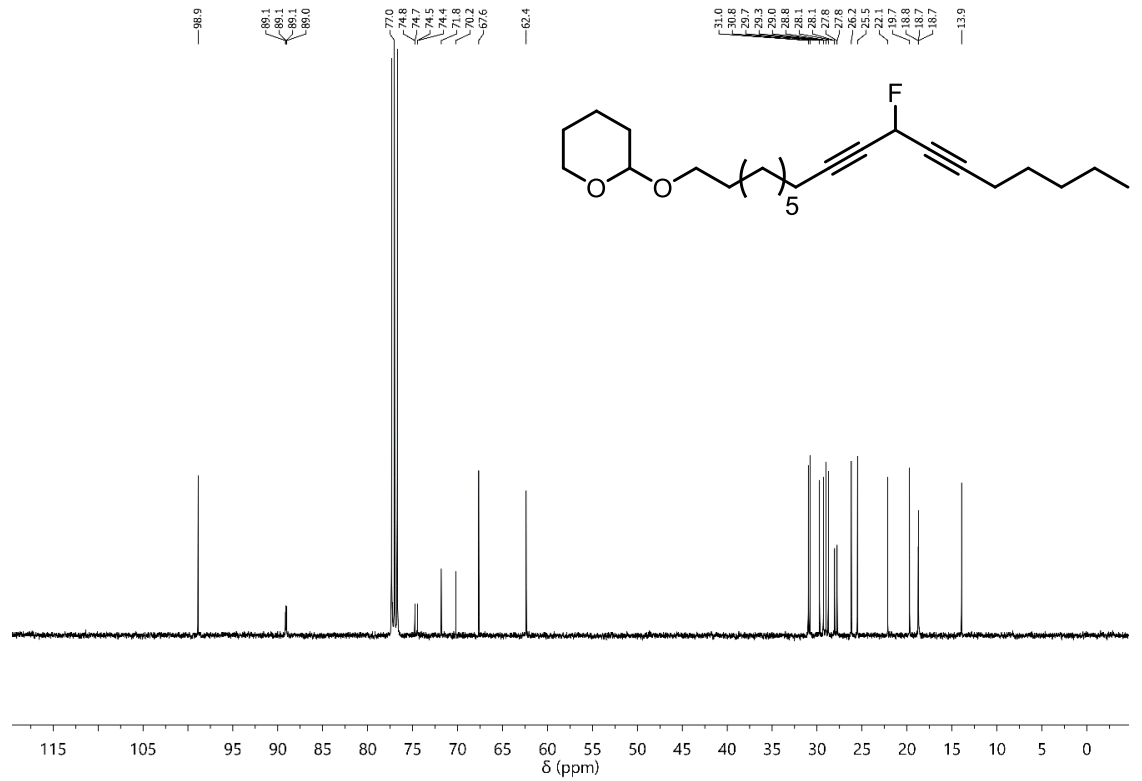
F
O
O
5
δ (ppm)

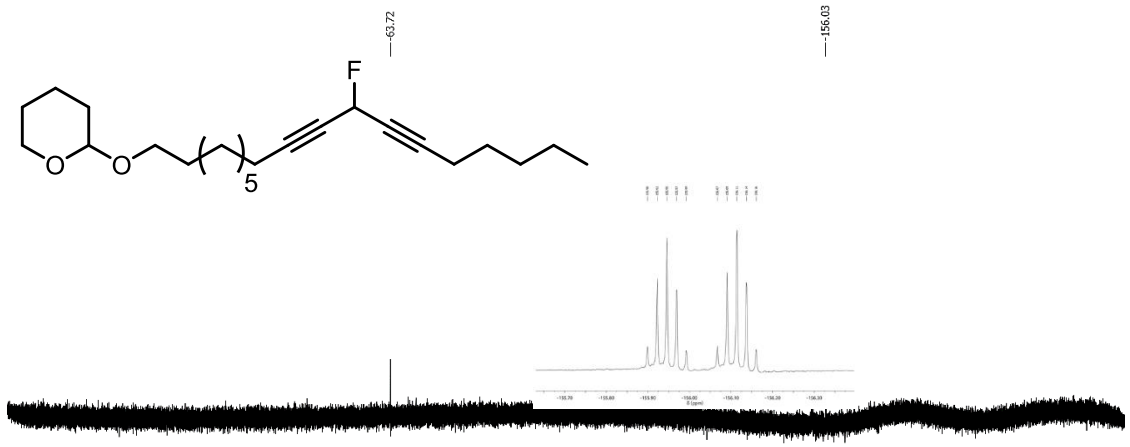
-63.72
-156.03
F
O
O
5

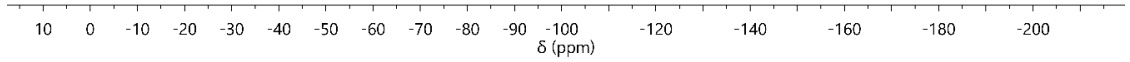
10 0 -10 -20 -30 -40 -50 -60 -70 -80 -90 -100 -120 -140 -160 -180 -200
δ (ppm)

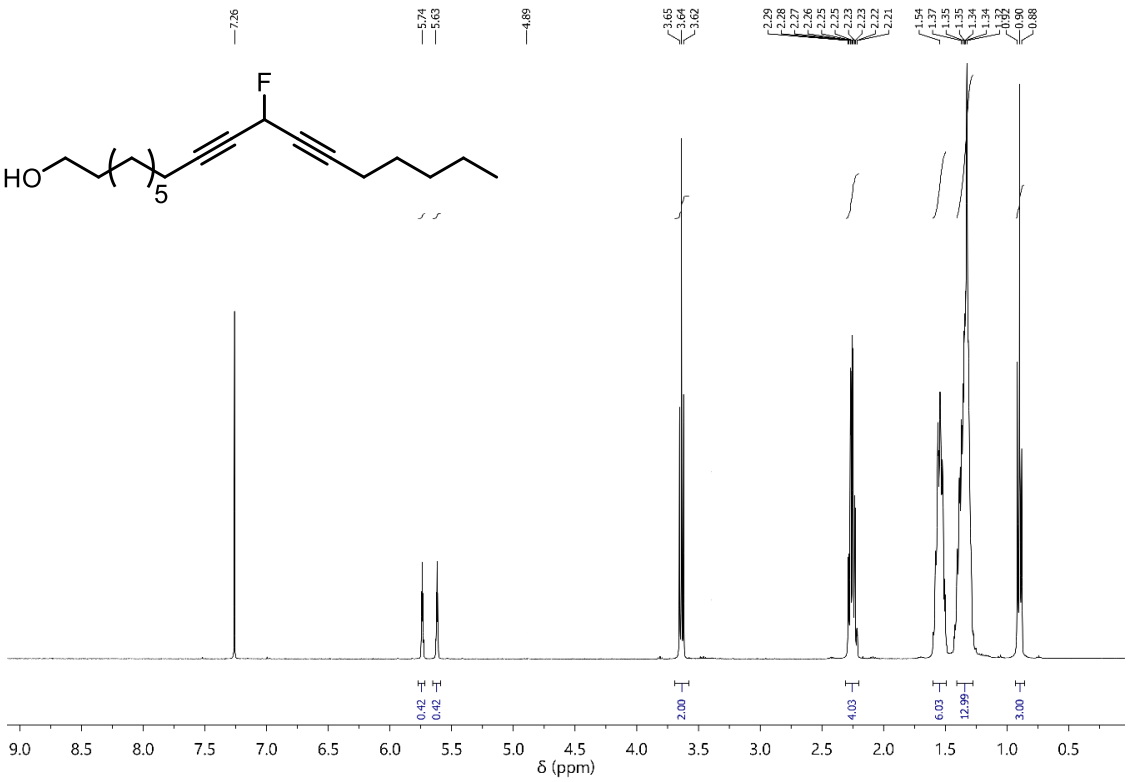
7.26
5.74
5.63
4.89
3.65
3.64
3.62
2.29
2.28
2.27
2.26
2.25
2.25
2.23
2.23
2.22
2.21
1.54
1.37
1.35
1.35
1.34
1.34
0.92
0.90
0.88
F
HO
5
0.42
0.42
2.00
4.03
6.03
12.99
3.00
9.0 8.5 8.0 7.5 7.0 6.5 6.0 5.5 5.0 4.5 4.0 3.5 3.0 2.5 2.0 1.5 1.0 0.5
δ (ppm)

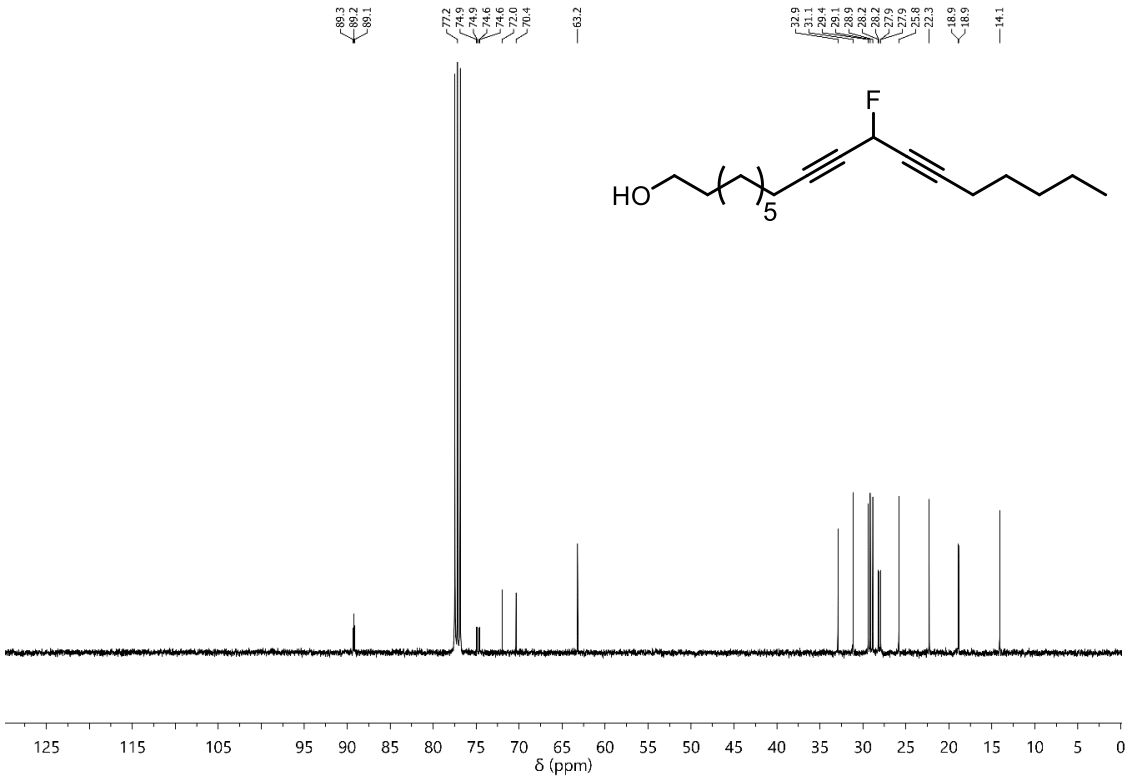
89.3
89.2
89.1
77.2
74.9
74.9
74.6
74.6
72.0
70.4
63.2
32.9
31.1
29.4
29.1
28.9
28.2
28.2
27.9
27.9
25.8
22.3
18.9
18.9
14.1
F
HO
5
125
115
105
95
90
85
80
75
70
65
60
55
50
45
40
35
30
25
20
15
10
5
0
δ (ppm)

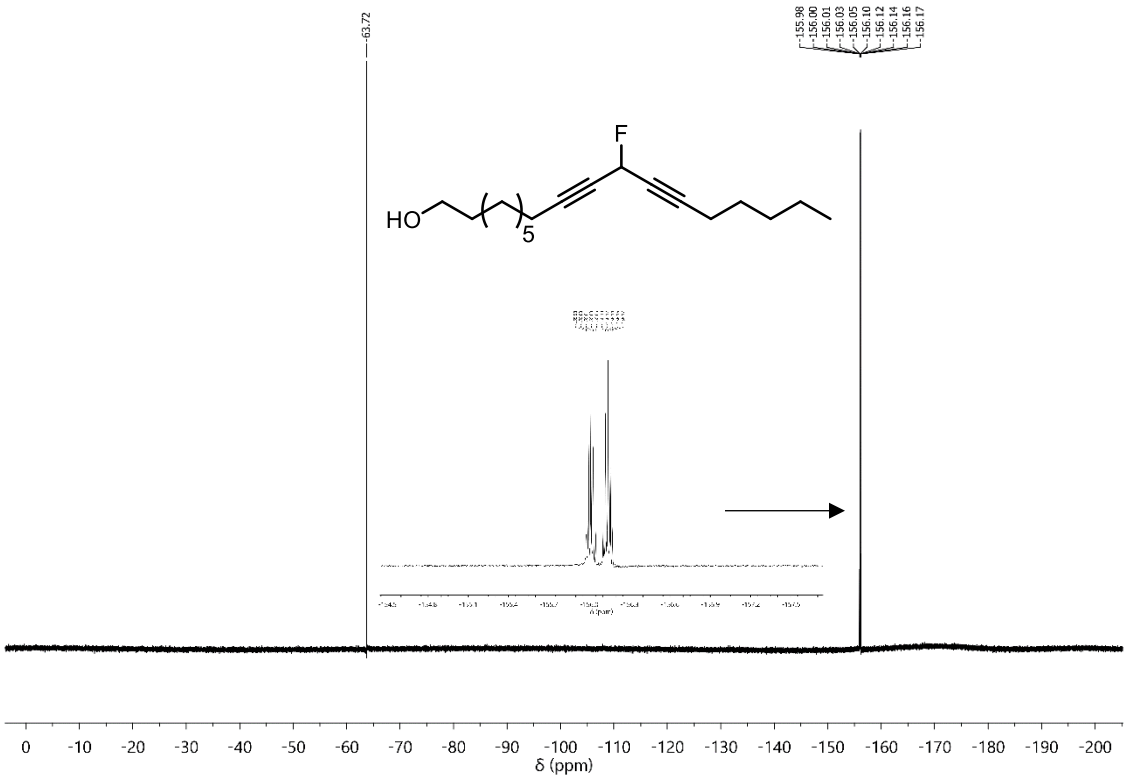
-63.72
-155.98
-156.00
-156.01
-156.03
-156.05
-156.10
-156.12
-156.14
-156.16
-156.17
F
HO
5
0
-10
-20
-30
-40
-50
-60
-70
-80
-90
-100
-110
-120
-130
-140
-150
-160
-170
-180
-190
-200
δ (ppm)

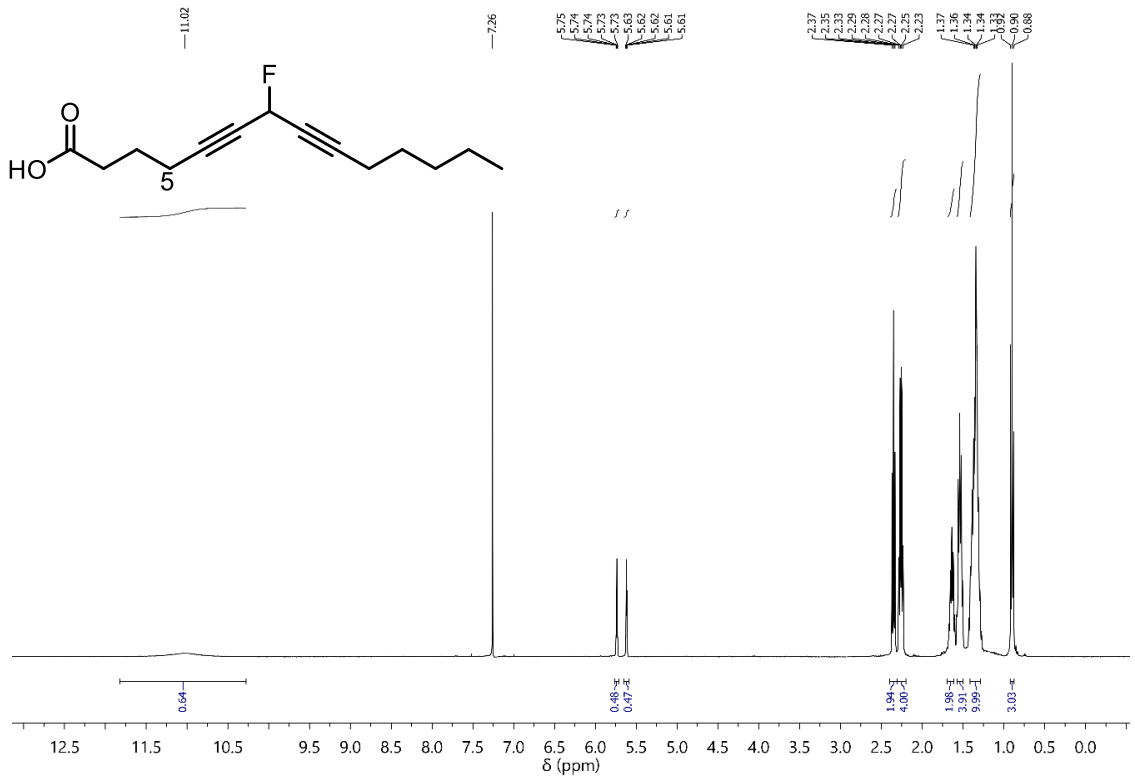
11.02
7.26
5.75
5.74
5.74
5.73
5.73
5.63
5.62
5.62
5.61
5.61
2.37
2.35
2.33
2.29
2.28
2.27
2.27
2.25
2.23
1.37
1.36
1.34
1.34
0.92
0.90
0.88
F
O
HO
5
0.64
0.48
0.47
1.94
4.00
1.98
3.91
9.99
3.03
12.5
11.5
10.5
9.5
9.0
8.5
8.0
7.5
7.0
6.5
6.0
5.5
5.0
4.5
4.0
3.5
3.0
2.5
2.0
1.5
1.0
0.5
0.0
δ (ppm)

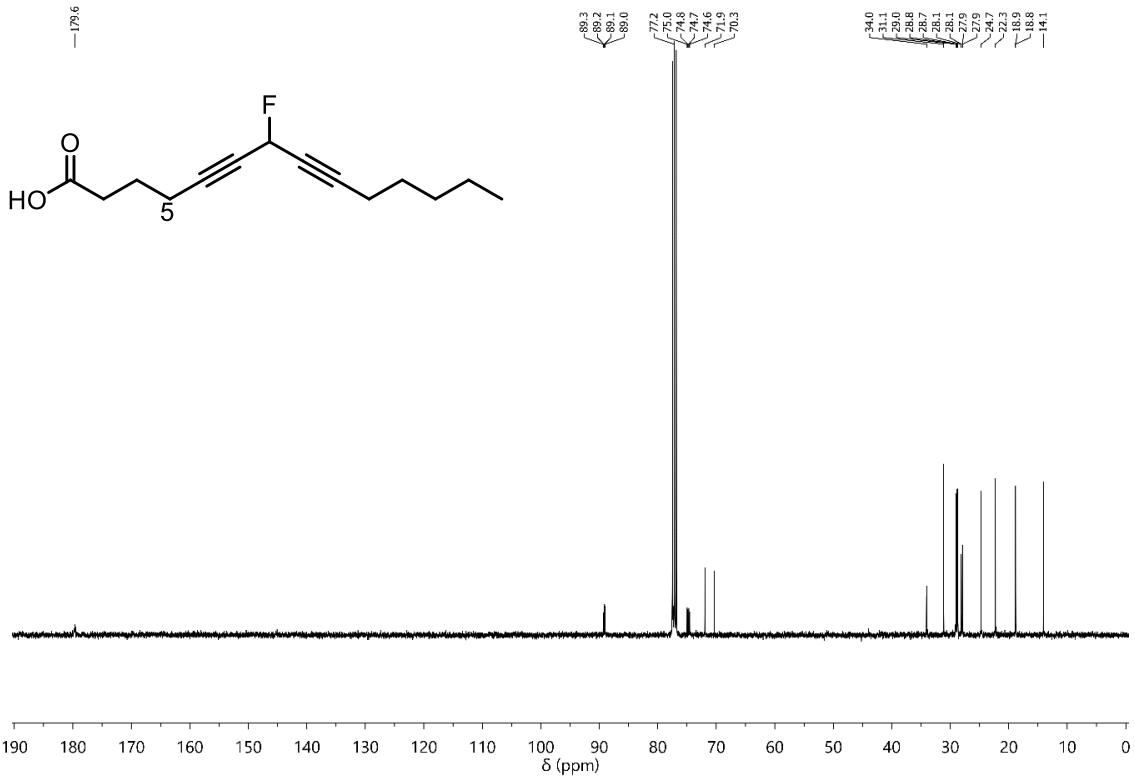
179.6
89.3
89.2
89.1
89.0
77.2
75.0
74.8
74.7
74.7
74.6
71.9
70.3
34.0
31.1
29.0
28.8
28.7
28.1
28.1
27.9
27.9
24.7
22.3
18.9
18.8
14.1
F
O
HO
5
190
180
170
160
150
140
130
120
110
100
90
80
70
60
50
40
30
20
10
0
δ (ppm)

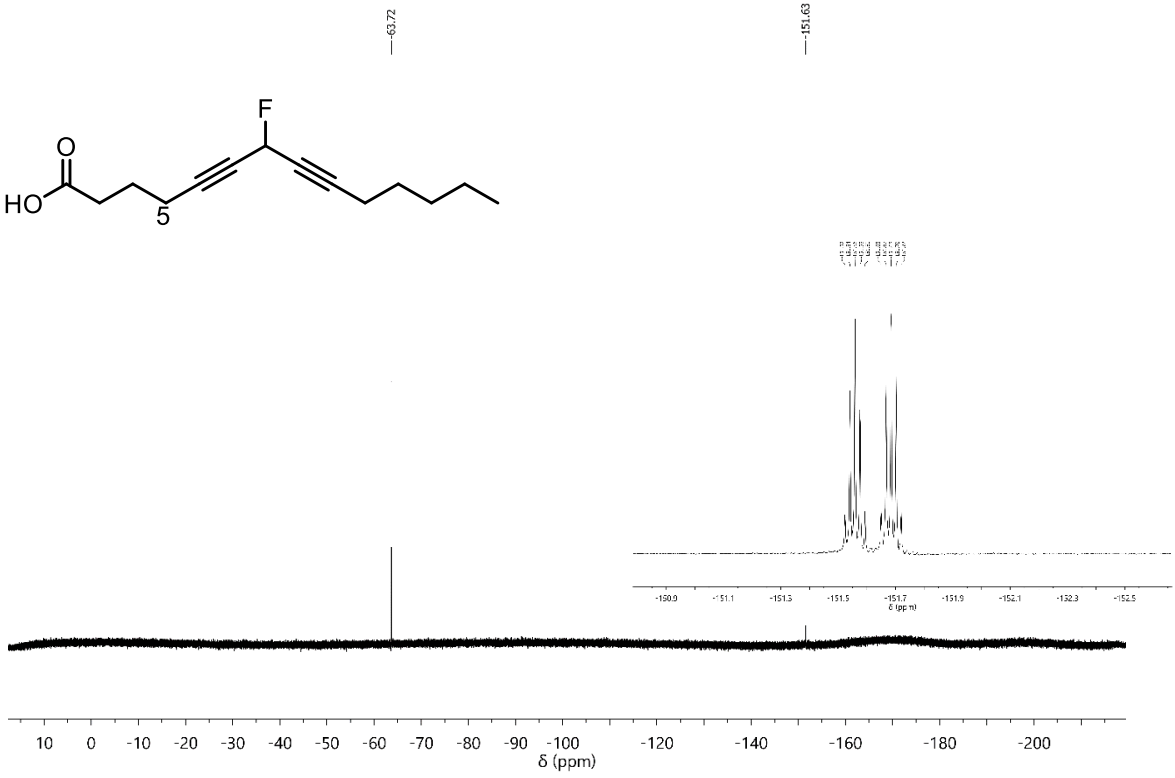
-63.72
-151.63
F
O
HO
5
-150.9
-151.1
-151.3
-151.5
-151.7
-151.9
-152.1
-152.3
-152.5
δ (ppm)
10
0
-10
-20
-30
-40
-50
-60
-70
-80
-90
-100
-120
-140
-160
-180
-200
δ (ppm)